Patrycja Rosa

Understanding of processes driving microglia repopulation in young and old mice by applying scRNA-seq technology

Ph.D. thesis
Completed in the Laboratory of Molecular Neurobiology
of the Nencki Institute of Experimental Biology
Polish Academy of Sciences

SUPERVISOR:
Prof. Bożena Kamińska-Kaczmarek, Ph.D., D.Sc.

Auxiliary supervisor:
Dr. Aleksander Jankowski, Ph.D.

Warsaw, 2025

This study was supported by following research grants:
NCN, OPUS 20 2020/39/B/NZ4/02683 to BK
NCN, SONATA 16 2020/39/D/NZ2/03461 to AJ
NAWA, Polish Returns 2019 to AJ

Part of the work presented in this dissertation has been published in following publication: Luczak-Sobotkowska Z.*, **Rosa P**.*, Banqueri Lopez M., Ochocka N., Kiryk A., Lenkiewicz A. M., Fuhrman M., Jankowski A., Kaminska B. "Tracking changes in functionality and morphology of repopulated microglia in young and old mice" *Journal of Neuroinflammation* **21**, 248 (2024).[1]

Acknowledgments

I would like to express my thanks and appreciation to everyone who contributed to the research enclosed in the following dissertation.

Prof. Bożena Kamińska- Kaczmarek, Ph.D., D.Sc., for giving me the opportunity to complete my Ph.D. thesis in Laboratory of Molecular Neurobiology, for her supervision and support in developing my research and gaining the experience in single-cell omics analysis.

I am deeply grateful to Dr. **Aleksander Jankowski Ph.D.,** for his great amount of help with finishing my dissertation and leading me through all bioinformatics analysis and statistical testing. Also for his great patience to explaining me difficult techniques in scientific world.

Zuzanna Łuczak-Sobotkowska for her tremendous contribution in microglial depletion/repopulation study, for performing experiments and for being not also my lab mate, but a great friend, who made me feel in lab like in home.
Dr. Anna M. Lenkiewicz, Ph. D., for performing single-cell experiments and for substantive discussions on scientific topics and more.
Dr. Bartosz Wojtaś, Ph. D., Ds. C., Dr. Bartłomiej Gielniewski Ph. D., and **Dr. Paulina Szadkowska Ph.D.,** for performing the sequencing of transcriptomics data.
Current and former lab members for a great opportunity to work with you, exchanging scientific and biological experiences.

Ogromne podziękowania kieruję, rodzinie oraz moim przyjaciołom za wiarę we mnie i wsparcie w najtrudniejszych momentach. W szczególności dziękuję **Dagmarze** za każde słowo otuchy podczas naukowych zmagań oraz mojemu bratu, **Mateuszowi**.

Ogromne słowa uznania kieruję mojemu narzeczonemu **Tomkowi**, za wsparcie w naukowej drodze, za jeszcze większe pokłady cierpliwości oraz za bycie moim najwierniejszym kibicem w tej ścieżce rozwoju.

Pracę dedykuję **Mamie** i **Tacie**, bez Waszej wiary w moje możliwości od najmłodszych lat nie byłoby to możliwe.

Table of contents

List of abbreviations

Act-MG – activated microglia

AD – Alzheimer's disease

ADT – antibody-dependent tag

ALS – amyotrophic lateral sclerosis

ARMs – activated response microglia

ATAC-seq – assay for transposase-accessible chromatin with high-throughput sequencing

ATMs – axon tract-associated microglia

BAM – border-associated macrophages

BBB – blood-brain barrier

BCL – binary base call

BDNF – brain-derived neurotrophic factor

CAMs – cytokine-associated microglia

ChIP-seq – chromatin immunoprecipitation followed by sequencing

CITE-seq – cellular indexing of transcriptomes and epitopes by sequencing

CNS – central nervous system

CPM – counts per million

CSF1 – colony-stimulating factor 1

M-CSF – macrophage colony-stimulating factor

CSF1R – colony-stimulating factor 1 receptor

DAMP – damage-associated molecular pattern

DAMs – disease-associated microglia

DGE – differentially expressed genes

ECM – extracellular matrix

FACS – fluorescence-activated cell sorting

FC – fold change

FDR – false discovery rate

FGF – fibroblast growth factor

FTD – frontotemporal dementia

GAMs – glioma-associated microglia

GDNF – glial cell line-derived neurotrophic factor

GEM – gel beads-in-emulsion

GLM – generalized linear model

HAMs – human Alzheimer's microglia

HTO – hashtag oligonucleotide

iPSC – induced pluripotent stem cell

IRMs – Interferon Response Microglia

KEGG – Kyoto Encyclopedia of Genes and Genomes

LDAMs – lipid droplet-accumulating microglia

Methyl-seq – methylation sequencing

MG – microglia

MGnD – microglial neurodegenerative phenotype

MIMS – multiple sclerosis-inflamed microglia

NB – negative binomial

NGS – next-generation sequencing

NO – nitric oxide

ONT – Oxford Nanopore technologies

PAMs – proliferative region-associated microglia

PCA – Principal Component Analysis

PCR – polymerase chain reaction

PD – Parkinson's disease

PVMs – perivascular macrophages

QC – quality control

RNA-seq – RNA-sequencing

ROS – reactive oxygen species

RPCA – reciprocal PCA

RT – reverse transcription

scRNA-seq – single-cell RNA sequencing

SMRT – single molecule real-time

sNN – shared nearest neighbor graph

SNPs – single nucleotide polymorphism

TMM – trimmed mean of M-values

UMAP – uniform Manifold approximation and projection

UMIs – unique molecular identifiers

WAMs – white matter-associated microglia

WES – whole-exome sequencing

WGS – whole-genome sequencing

1. Abstract

Microglia, the resident immune cells of the central nervous system (CNS), are critical for maintaining neuronal homeostasis, supporting synaptic plasticity, and mounting immune responses to injury and disease. Unlike most CNS-resident cell populations, microglia possess a unique regenerative capacity: following depletion, they are able to repopulate the brain and restore density within days. Microglia viability is regulated by colony stimulating factor 1 receptor (CSF1R) signaling. However, whether these repopulated microglia fully reacquire the functional heterogeneity and homeostatic states of their counterparts, and how this process is influenced by aging, remains poorly understood.

In this study, we combined pharmacological depletion using the CSF1R inhibitor BLZ-945 with single-cell RNA sequencing (scRNA-seq) of CD11b+ cells to examine the molecular programs underlying microglial repopulation in both young and aged mice. Complete depletion was achieved after 21 days of BLZ-945 treatment, and repopulation occurred within 7 days following withdrawal of the inhibitor. The analyses of the acquired dataset revealed that repopulated microglia reestablish many of the transcriptional states observed in control animals, but only after passing through distinct, transiently activated phenotypes (Act-MG1, Act-MG2, Act-MG3). These activation states were marked by expression of genes involved in proliferation (*Mki67, Top2a*), motility and cytoskeletal remodeling (*Rac1, P2ry12*), extracellular matrix (ECM) degradation (*Cstb, Ctsd*), and inflammatory cytokine signaling *(Il1b, Tnf, Il6*).

Trajectory analyses demonstrated that repopulated microglia originate from proliferating precursors and move through activated states before reaching a homeostatic phenotype.

Age emerged as a major determinant of repopulation efficiency and outcome. While young mice successfully generated homeostatic microglia following transient activation, aged mice displayed impaired maturation of repopulated cells. Repopulated microglia from older animals exhibited heightened proliferation, persistent inflammatory signaling, and reduced representation of homeostatic clusters. Bulk RNA sequencing (RNA-seq) further confirmed downregulation of core homeostatic genes (*P2ry12, Tmem119, Trem2*) and upregulation of pro-apoptotic and senescence-associated genes in repopulated microglia from aged mice. Pathway-level analysis implicated dysregulation of RhoA-ROCK signaling, which regulates

microglial motility, cytoskeletal dynamics, and inflammatory responses, as a central feature of the aging-associated deficits.

Comparative analysis revealed striking similarities between the transient Act-MG states of repopulated microglia and the transcriptional programs of glioma-associated microglia. Integration of the presented scRNA-seq dataset with CITE-seq data from murine glioma models identified overlapping clusters enriched for migratory, phagocytic, and inflammatory signatures. These results suggest that microglia repopulation recapitulates transcriptional programs exploited in pathological contexts, highlighting conserved mechanisms of microglial plasticity.

These findings have several implications. First, they demonstrate that repopulation is not a simple return to baseline but a dynamic, multi-stage process requiring activation, migration, and eventual resolution to homeostasis. Second, they reveal that aging disrupts this trajectory, leaving microglia in maladaptive states that may compromise neuronal support and increase vulnerability to neurodegeneration. Third, the shared transcriptional features between repopulated and glioma-associated microglia suggest that cellular programs enabling regeneration may also predispose microglia to pathological reprogramming in disease.

In conclusion, our study establishes a comprehensive transcriptional framework for microglial repopulation in young and aged brains. By identifying conserved activation programs that bridge regeneration and pathological activation , we highlight new opportunities for therapeutic strategies aimed at harnessing microglial plasticity while mitigating age-related dysfunction. This work underscores the dual nature of microglial repopulation, as both a regenerative mechanism and a potential point of vulnerability in the aging brain.

2. Streszczenie

Mikroglej, komórki odpornościowe w ośrodkowym układzie nerwowym (OUN), odgrywają kluczową rolę w utrzymaniu homeostazy, wspierają plastyczność synaptyczną oraz uczestniczą w odpowiedzi układu odpornościowego na urazy i choroby. W odróżnieniu od większości populacji komórek OUN, mikroglej ma unikalną zdolność do odnowy: po farmakologicznej eliminacji dochodzi do odnowy populacji w OUN i odtworzenia prawidłowej gęstości komórek w ciągu kilku dni. Nadal jednak nie wiadomo, czy nowe, zasiedlające OUN komórki mikrogleju w pełni odtwarzają heterogenność funkcjonalną i stan prawidłowego mikrogleju oraz w jaki sposób proces ten ulega modyfikacji w trakcie starzenia OUN.

W niniejszej pracy połączono farmakologiczne usunięcie mikrogleju przy użyciu inhibitora CSF1R (BLZ-945) z sekwencjonowaniem RNA pojedynczych komórek (scRNA-seq) w populacji komórek mieloidalnych sortowanych jako komórki CD11b+ w celu zbadania programów molekularnych leżących u podstaw odnowy mikrogleju u młodych i starych myszy. Całkowitą eliminację mikrogleju osiągnięto po 21 dniach podawania BLZ-945, a odnowa nastąpiła w ciągu 7 dni od odstawienia inhibitora. Uzyskane dane pokazały, że nowy mikroglej (MG) odtwarza wiele stanów transkrypcyjnych obserwowanych u zwierząt kontrolnych, ale przechodzi wcześniej przez przejściowe stany aktywacji (Act-MG1, Act-MG2, Act-MG3). Stany te charakteryzowały się ekspresją genów związanych z proliferacją (*Mki67, Top2a*), migracją i przebudową cytoszkieletu (*Rac1, P2ry12*), degradacją macierzy pozakomórkowej (*Cstb, Ctsd*) oraz sygnalizacją cytokin zapalnych *(Il1b, Tnf, Il6*).

Analizy trajektorii rozwojowych pokazały, że odtworzony mikroglej wywodzi się z nielicznych prekursorów, które proliferują i przechodzą przez stany aktywacji, zanim osiągną fenotyp homeostatyczny. Starzenie jest kluczowym czynnikiem determinującym efektywność i wynik odnowy MG. Podczas gdy w mózgu młodych myszy MG osiągał stan homeostatyczny po fazie przejściowej aktywacji, u starych osobników obserwowano upośledzone dojrzewanie MG. Komórki te cechowały się zwiększoną proliferacją, utrzymującą się sygnalizacją zapalną i zmniejszoną reprezentacją komórek w stanie homeostatycznym. Sekwencjonowanie RNA (bulk RNA-seq) mikrogleju dodatkowo potwierdziło obniżoną ekspresję genów homeostatycznych (*P2ry12, Tmem119, Trem2*) oraz zwiększoną ekspresję genów proapoptotycznych i związanych ze starzeniem. Analizy szlaków powiązanych z ekspresją genów wskazały na deregulację sygnalizacji RhoA-ROCK – kluczowej dla migracji, dynamiki cytoszkieletu i odpowiedzi zapalnej mikrogleju związanych ze starzeniem.

Analiza porównawcza ujawniła uderzające podobieństwa między przejściowymi stanami Act-MG a programami transkrypcyjnymi mikrogleju związanego z glejakiem. Integracja przedstawionego w rozprawie zbioru danych scRNA-seq z danymi CITE-seq z modeli mysich glejaków wykazała obecność mikrogleju z ekspresją podobnych genów wzbogaconych w sygnatury migracyjne, fagocytarne i zapalne. Wyniki te sugerują, że programy transkrypcyjne w procesie odnowy mikrogleju są wykorzystywane w kontekstach patologicznych, co podkreśla konserwatywne mechanizmy plastyczności mikrogleju.

Podsumowując, wyniki przedstawionych badań dostarczyły kompleksowych profili transkrypcji występujących w czasie odnowy mikrogleju w młodym i starym mózgu. Pokazano, że choć mikroglej u młodych myszy odtwarza pełną różnorodność i funkcjonalność, starzenie głęboko zakłóca ten proces, uniemożliwiając przywrócenie pełnej homeostazy. Identyfikacja konserwatywnych programów aktywacji, które łączą odnowę mikrogleju z patologiczną aktywacją, otwiera nowe perspektywy terapeutyczne, ukierunkowane na wykorzystanie plastyczności mikrogleju przy jednoczesnym ograniczaniu dysfunkcji związanych z wiekiem. Nasze wyniki podkreślają dwoistą naturę odnowy mikrogleju – jako mechanizmu regeneracyjnego, ale również potencjalnego punktu podatności w starzejącym się mózgu.

3. Introduction

3.1 Overview of microglia origin and functions

3.1.1 Microglia as myeloid cells in the central nervous system

Microglia (MG) are myeloid cells that reside permanently within a parenchyma of the central nervous system (CNS), where they function as its principal innate immune component. Unlike peripheral immune cells that originate from hematopoietic stem cells in the bone marrow, microglia arise from erythromyeloid precursors in the yolk sac during early embryogenesis[2–4]. Around embryonic day 8.5 in mice, these precursors migrate into the developing CNS before the blood-brain barrier (BBB) is fully formed, establishing a self-renewing population of microglia that persists throughout life under homeostatic conditions.

Together with other CNS-resident myeloid cells (including perivascular, choroid plexus, and meningeal macrophages, collectively termed border-associated macrophages (BAMs)), microglia constitute the resident innate immune cells of the CNS. In contrast to BAMs, which occupy barrier niches, microglia populate the CNS parenchyma, where they play an essential role in preserving homeostasis, monitoring the neural environment, and orchestrating immune responses[5,6].

Functionally, microglia act as the primary immune sentinels of the CNS. In the healthy brain, they typically adopt ramified morphology, characterized by a small cell body and highly motile processes, which allow continuous surveillance of the local microenvironment for signs of infection, injury or cellular stress. This surveillant state, previous described as a “resting” state is in fact highly dynamic and underpins the homeostatic functions of microglia. When confronted with perturbations such as infection, trauma, neurodegeneration or autoimmune inflammation, microglia rapidly undergo morphological, transcriptional and functional transformations, transitioning into various activated states tailored to context specific demands[7]. These activated microglial states reflect their remarkable plasticity and can promote neuroprotection, tissue repair or neurotoxicity (in cases of chronic or dysregulated activation)[8].

Quantitatively, microglia constitute approximately 5-12% of the total glial cell population in the mouse brain, though this proportion varies depending on the brain region, age and disease state[9]. Their dual capacity for beneficial or detrimental roles makes them central

players in CNS pathologies. Dysregulated or senescent microglia have been implicated in a broad spectrum of CNS disorders, including Alzheimer's disease, multiple sclerosis, Parkinson's disease, stroke and psychiatric conditions. Importantly, their distinct developmental lineage sets them apart from other CNS-resident cells derived from the neuroectoderm (neurons, astrocytes, oligodendrocytes), equipping them with unique immune capabilities such as phagocytosis, cytokine release and antigen presentation[10,11].

3.1.2 Role of microglia in maintaining CNS homeostasis

Microglia play a fundamental role in maintaining homeostasis in CNS across all stages of life, including development, adulthood, aging, and disease. As the brain's resident immune and surveillance cells, microglia are uniquely equipped to monitor and respond to changes in the neural environment, thereby ensuring tissue integrity and functional stability. In their surveillant state, microglia exhibit a highly branched morphology, enabling them to continuously scan the CNS microenvironment with dynamic, motile processes[12]. This constant surveillance allows microglia to detect subtle alterations in neuronal activity or injury-related signals, such as damage-associated molecular pattern (DAMP) molecules, which are released by stressed or dying cells[13].

During embryonic and early postnatal development, microglia are critical for forming the nervous system. Depletion studies in mice have shown that microglia support the survival and maturation of developing neurons by releasing neurotrophic factors such as brain-derived neurotrophic factor (BDNF) and insulin-like growth factor 1 (IGF-1)[14]. In addition to promoting neuronal survival, microglia play an essential role in removing apoptotic cells and cellular debris through phagocytosis, a function crucial for proper synaptic pruning and circuit formation during early brain development[15].

As the brain ages, microglia continue to modulate their functions to adapt to changing physiological demands. Aging is associated with a shift in microglial phenotype, often resulting in a more pro-inflammatory state characterized by increased cytokine production and reduced phagocytic efficiency. These changes can contribute to age-related cognitive decline and increased vulnerability to neurodegenerative disorders. Recent advances in single-cell transcriptomics, fate mapping, and high-resolution imaging have revealed that microglia exhibit remarkable context-dependent plasticity[16,17]. In response to injury, disease, or neurodegeneration, microglia undergo profound transcriptional, morphological, and functional reprogramming. Microglia in activated states can be either neuroprotective

by promoting repair, clearing debris, and resolving inflammation, or neurotoxic, contributing to synaptic loss, chronic inflammation, and neuronal damage[16,17].

The ability of microglia to adapt to local cues underscores their dual nature: while essential for maintaining CNS homeostasis, dysregulated microglial activity can also drive pathology. Understanding the factors that influence microglial phenotypes and functions remains a critical area of research, with significant implications for therapeutic strategies targeting neuroinflammatory and neurodegenerative diseases.

3.1.3 Importance of microglia during development, aging, and disease

Microglia are recognized as key regulators of CNS homeostasis, with critical roles that extend from embryonic development through aging and into the pathophysiology of numerous neurological diseases. Because the microglial population is established early during embryogenesis from yolk sac progenitors, it is uniquely vulnerable to long-term physiological perturbations. As a result, age-related changes in microglial function are now understood to contribute significantly to the onset and progression of both psychiatric and neurodegenerative disorders[7]. Senescent microglia show the impaired neuroprotective ability and the low but sustained secretion of inflammation molecules. Some studies showed the presence of an aberrant phenotype referred to as dystrophic or senescent. Aged microglia have been identified in neurodegenerative diseases such as Alzheimer's disease, but there is no conclusive evidence that proves a causal role due to a lack of models of aged microglia. One of the models of senescent microglia is based on iron overload in dystrophic microglia. Cultured iron-overloaded microglia acquire a senescent phenotype and show some changes similar to those observed during neurodegeneration in patients[7].

One of the most compelling pieces of evidence for microglial involvement in disease comes from human genetic studies. Variants in several microglia-associated genes have been identified as risk factors for major neurodegenerative diseases, including Alzheimer’s disease (AD)[15,18], frontotemporal dementia (FTD)[19], Parkinson’s disease (PD)[20], and amyotrophic lateral sclerosis (ALS)[21]. Activated microglia are frequently found in proximity to pathological markers in these diseases (such as amyloid-beta plaques in AD)[22], suggesting a reactive and potentially causal role in disease progression.

Among the most studied genetic risk factors is a rare variant of the triggering receptor expressed on myeloid cells 2 (TREM2) gene, which increases the risk for developing AD by three – to fourfold and is associated with more severe neuropathology[23]. TREM2 is believed

to interact with apolipoprotein E (APOE) to regulate pathways involved in microglial activation, survival, lipid metabolism, and phagocytosis[24]. In models of neurodegenerative and neuroinflammatory diseases (i.e. AD), microglia exhibit upregulation of genes associated with metabolism and inflammation, including *Spp1* and *Apoe*, marking a shift from homeostatic to a disease-associated phenotype[24,25].

Microglia also contribute to the modulation of synaptic function across the lifespan. In early adulthood, they are involved in learning-dependent synaptic remodeling and plasticity. In neurogenic regions of the adult brain, microglia facilitate the clearance of apoptotic neuronal progenitors, thereby shaping neurogenesis[14]. Their interaction with the extracellular matrix (ECM) also appears to be critical for maintaining synaptic structure and function. Recent studies have shown that neuronal expression of interleukin-33 (IL-33) can induce microglial-mediated ECM clearance, which promotes synaptic remodeling. Mice with neuron-specific IL-33 deletion or microglia-specific deletion of the IL-33 receptor exhibit mislocalization of ECM material, reduced dendritic spine density in the hippocampus, and impaired memory recall, underscoring the importance of neuron-microglia signaling for cognitive function[14,25].

Across species and disease models, microglia display a wide range of transcriptional states reflecting their high degree of plasticity and context-dependent specialization. These include:

- Disease-associated microglia (DAMs): initially characterized in mouse models of AD, marked by downregulation of homeostatic genes and upregulation of phagocytic and lipid metabolism pathways.
- Microglial neurodegenerative phenotype (MGnD): observed across multiple models, sharing features with DAMs.
- Activated response microglia (ARMs) and interferon-responsive microglia (IRMs): identified in AD models, displaying antiviral and inflammatory gene signatures.
- Human Alzheimer's microglia (HAMs): human-specific microglial signatures found in AD patients.
- Multiple Sclerosis-inflamed microglia (MIMS) and lipid droplet-accumulating microglia (LDAMs): linked to neuroinflammation and aging.
- Glioma-associated microglia (GAMs): found in brain tumor environments.
- ALS- and PD-associated microglia signatures: reflect disease-specific alterations in microglial states.

In both the developing and aging brain, microglia further adopt specialized subtypes that support region-specific functions. For instance:

- White matter-associated microglia (WAMs) and axon tract-associated microglia (ATMs) are involved in axonal support and myelin maintenance.
- Proliferative region-associated microglia (PAMs) contribute to the phagocytosis of developing oligodendrocytes in proliferative CNS zones.

Interestingly, many of these developmental microglial states share transcriptomic features with the DAM and MGnD profiles observed in disease, suggesting conserved mechanisms that are re-engaged in pathology[8].

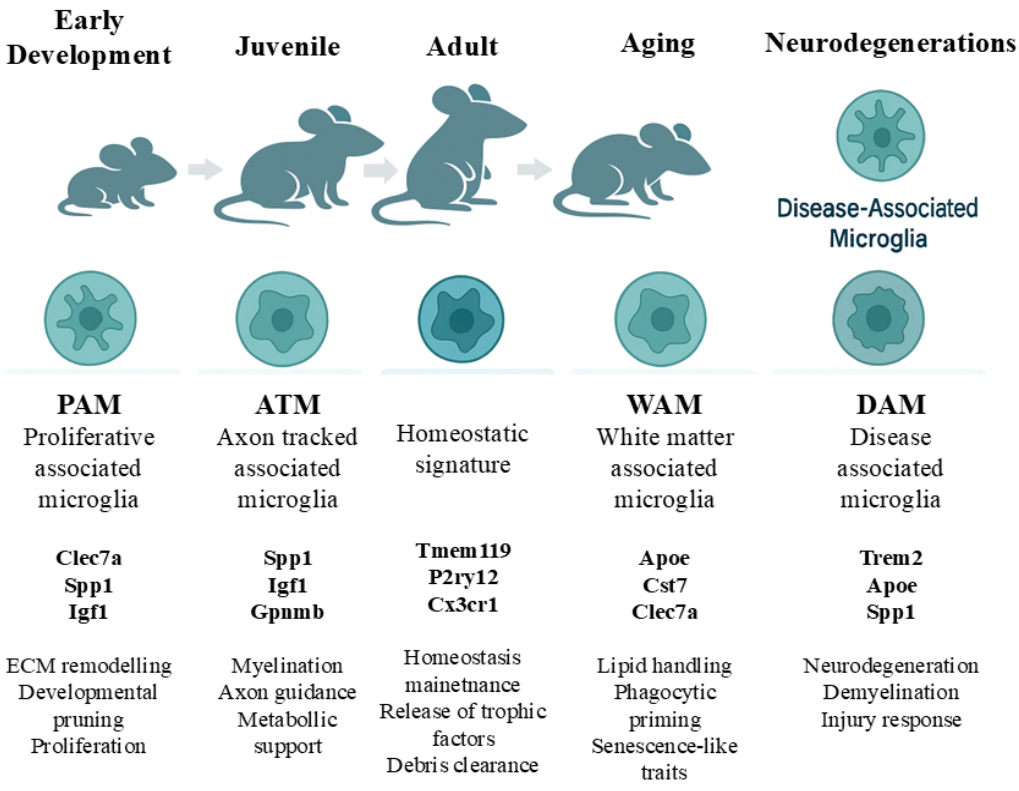

Figure 3.1 | Microglial transcriptional states across mouse development, aging and neurodegeneration. Schematic representation of major microglial phenotypes observed at different life stages in mice. Early development features proliferative (PAM) microglia, followed by axon tract-associated microglia (ATM). In adulthood, microglia adopt a stable homeostatic signature characterized by *Tmem119, P2ry12,* and *Cx3cr1*. Aging is associated with white matter-associated microglia (WAM), expressing *Apoe, Cst7,* and *Clec7a*. Neurodegenerative conditions induce disease-

associated microglia (DAM), marked by *Trem2, Apoe,* and *Spp1*. Figure created by the author of the dissertation. Microglial state categories were conceptually informed by Paolicelli et al., Neuron (2022), but no original artwork or copyrighted elements were reproduced[8].

3.1.4 Implications of microglial dysfunctions in aging

Aging has profound effects on microglial morphology, function, and gene expression, leading to a state often referred to as microglial senescence or dysfunction, which has critical implications for CNS homeostasis and vulnerability to neurodegenerative diseases. Morphologically, aged microglia exhibit a distinct dystrophic phenotype characterized by deramification, shortening and thickening of processes, the formation of cytoplasmic spheroids, and fragmentation of cellular processes[7]. These features suggest a loss of structural integrity and cellular homeostasis, which may compromise the cellular capacity to perform essential surveillance and immune functions. Functionally, aging microglia show reduced process motility, impairing their ability to effectively scan the CNS environment[26–29]. This altered surveillance phenotype leads to delayed or diminished responses to pathological stimuli.

Upon injury, aged microglia demonstrate slower migration to lesion sites and exhibit a more prolonged and dysregulated inflammatory response, rather than the transient and balanced response seen in younger microglia[30]. At the molecular level, aged microglia undergo significant shifts in their transcriptomic and functional profiles. They tend to adopt a pro-inflammatory cytokine signature, characterized by elevated expression of interleukins (e.g., IL-1β, IL-6), tumor necrosis factor-alpha (TNF-α), and other inflammatory mediators[31,32]. Simultaneously, their phagocytic capacity-critical for clearing apoptotic cells, debris, and misfolded proteins is notably reduced. This combination of chronic inflammation and impaired clearance contributes to a feed-forward loop that exacerbates neuronal damage and may accelerate cognitive decline. Additionally, aged microglia produce increased levels of reactive oxygen species (ROS), promoting oxidative stress in the CNS, which can damage both neuronal and glial cells. This oxidative environment, paired with sustained inflammation, creates a milieu conducive to neurodegenerative processes[33,34].

Recent meta-analyses of gene expression datasets have shown that aged microglia do not simply reflect classical activation states induced by lipopolysaccharide (LPS) or IL-4 stimulation. Instead, they exhibit a unique gene expression profile that overlaps with “premature microglia”, a phenotype associated with increased responsiveness

to secondary insults and a propensity toward neurotoxicity[35]. These findings suggest that microglial aging represents a distinct, maladaptive state that may render the aging brain more susceptible to injury and disease. Collectively, these abnormalities undermine the neuroprotective and homeostatic roles of microglia, contributing to age-associated CNS pathologies such as Alzheimer's disease, Parkinson's disease, and vascular cognitive impairment[27,36]. Understanding the mechanisms driving microglial aging is therefore critical for developing interventions aimed at restoring microglial function or preventing their deleterious activation in the aging brain.

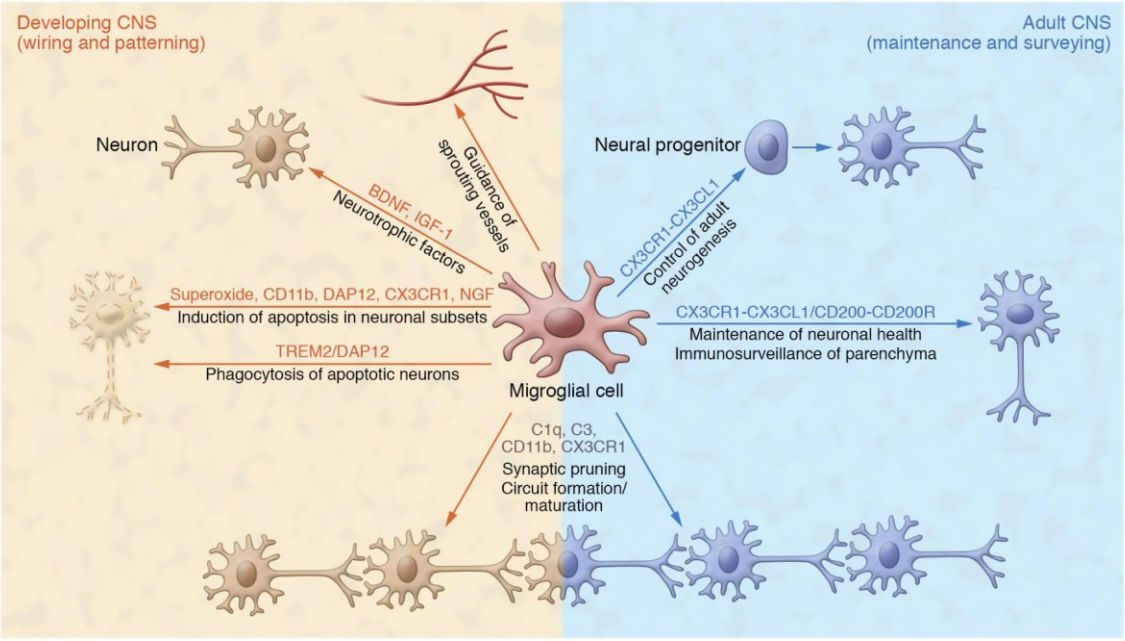

Figure 3.2 | Developmental and adult functions of microglia mediated by neuron-microglia signaling pathways. Figure from Kierdorf, K. & Prinz, M. Microglia in steady state. J. Clin. Invest. 127, 3201–3209 (2017)[37], used under CC BY 4.0 license (http://creativecommons.org/licenses/by/4.0/).

3.1.5 Microglial function and plasticity

Throughout life, but especially during CNS development, microglia engage in a wide range of dynamic activities including neurogenesis, apoptotic cell clearance, synaptic pruning, and the modulation of neural network architecture[38]. These processes are essential for shaping functional neural circuits and ensuring proper CNS maturation.

One of the most defining features of microglia is their remarkable plasticity. They are highly responsive to changes in their environment, capable of undergoing rapid and reversible shifts in both morphology and molecular phenotype in response to physiological

and pathological stimuli[7]. Depending on the context, microglia can adopt various functional states ranging from supportive and neuroprotective to reactive and neurotoxic. In the setting of CNS injury or disease, microglia become activated, a process involving extensive remodeling of gene expression, cytoskeletal structure, and secretory profiles. This activation is not binary but occurs along a spectrum of phenotypic states that evolve over time and vary between different diseases[39,40].

Throughout disease progression, activated microglia often shift between these states, influencing the progression of neurodegeneration or instigating a recovery[41,42]. Activated microglia engage in direct physical interactions with neurons, playing a dual role in either promoting neuronal survival or contributing to neuronal damage[43,44]. One notable mechanism of interaction involves the elimination of synapses on injured or dysfunctional neurons[45,46], a process sometimes beneficial for limiting excitotoxicity or inflammation, but also potentially detrimental when excessive, as it can disrupt neural connectivity[5]. Microglia are finely tuned to detect neuronal distress through a combination of chemotactic and phagocytic signals[44,47,48]. Upon CNS injury, neurons and other glial cells release molecular cues that guide microglial responses. These include:

- **"Find-me" signals** (e.g., adenosine triphosphate (ATP), chemokines such as *Cx3cl1*) that attract microglia to sites of injury.
- **"Eat-me" signals** (e.g., phosphatidylserine) that promote recognition and phagocytosis of apoptotic cells or cellular debris[49].

In response to injury or inflammation, microglia release a diverse array of neurotrophic factors that promote cell survival and repair, including nerve growth factor (NGF)[50,51], neurotrophin-4/5 (NT-4/5), transforming growth factor-beta 1 (TGF-β1)[52,53], glial cell line – derived neurotrophic factor (GDNF), fibroblast growth factor (FGF), and interleukin-3 (IL-3). These factors can support neuronal regeneration, modulate synaptic plasticity, and help restore tissue homeostasis. However, microglial activation is a double-edged sword. In chronic or unresolved pathological conditions, microglia may transition into a pro-inflammatory and cytotoxic state, marked by the release of pro-inflammatory cytokines, reactive oxygen species (ROS), and nitric oxide (NO)[54–56]. These molecules can induce retrograde apoptosis in neurons connected to already degenerating cells, thereby facilitating the spread of neural damage across functional circuits and exacerbating disease progression (Fig. 3.2).

In the adult CNS, microglia maintain tissue integrity through continuous interactions with neurons mediated by homeostatic signaling pathways. Two major neuron-derived regulatory axes provide inhibitory input that restrains microglial activation and support their surveillant phenotype[57–59]. Neuronal fractalkine (CX3CL1) engages microglial chemokine receptor (CX3CR1) to limit inflammatory signaling, stabilize microglial-synaptic interactions and support neuronal survival[57,58]. This pathway also contributes to adult neurogenesis, influencing the integration and maintenance of newly generated neurons[60]. Complementing this system, neuronal CD200 binds microglial CD200R to suppress activation and prevent excessive cytokine release, which loss of CD200 leading to chronically activated microglia and sensitization to inflammatory stimuli[59,61,62]. Disruption of either inhibitory axis is observed across aging and neurodegenerative conditions, where reduced fractalkine or CD200 signaling correlated with heightened microglial reactivity and increased neuronal vulnerability[61,63,64]. Together, these pathways constitute core mechanisms through which neurons actively maintain microglial homeostasis and preserve a stable, non-injurious immune environment in the adult brain.

3.1.6 Microglial identity, heterogeneity, and markers

The identity of microglia is defined by a set of genes highly enriched in these cells, commonly referred to as “microglial markers”. These include *P2ry12*, *Tmem119*, *Cx3cr1*, and AIF1 (*Iba1*), among others[65]. The expression of any single marker is insufficient to definitively establish microglial identity, as these genes exhibit plastic expression in response to local CNS signals and environmental context[8]. Moreover, under pathological conditions, these markers can be downregulated or shared with BAMs (perivascular and meningeal macrophages)[8,66].

Single-cell RNA sequencing (scRNA-seq) has revealed substantial transcriptional heterogeneity among brain myeloid cells, primarily microglia, even in the naïve adult brain. While some diversity is observed during adult homeostasis, microglial heterogeneity is particularly prominent during early postnatal development, likely reflecting microglial adaptation to dynamic CNS environments[8,67]. In adult brains, scRNA-seq clusters are often positioned on a transcriptional continuum, rather than forming distinct, stable states, indicating that microglial states are highly plastic and context-dependent[68–70]. Upon detection of CNS injury or disease-associated signals (e.g., amyloid, α-synuclein, apoptotic cells, BBB disruption), microglia undergo morphological and functional transformation, transitioning

into activated states[71,72]. These include non-phagocytic reactive microglia (with thickened branches and increased MHC expression) and phagocytic microglia, which assume a rounded amoeboid morphology and express pro-inflammatory cytokines like IL-1β, TNF-α, and IL-6[47,73,74].

Transcriptomic studies have identified several distinct microglial subclusters with functional implications:

- **MG1:** Enriched in microglial signature genes such as *Crybb1*, *Cst3*, *P2ry12*, and *Pros1*[75].
- **MG2:** Characterized by immediate-early gene expression (*Jun, Fos, Egr1*) and increased NF-κBA, suggesting a transcriptionally responsive state[76–78].
- **MG3:** Displays upregulation of signaling inhibitors (*Bmp2k*) and transcriptional repressors (*Bhlhe41*, *Ncoa3*, *Notch2*) with potential anti-inflammatory roles[79,80].
- **PreMG**: A "premature" microglial cluster expressing genes related to interferon signaling (*Ifit1, Ifitm, Ifitx, Isg15, Usp18*), cytokines, and pan-macrophage markers like *Aif1*[81,82].

In addition to these, specialized or context-responsive clusters have been described:

- **Axon Tract-Associated Microglia (ATMs):** Defined by expression of *Lgals1*, *Apoc1*, *Spp1*, and *Ftl*, and associated with white matter regions[68].
- **Cytokine-Associated Microglia (CAMs):** Expressing *Ccl3*, *Il1b*, and *Cxcl8*, indicative of inflammatory activation[68,69,82].
- **Ex Vivo-Activated Microglia:** Characterized by heat shock and stress-response genes (*Hspa1a, Jun, Dnajb1*) likely induced during tissue processing[82,83].
- **Homeostatic Microglia:** Defined by *P2ry12, Cx3cr1* and *Pros1*, considered representative of microglia in steady-state conditions[84–86].
- **Perivascular Macrophages (PVMs):** A separate small cluster expressing *F13a1, Mrc1*, and *Lyve1*, distinct from microglia[82].

In vitro, primary microglia rapidly lose their homeostatic gene signature, while induced pluripotent stem cell (iPSC)-derived microglia often exhibits a hybrid phenotype resembling both microglia and peripheral macrophages[87,88]. Interestingly, while certain microglial

subtypes such as the ATM cluster are transient in early mouse development, the evidence suggests that humans retain MG with these transcriptional features into adulthood, particularly clusters enriched in *Apoe* and *Trem2*, both genes implicated in Alzheimer's disease[68,82].

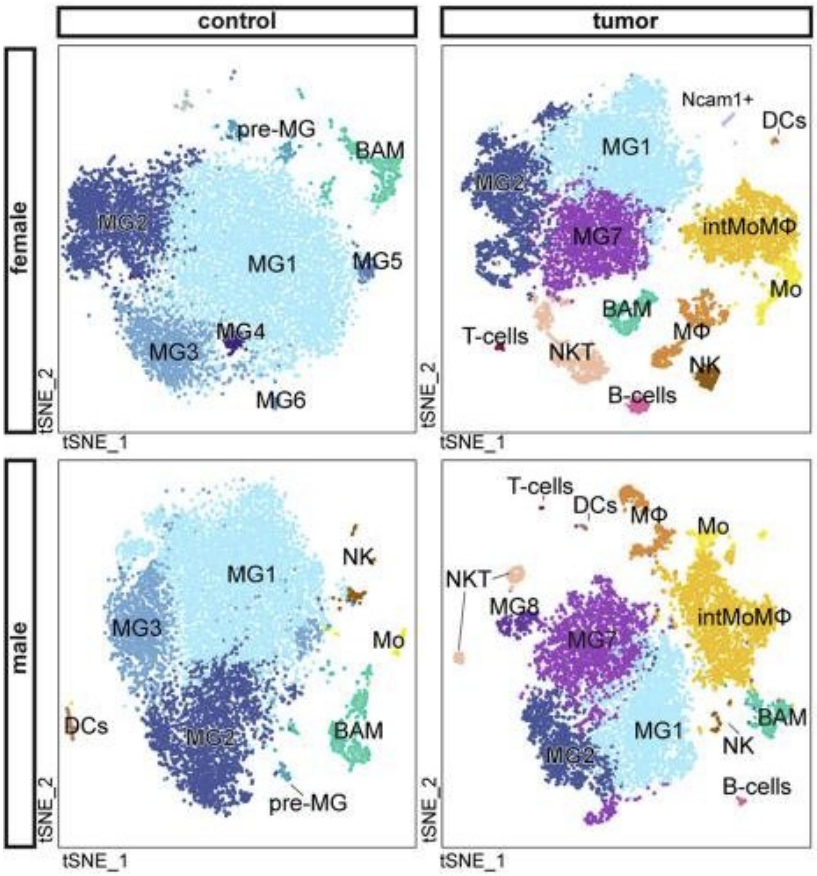

Figure 3.3 | Subpopulations of microglia and myeloid cells identified after clustering of scRNA-seq data from CD11b+ sorted cells from brains of naïve mice or tumor-bearing hemispheres. Figure from Ochocka, N. et al. Single-cell RNA sequencing reveals functional heterogeneity of glioma-associated brain macrophages. Nat. Commun. 12, 1151 (2021)[67], used under CC BY 4.0 license (http://creativecommons.org/licenses/by/4.0/).

3.2 Microglia depletion and repopulation processes

3.2.1 CSF1R inhibitors and their effects on microglia

Microglia are unique among brain cells in that they are not continuously replenished by circulating myeloid progenitors. Instead, they maintain their population primarily through self-renewal via cell division[7,89]. A key regulator of microglial survival, proliferation,

and differentiation is the colony-stimulating factor 1 receptor (CSF1R), a transmembrane tyrosine kinase receptor predominantly expressed in microglia within the CNS[14,90]. CSF1R mediates signaling from two known ligands: colony-stimulating factor 1 (CSF1), also known as macrophage colony-stimulating factor (M-CSF), and interleukin-34 (*Il-34*)[91]. These ligands act as hematopoietic growth factors that regulate macrophage and microglial development and homeostasis[92]. Importantly, CSF1R expression is largely restricted to cells of the mononuclear phagocyte lineage, including microglia and macrophages, as confirmed by *in situ* hybridization studies[93,94]. The signaling axis involving CSF1/IL-34 and CSF1R is not only critical during early development, but remains essential throughout life[95].

Pharmacological or genetic inhibition of CSF1R has been instrumental in creating models for microglial depletion, allowing to study microglial function in health and disease. Administration of CSF1R inhibitors in adult mice has been shown to result in the elimination of approximately 99% of microglia across the brain, highlighting the absolute dependency of adult microglia on CSF1R signaling for survival[95]. Remarkably, despite near-complete ablation of microglia, mice typically show no overt behavioral or cognitive impairments under baseline conditions, suggesting a degree of CNS plasticity or compensation in the short term. Following the cessation of CSF1R inhibitor treatment, the brain undergoes rapid and robust microglia repopulation. This process typically occurs within one week and is driven by nestin-positive progenitor-like cells residing in the CNS, which proliferate and differentiate into new microglia[14]. These findings demonstrate not only the resilience of the microglial compartment but also the regenerative potential of the CNS microglial niche.

The development of CSF1R-targeting compounds has been pivotal for advancing our understanding of microglial biology and has clinical relevance for disorders where microglial overactivation contributes to pathology, such as Alzheimer's disease, multiple sclerosis, and brain tumors. However, the long-term consequences of sustained microglial depletion or repopulation, particularly in the aging brain or in disease contexts, remain areas of active investigation.

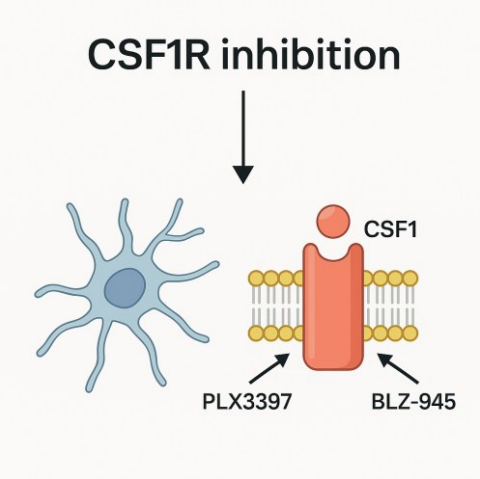

Figure 3.4 | A scheme representing a CSF1R receptor inhibition in microglia. The illustration depicts the mechanism of colony-stimulating factor 1 receptor (CSF1R) blockade in microglial cells.

3.2.2 Microglial depletion and repopulation

Under physiological conditions, microglia maintain region-specific densities through slow but consistent self-renewal, independent of peripheral hematopoietic sources[6]. However, recent advances in microglial depletion models have allowed to interrogate the essential roles of microglia in maintaining CNS homeostasis, as well as in pathological states such as neuroinflammation, injury, and neurodegeneration[13,49]. Pharmacological depletion of microglia is most commonly achieved through administration of CSF1R inhibitors, such as PLX3397 or BLZ-945, which cross the BBB and target microglial survival signaling pathways[95,96]. These compounds have been shown to induce rapid and near-complete ablation of resident microglia when administered over the course of several days to weeks. For instance, 7-day administration of BLZ945 in Cx3cr1^GFP/+ mice led to a profound depletion of microglia in the white matter[96].

The mechanism of depletion involves apoptotic cell death, rather than mere inhibition of proliferation. This has been evidenced by the upregulation of active caspase-3, a marker of apoptosis, in *Iba1*+ cells following CSF1R inhibition. Additionally, significant reduction in the expression of key microglial marker genes, including *Iba1* (AIF1, Allograft inflammatory factor 1), Cx*3cr1*, *Fcgr1*, *Itgam*, *Trem2*, Cd68, Cd86, MHC II (*H2-Eb1*), and CD45 (*Ptprc*) further confirm the depletion of the microglial population[87,95]. Importantly, this loss of microglia is not associated with an overt inflammatory response in other CNS cells, indicating a non-disruptive depletion protocol. Following inhibitor withdrawal, microglial repopulation occurs rapidly and robustly, with Iba1+ cells reappearing in the brain within

3 days[95]. These early repopulating cells exhibit a unique morphology: they are larger, possess short, stubby processes, and express markers such as *Ib4*, *Cd45*, *Nestin*, and *Mki67*, indicating a proliferative and potentially progenitor-like state. By 7 days after inhibitor withdrawal, the microglial population exceeds that of control brains and assumes more intermediate morphologies. By 14 days, the repopulating cells become morphologically indistinguishable from homeostatic ramified microglia and stabilize in number[95,97].

The initial repopulating phase is accompanied by elevated expression of cell cycle-related genes, including *Mki67, Ube2c, Ccna2, Prr11*, and *Top2a*, consistent with a strong proliferative response. Chemokines such as *Ccl2*, *Ccl3*, and *Ccl5* also surge at this stage, acting as signals to orchestrate the replenishment of the depleted niche[95,98,99]. The kinetics of repopulation s remarkable: within 72 hours, the brain can contain ~14,000 microglial cells per section, up from ~600 cells per section immediately following depletion[95]. While some studies suggest that residual surviving microglia could contribute to repopulation through rapid division (requiring a doubling time of ~5–6 hours), the presence of Nestin+ cells early in repopulation supports the idea that a progenitor-like population may also contribute to this process[49,54].

Microglia depletion models have revealed important insights into the essential, yet context-dependent, functions of microglia. In the healthy adult mouse brain, long-term depletion using CSF1R inhibitors (CSF1Ri) does not lead to obvious behavioral, cognitive, or pathological abnormalities, indicating that under homeostatic conditions, microglia may not be strictly required for routine neural function[49]. However, microglia are known to play critical roles during development, including synaptic pruning, regulation of neurogenesis, and removal of apoptotic cells, highlighting the importance of temporal context when interpreting depletion studies[14,37]. The timing and context of microglia depletion relative to disease progression are crucial factors influencing outcomes. For instance, CSF1Ri-induced microglia elimination following neuronal injury or during neurodegenerative disease progression has been shown to be neuroprotective, improving cognitive function and reducing inflammation in mouse models of AD and acute injury[14,37,100].

However, early elimination of microglia during the acute phase of injury may exacerbate damage, underscoring the biphasic and dynamic nature of microglial involvement in CNS pathology. Importantly, microglia repopulation itself is beneficial in certain contexts. For example, when microglia repopulation occurs after injury, it can enhance functional recovery, suggesting that newly generated microglia may adopt a more homeostatic or reparative phenotype. These findings are not limited to rodents. CSF1R inhibitors have been

shown to effectively deplete microglia in non-human primates and humans, with similar patterns of robust repopulation following inhibitor treatment cessation[95,101]. This translational relevance positions CSF1R inhibitors as promising tools in future therapeutic strategies aimed at resetting microglial populations in the context of chronic neuroinflammation or neurodegenerative disease.

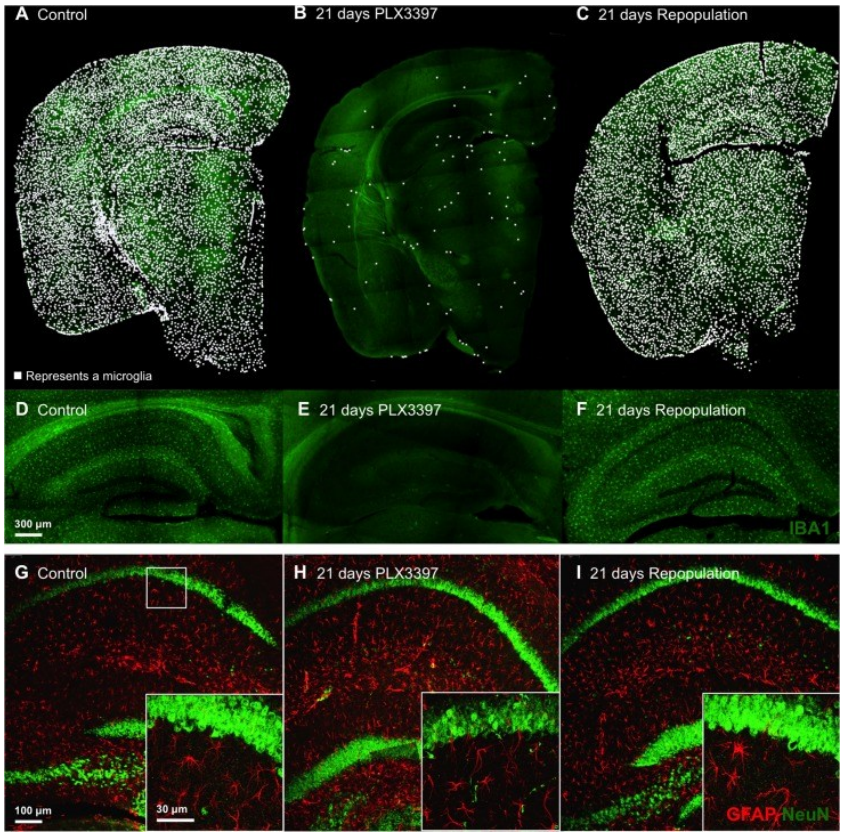

Figure 3.5 | CX3CR1-GFP positive microglia in under control conditions, after depletion and repopulation. The upper panel shows CX3CR1-GFP+ MG under various conditions in the hemispheres (A–C) or hippocampi (D–F). The density of MG is fully restored without significant changes in GFAP and NeuN reactivity (G–I). Figure from Elmore et al, Plos One 2015[102], used under CC BY 4.0 license (http://creativecommons.org/licenses/by/4.0/).

3.2.3 Origin of repopulated microglia

The origin of microglial repopulation following CSF1R inhibitor (CSF1Ri)-induced depletion has been a subject of considerable investigation. Fate-mapping and parabiosis experiments have now conclusively demonstrated that repopulated microglia arise exclusively from the proliferation of a small population of residual microglia, rather than from infiltration of peripheral myeloid cells or local progenitor-like cells[101]. Despite early observations

of transient nestin expression in newly forming microglia, careful lineage tracing confirmed that nestin-positive, non-microglial cells do not contribute to the new microglial pool. These findings exclude the participation of local CNS stem or progenitor cells in microglia repopulation, despite temporary expression of stemness-associated markers. Additionally, no evidence of contribution from blood-derived monocytes or macrophages has been found, further emphasizing that microglia form an autonomous, self-renewing population under both homeostatic and post-depletion conditions[5,53].

During early development, microglia arise from uncommitted c-Kit+ progenitor cells in the yolk sac, which differentiate into CD45+/c-Kit−/CX3CR1+ cells that migrate into the developing CNS prior to the closure of the BBB[103]. Once the BBB is established, the CNS becomes impermeable to peripheral immune cell infiltration under non-pathological conditions, reinforcing the notion of microglial independence from systemic myeloid lineages. Genetic studies have shown that the developmental program of microglia is regulated by key transcription factors such as *Pu1* and *Irf8*, as well as CSF1R signaling, all of which are critical for establishing and maintaining the resident microglial population[4]. Using tdTomato-labeled fate-mapping systems, it was demonstrated that all tdTomato+ repopulated cells also expressed Iba1 (ionized calcium-binding adapter molecule 1), confirming that repopulated microglia maintain their lineage identity throughout the repopulation process[101].

These surviving microglia undergo a process of partial dedifferentiation, temporarily downregulating key microglial markers, and then re-differentiating into fully functional homeostatic microglia once CSF1R signaling is restored[95,104,105]. Crucially, no evidence supports the idea that these cells transdifferentiate into other lineages or arise from dedifferentiated progenitors. While some proliferating non-microglial cells may appear during the early repopulation phase, comprehensive analyses confirmed that they do not contribute to the regenerating microglial population, highlighting the highly lineage-restricted nature of microglial self-renewal in the adult CNS[95,101,106]. The evidence indicates that repopulated microglia derive exclusively from the proliferation of residual microglia following CSF1Ri-induced depletion. This finding underscores the remarkable plasticity, resilience, and self-renewal capacity of the resident microglial population, and rules out the existence of a latent, multipotent microglial progenitor pool in the adult brain[95,98,99].

3.2.4 Characteristics of morphology of repopulated microglia

Microglia are among the most morphologically dynamic and functionally adaptable cells in the brain. They constantly survey their environment by extending and retracting thin cytoplasmic extensions, forming transient contacts with synapses, and releasing regulatory molecules that influence neuronal function[107]. Their morphology is tightly coupled to functional state, with transitions reflecting shifts in activation, surveillance, or phagocytic roles[12]. Following CSF1R inhibitor (CSF1Ri)-induced depletion and withdrawal, repopulated microglia exhibit distinct morphological characteristics during preliminary stages of re-establishment[95,99,105]. Initially, these cells display larger cell bodies and reduced process complexity, with short, stubby, and less branched extensions, compared to the highly ramified morphology seen in homeostatic microglia[95]. These changes resemble a reactive or transitional phenotype and gradually resolve over time, as the microglia mature and regain features of the surveillant, ramified state in which they. actively participate in immune surveillance, synaptic pruning, neurogenesis, and homeostasis[8]. Conversely, "activated" microglia, typically observed in pathological contexts, exhibit a more amoeboid morphology, rounded cell bodies with fewer and shorter processes, which is commonly associated with heightened inflammatory responses and increased phagocytic activity[5,8,108].

Another functionally significant morphology is that of "amoeboid" microglia, historically considered to be highly phagocytic[109]. Yet, recent findings have revealed that even ramified microglia can perform phagocytosis, particularly through specialized "en passant" or terminal branches, such as during adult neurogenesis[110]. Interestingly, in certain disease states like epilepsy, amoeboid microglia may exhibit reduced phagocytic capacity, further decoupling morphology from function[111,112]. Additional morphologies, such as "rod-shaped" microglia, characterized by elongated cell bodies and polarized processes, have been reported to increase in prevalence with aging, suggesting another form of functional adaptation[42,95,113].

In the context of microglia repopulation, the early morphological profile suggests a transient reactive state, linked to the high proliferative and migratory demands during recolonization of the CNS[95,105]. However, over time (by ~14 days post-inhibitor withdrawal), repopulated microglia gradually regain typical ramified morphologies, with branching complexity and cell size comparable to those of untreated controls[95]. These findings emphasize that microglial morphology reflects, but does not solely define, their functional state. The increasing complexity of microglial classification revealed by scRNA-seq has introduced numerous subtypes and acronyms[8,114]. Yet, without consistent nomenclature and rigorous

functional validation, these classifications may hinder rather than clarify our understanding of microglial biology[8].

3.2.5 Functional profile and transcriptomic identity of repopulated microglia

Repopulated microglia closely resemble their resident counterparts in both morphology and functional gene expression, although transient differences emerge during the preliminary stages of re-establishment. One key molecular mechanism influenced by tissue damage involves activation of P2Y12 receptor (encoded by *P2ry12*), a purinergic receptor highly expressed in homeostatic microglia[115]. Upregulation of *P2ry12* by tissue damage signals enhances the activity of the tonically active potassium channel THIK-1, leading to a reduction in microglial process complexity (i.e., decreased ramification) and activation of inflammasome pathways[116,117]. This inflammasome activity facilitates the maturation of pro-inflammatory cytokines such as IL-1β, implicating *P2ry12* signaling in microglial reactivity and inflammatory readiness[8,117]. Despite undergoing significant morphological and proliferative changes, repopulated microglia maintain functional integrity and responsiveness[95,101]. When challenged with LPS, a potent inducer of innate immune responses, repopulated microglia exhibited inflammatory gene expression profiles similar to control (non-depleted) microglia, indicating that their immune competence is preserved post-repopulation[82,101].

RNA-seq analyses revealed that repopulated microglia initially display a distinct transcriptomic identity compared to resident microglia. For instance, cell cycle–related genes such as *Mki67* and *Cdk1*, and migration-associated genes like *Cd36*, are significantly upregulated during the early phases of repopulation, reflecting the intense proliferative and migratory activity required to repopulate the brain[98,101]. Importantly, during CSF1R inhibitor-induced depletion, classic microglial genes such as *Aif1*, *Tmem119*, *Trem2*, and *Cx3cr1* are significantly downregulated, affirming the effective removal of microglia[95,101]. Notably, this depletion is not accompanied by an upregulation of inflammatory genes, suggesting that microglial loss does not provoke a cytokine storm or pathological inflammation within the CNS environment[73]. Over time, the transcriptomic differences between repopulated and resident microglia diminish. By day 60 post-repopulation, only three genes remain differentially expressed compared to baseline controls, highlighting a remarkable convergence toward the native microglial gene signature and suggesting functional equivalence under homeostatic conditions[73].

3.2.6 Inflammatory responsiveness and heterogeneity of repopulated microglia

Although repopulated microglia achieve homeostatic gene expression and morphology over time, their ability to respond to acute neuroinflammatory stimuli is a critical measure of their functional equivalence to resident MG. Acute systemic inflammation, such as that induced by LPS, is known to drive robust microglial activation and production of interleukin-1β (IL-1β), among other pro-inflammatory mediators like *Tnf*, *Il-6*, and nitric oxide (NO)[8,118,119]. These responses contribute to microglia-mediated neurotoxicity and are shaped by factors including disease stage, local microenvironment, and genetic background.

To test the inflammatory competence of repopulated MG, LPS (1 mg/kg, i.p.) was administered to mice with either resident or repopulated microglia. Transcriptomic profiling revealed a comparable inflammatory gene expression response in both groups. Specifically, the LPS challenge upregulated 455 genes and downregulated 34 genes in the brains of mice with resident microglia. The LPS-induced transcriptional response in mice with repopulated microglia was nearly identical, with no significant differences between the two groups[51,101,118]. These findings suggest that repopulated MG retain a fully functional capacity to respond to systemic inflammatory stimuli, including upregulation of key cytokines and immune-related pathways[97,104,120].

Despite their acute functional competence, the ability of repopulated microglia to fully re-establish a spectrum of microglial heterogeneity (a key feature of microglial specialization) is influenced by age[121,122].

3.3 Future directions for studying microglial roles in health and disease

Future research on microglial roles in health and disease should focus on several key directions. First, advanced single-cell and spatial transcriptomic technologies could be used to map microglial heterogeneity and dynamics across development, aging, and diverse pathological contexts. Second, longitudinal *in vivo* imaging and novel lineage tracing tools could clarify how microglia transition between functional states during disease progression or recovery. Third, there is a need for improved models that more closely mimic human microglial biology, such as human iPSC-derived microglia and organoid co-cultures, to better understand species-specific mechanisms. Finally, investigating the interactions between

microglia and other CNS cell types, the peripheral immune system, and the gut–brain axis may reveal novel therapeutic targets for neuroinflammatory and neurodegenerative disorders.

3.4 Overview of applied methodologies

3.4.1 Low throughput technologies

Low-throughput sequencing technologies refer to methods for sequencing genetic material that produce relatively insignificant amounts of data per run. These methods often provide lower parallelization but can offer higher accuracy, longer read lengths, or a targeted focus. They are particularly useful when sample availability is limited or when only a small number of genes need to be analyzed. Low-throughput sequencing is primarily used in clinical diagnostics, particularly for identifying rare mutations associated with diseases or for preparing small genetic panels. Additionally, these technologies are beneficial for educational and training purposes, forensic analysis, microbial strain typing, and pharmacogenomics. Their advantages include high accuracy of sequenced data and well-established protocols and software. In small projects, using low-throughput sequencing can help save both costs and time associated with data analysis[123]. Several methods, which are classified as low-throughput sequencing, with the most popular being:

1. Sanger Sequencing: Developed by Frederick Sanger in 1970, this first-generation method is considered the gold standard for DNA sequencing. It typically generates reads of approximately 500-1,000 base pairs (bp). This technique is primarily used for small-scale gene sequencing, validating variants such as single nucleotide polymorphism (SNPs) or mutations, verifying clones, and clinical diagnostics. Although it is highly accurate and straightforward to interpret, Sanger sequencing is not suitable for large-scale genome sequencing due to its limited scalability and high costs[124].

2. Amplicon Sequencing (Targeted): This methodology focuses on sequencing specific regions of DNA, such as particular genes or loci. It is commonly used to analyze genetic variability in selected genes or regions of interest. The output varies depending on the sequencing platform used, ranging from 100-300 bp for next-generation

sequencing (NGS) and about 700 bp for Sanger technology. Amplicon sequencing targets variant detection, microbial profiling, plant breeding, CRISPR screenings, and cancer mutation analysis. It offers high sensitivity and is cost-effective for small targets; however, its genomic scope is limited, and it can be affected by large polymerase chain reaction (PCR) biases and amplification errors[125].

3. Pyrosequencing: This method provides real-time detection of nucleotide incorporation through light emission. It is often used to sequence specific targeted regions, typically generating noticeably short reads of about 100 bp. Pyrosequencing is utilized for SNP genotyping, methylation analysis, and short amplicon sequencing. While it is effective for SNP detection, its short reads and lower throughput, along with reduced accuracy for complex genomes, can pose challenges for its use[126].

4. Oxford Nanopore MinION: This portable and flexible technology is suitable for low-throughput applications, being used for small genome sequencing, pathogen surveillance, and fieldwork. It excels at long-read sequencing; however, it has lower accuracy and a higher error rate compared to other sequencing technologies[127].

3.4.2 High-throughput sequencing technologies

High-throughput sequencing technologies, commonly known as NGS, enable the simultaneous sequencing of millions to billions of DNA fragments in parallel. These platforms are designed for large-scale genomic studies, offering substantial data output, scalability, and a lower cost per base compared to traditional methods like Sanger sequencing. NGS is widely used for whole-genome sequencing (WGS), variant calling, and the detection of genetic populations.

In transcriptomics, NGS is utilized in RNA-seq and scRNA-seq. In epigenomics, it is applied in methylation sequencing (Methyl-seq), Assay for Transposase-Accessible Chromatin using sequencing (ATAC-seq), and chromatin immunoprecipitation sequencing (ChIP-seq), among others. Additionally, NGS is employed in clinical diagnostics, including cancer panels and rare disease detection, as well as in metagenomics for microbiome profiling[123]. Below are some prominent high-throughput sequencing technologies:

1. Illumina Sequencing: This method is performed on various platforms such as HiSeq, NovaSeq, NextSeq, and MiSeq. Sequencing is done via synthesis, producing short reads (75-300 bp). The data output can reach up to 6 TB per run on the NovaSeq platform. It is used for WGS, whole-exome sequencing (WES), RNA-seq, scRNA-seq, ChIP-seq, and ATAC-seq. Illumina sequencing is known for its high accuracy and extremely high throughput, with a well-established ecosystem. However, the short read length limits structural variant resolution, and substantial infrastructure is required[128].

2. BGI/MGI Sequencing (DNBSEQ): This is conducted on MGISEQ and DNBSEQ platforms, and it sequences DNA nanoballs. The read length is similar to Illumina (75-300 bp), with data output comparable to the NovaSeq, reaching up to 5 TB per run. It is applied to WGS, WES, RNA-seq, scRNA-seq, ChIP-seq, ATAC-seq, and some low-cost applications. This method offers high throughput and lower costs compared to other technologies, and it is faster as well. Nevertheless, it is primarily established in Asia, leading to limited knowledge and support outside that region. Additionally, it requires proprietary reagents and systems[129].

3. PacBio SMRT Sequencing: This technology is performed on the Sequel IIe and Revio platforms and utilizes Single Molecule Real-Time (SMRT) technology. Read lengths range from 10–50 kb, with potential lengths exceeding 100 kb. Each run consumes up to 360 GB of data. It is useful for de novo genome assembly, Iso-Seq (full-length transcriptomics), structural variation analysis, and epigenetics. Some advantages include long reads with high accuracy (HiFi reads), making it ideal for complex genomes. However, it has a higher cost per Gb compared to Illumina and lower throughput for short-read applications[130].

4. Oxford Nanopore Technologies (ONT): This method is performed on platforms like PromethION, GridION, and MinION, utilizing nanopore sequencing. Read lengths are ultra-long, ranging from 10 kb to over 1 Mb, with output reaching up to 290 Gb per flow cell on PromethION. ONT is applied in real-time genome surveillance, structural variation analysis, metagenomics, and transcriptomics. Its key benefits include real-time sequencing capabilities, portable platforms, and the elimination of the need

for PCR/amplification. However, it does come with a higher error rate (though this improves with Q20+ chemistry) and necessitates robust error correction mechanisms[131].

3.4.3 Introduction to single-cell RNA-seq technology

Single-cell RNA sequencing (scRNA-seq) measures the gene expression of the entire transcriptome in individual cells, providing a detailed view of how cells function and interact within complex tissues. By tracing individual transcripts back to their cells of origin, it helps to identify unique gene expression profiles in highly heterogeneous samples. This approach reveals rare cell types and dynamic cell states that other methods often overlook. Advancements in scRNA-seq enable the integration of comprehensive information about various molecular states, the inference of functional phenotypes, and the deduction of potential relationships between individual cells.

Single-cell technologies, multi-omics, and integrative analyses of gene and protein expression not only help identify cells but also offer new insights into the molecular mechanisms that shape and regulate specific cell states in different contexts. Improvements in computational tools and techniques that facilitate the alignment and integration of single-cell datasets are crucial for addressing these challenges. They provide a powerful means to discern similarities in microglial states across various contexts. However, a practical limitation of defining functional states solely based on their transcriptional signatures is that mRNA expression may not directly predict protein levels. Importantly, mRNA or protein expression alone does not necessarily predict microglial function, although they can be used to formulate functional hypotheses that require experimental validation. Numerous methods exist for classifying microglia based on their constituent states, including gene expression, protein expression, post-translational modifications, mRNA profiling, morphology, and ultrastructure. Each of these approaches can vary in coverage, such as single-cell versus whole-transcriptome profiling, contributing to confusion and mislabeling in the field. Single-cell sequencing technology can reveal cell heterogeneity and provide unprecedented insight into cell functions, interactions, and disease mechanisms.

scRNA-seq provides high-resolution insights into the heterogeneity of microglia populations, enabling precise detection of gene expression at the level of individual cells. This approach is particularly valuable in distinguishing transcriptionally distinct microglia subtypes, identifying rare activation states, and uncovering low-abundance transcripts that are frequently undetectable using conventional bulk RNA sequencing methods. In the context

of the study, scRNA-seq allowed the systematic annotation of microglia clusters based on both canonical and novel marker genes, facilitating the refinement of subtype definitions and the exclusion of irrelevant or contaminating populations.

The ability to quantify tens of thousands of genes across thousands of single cells in parallel yields comprehensive datasets that capture the diversity of transcriptional states within the microglia compartment. This capability supports large-scale comparative analyses, reconstruction of lineage trajectories, and detection of subtle changes in cluster composition under different experimental conditions. Such high-resolution data are essential for dissecting complex processes, including microglial activation, proliferation, and transitions between homeostatic and reactive states.

However, the implementation of scRNA-seq is not without limitations. The technique involves higher costs and longer processing times compared to bulk RNA sequencing, alongside substantial demands for computational power and bioinformatics expertise. The requirement to dissociate brain tissue into single-cell suspensions can alter transcriptomic profiles and introduce technical artifacts. Furthermore, dropout effects, where transcripts present in a cell are not detected, pose challenges for quantitative analysis, particularly for genes expressed at low levels. While scRNA-seq provides unparalleled granularity, the sequencing depth per gene is lower than in bulk RNA-seq, potentially reducing sensitivity for detecting uniformly low-abundance transcripts.

Overall, scRNA-seq is a powerful and versatile approach for investigating microglia heterogeneity, offering detailed mapping of transcriptional states and discovery of previously unrecognized subtypes. Nonetheless, careful experimental design, the use of appropriate controls, and complementary validation methods are necessary to mitigate its technical constraints and ensure robust interpretation of results.

3.4.4 Applications of single-cell RNA-seq

scRNA-seq enables to understand the diverse cell populations within tumors, helping to identify sub-clonal structures that may drive disease progression and therapeutic resistance. By analyzing changes in gene expression over time, tumor evolution can be tracked, providing insights into metastatic behavior and treatment responses. This technology also facilitates real-time monitoring of gene expression dynamics as stem cells differentiate into various lineages, capturing the regulatory networks involved in development. scRNA-seq allows identifying key

transcription factors and signaling pathways that regulate stem cell fate decisions, thereby advancing stem cell therapy.

Furthermore, scRNA-seq can be used to examine the complex cellular composition of the nervous system, exploring the unique transcriptional profiles of different neuron types and supporting glial cells. This approach reveals temporal changes in gene expression that occur during neural differentiation and development, providing valuable insights into developmental neurobiology. It can also shed light on the molecular mechanisms underlying various neurological disorders by identifying disrupted gene expression patterns within affected cell types. scRNA-seq can analyze gene expression patterns that dictate cell fate decisions during embryonic development and tissue morphogenesis. This offers insights into normal developmental processes and congenital disorders.

By studying gene expression in affected cells, potential causal genes and pathways implicated in developmental disorders can be identified, contributing to improved diagnostics and therapies. Additionally, scRNA-seq allows for detailed profiling of immune cell populations, enabling the study of their roles in health and disease. It helps to investigate how immune cells respond at the single-cell level during infections and inflammatory processes, leading to a deeper understanding of autoimmune conditions and potential therapeutic interventions.

10x Genomics platforms combine microfluidic technology with droplet packaging for high-throughput sequencing of single cells. Their technology encapsulates single cells and reaction reagents in nanoscale droplets, enabling high-throughput and high-precision single-cell analysis through the Gel Beads-in-Emulsion (GEM) structure. By allowing for in-depth exploration of cellular processes, molecular interactions, and disease pathways, the platform has established new standards in genomic research. Using advanced microfluidic systems and precision droplet formation, their Chromium technology allows for the comprehensive examination of large numbers of distinct cells simultaneously.

3.4.5 Droplet based single-cell RNA-seq system

The employ a microfluidic system based on a water-in-oil emulsion to mix single cells with primers, enzymes, and reverse transcription reagents, resulting in the formation of GEMs. Each GEM comprises a single cell along with its transcriptome or genomic information. A GEM acts as a drop-like microreactor that contains a Gel Bead and a water-in-oil emulsion. The surface of the bead is coated with various barcodes: a coded barcode (10x barcode),

a molecular barcode, and reverse transcription (RT) primers for subsequent decoding and quantification of transcripts. The beads within each GEM carry unique molecular barcodes that distinguish sequencing data from different cells. These barcodes bind to unique identifiers, ensuring the exclusivity of each transcript. The recent Chromium platform can simultaneously process thousands to tens of thousands of single cells, with each chip capable of capturing up to 80,000 cells, significantly enhancing the efficiency of single-cell sequencing[132].

ScRNA-seq using the 10x Genomics Chromium system enables the high-throughput characterization of transcriptomes at single-cell resolution. The workflow consists of sequential steps encompassing sample preparation, single-cell encapsulation and barcoding, library construction, sequencing, and bioinformatics analysis, each of which contributes to the generation of accurate and robust gene expression data.

Tissue is dissociated into a single-cell suspension, filtered and assessed for viability (target >80%). Cell concentration is adjusted to the recommended range (700–1200 cells/μL).

Cells are then encapsulated with barcoded gel beads into droplets (GEMs) using the 10x Genomics Chromium system. Inside each GEM, cells are lysed and mRNA molecules are captured by barcoded oligos, assigning each transcript a unique cell barcode and Unique Molecular Identifier (UMI). Reverse transcription produce barcoded cDNA, which is pooled and amplified by PCR.

Amplified cDNA is fragmented, end-repaired, and adaptor-ligated and quality-checked before sequencing on Illumina platforms (e.g., NextSeq or NovaSeq). Sequencing data are processed with Cell Ranger for alignment and generation of a gene expression matrix. Downstream analysis (Seurat/Scanpy) induced dimensionality reduction, clustering, and annotation based on reference datasets, followed by differential expression analysis. This workflow enables high-resolution characterization of cellular heterogeneity, though it is sensitive to dissociation artifacts and transcript dropout[132]. Cell hashing employs barcoded antibodies (often targeting universal cell surface proteins like CD45) conjugated to oligonucleotides. Each sample is labeled with a unique hashtag oligonucleotide (HTO) prior to pooling. After sequencing, the HTOs are used to demultiplex the pooled data back to individual samples. Genetic polymorphisms specific to samples can act as fingerprints, allowing cells to be assigned to their origin after sequencing. This workflow facilitates the detection of multiplets from two different or more individuals, leading to a decrease in non-identifiable multiplets that directly correlate with the number of multiplexed samples.

By using a defined set of oligo-tagged antibodies against common surface proteins, samples from different experiments can be uniquely labeled. This enables pooling samples together,

using the barcoded antibody signal for reliable demultiplexing. The technology is called Cellular Indexing of Transcriptomes and Epitopes by Sequencing (CITE-seq). Cell hashing supports robust sample multiplexing, accurate multiplets identification, and the differentiation of low-quality cells from ambient RNA, resulting in substantial cost reductions. This approach allows CITE-seq and cell hashing to be conducted simultaneously, while generating separate sequencing libraries. This means that HTOs, antibody-dependent tags (ADTs), and scRNA-seq libraries can be independently amplified and pooled.

The background signal for each HTO as a negative binomial distribution, estimating background cells based on initial k-medoids clustering of all HTO reads. Barcodes with HTO signals above the 99th percentile of this distribution are classified as "positive", while those positive for multiple HTOs were classified as multiplets. Profiling diverse environmental and genetic perturbations simultaneously enhances experimental workflows, such as optimizing antibody concentrations for CITE-seq experiments. In flow cytometry, antibodies are usually tested individually over a wide dilution series to establish signal-to-noise ratios and locate optimal concentrations[133].

The methodology improves several aspects of technological application, such as significantly reducing sequencing costs by enabling multiple samples to be analyzed in a single run, minimizing technical variation as samples are processed together, improving the identification and removal of doublets (cells from two or more individuals captured in the same droplet), and processing more samples without a proportional increase in experimental workload, which shows up better results compared to other sequencing methods. Compared with alternative multiplexing approaches, such as genetic barcoding or lipid-tagged oligonucleotide labeling, HTO-based hashing offers several advantages. Unlike genetic barcoding, which requires prior engineering of the cells, hashing can be readily applied to primary tissues without the need for genetic manipulation. In contrast to lipid-tagged oligos, which may introduce variability in labeling efficiency, HTO-based methods rely on well-established antibody–epitope interactions, ensuring stable and reproducible labeling across diverse cell types. These characteristics make HTO hashing particularly suitable for studies of primary microglia, where genetic modification or extensive *in vitro* manipulation is not feasible.

However, cell hashing also has some limitations that hinder its application, such as poor antibody staining can lead to ambiguous assignments or unidentified "negative" cells (no hashtag detected). While HTOs can help identify inter-sample doublets, detecting intra-sample doublets remains challenging. Hashtag signals may spill over due to ambient RNA

or insufficient washing, resulting in misclassification. Demultiplexing and quality control require careful normalization and statistical modeling (using tools like Seurat, Demuxlet, or HTODemux). The number of distinct HTOs is finite (typically between 4 and 12), which limits the number of samples that can be multiplexed. Newer methods, such as MULTI-seq and cell hashing with lipid-tagged indices, continue to enhance and expand the capabilities of cell hashing techniques.

4. Aims of the study

Microglia have a unique capacity among CNS-resident cells to self-renew and are capable of repopulating the CNS after depletion restoring their density within a few days. Yet, it remains unclear whether repopulated microglia fully regain the functional heterogeneity and homeostatic states of their counterparts, and how this process is shaped by aging.

The central goal of this study was to understand the origin and functionality of microglia repopulating the brain after pharmacological depletion, with particular attention to how this process differs between young and aged mice.

To address these questions, our study was designed with the following aims:

1. The analysis of heterogeneity of repopulated microglia in young mice with scRNA-seq.
2. A comprehensive characterization of repopulated microglia at the transcriptional and functional level.
3. Defining the origin of repopulated microglia.
4. Comparison of repopulated microglia at the transcriptional and functional level in young and old mice using scRNA-seq data.
5. Characterization of repopulated microglia at the transcriptional and functional level in old mice using bulk RNA seq data.
6. Comparison of activated microglia in various pathologies and in public datasets.

These aims were designed to build a unified framework for understanding microglial plasticity. At its core, the study asks whether repopulated microglia can truly restore heterogeneity and homeostasis, how aging alters this capacity, and whether the activation programs of repopulated cells overlap with those driving pathological states such as glioma or neurological disorders.

5. Materials and methods

5.1 Mouse microglia depletion/repopulation experiment

To investigate the dynamics of microglial repopulation following depletion, we employed a well-established mouse model of targeted CD11b^{+} cell depletion with oral administration of CSF1R inhibitor (BLZ495). Using Tmem119 staining we confirmed efficient depletion (>90%) of resident microglia and minor populations of myeloid cells. Upon withdrawal of the CSF1R inhibitor for 7 days, numbers of microglia in all tested structures were restored. All experimental procedures involving animals were approved by the First Local Ethics Committee for Animal Experimentation in Warsaw (836/2019; 1364P1/2022). Young (3 months old), aging (12 months old) or aged (18–22 months old) female and male GFP-M: Cx3cr1-CreERT2fl/fl: Rosao 26-tdTomatotg/tg mice were housed at the Nencki Institute, Poland. The animals were kept in individually ventilated cages, with free access to food and water, at a temperature of 21–23 °C, and 50–60% humidity, under a 12 h/12 h day and night cycle. The animals were habituated for 3–4 days by being placed individually in a cage for 3 h, where a small amount (~ 100 µL) of the peanut butter (PB) was provided. The mice were fed with BLZ-945 (MedChemExpress, HY-12768) at a dose of 200 mg/kg b.w. daily in 100 µL PB (Peanut butter, GoOn, Santé); the controls received PB. BLZ-945 was delivered for 14 or 21 days to establish the kinetics of depletion; repopulation was studied 7 days after cessation of the treatment. The studies were performed by Dr. Maria Banqueri Lopez Ph.D. and Dr. Anna Kiryk Ph.D. for the ERANET MicrosynDep project.

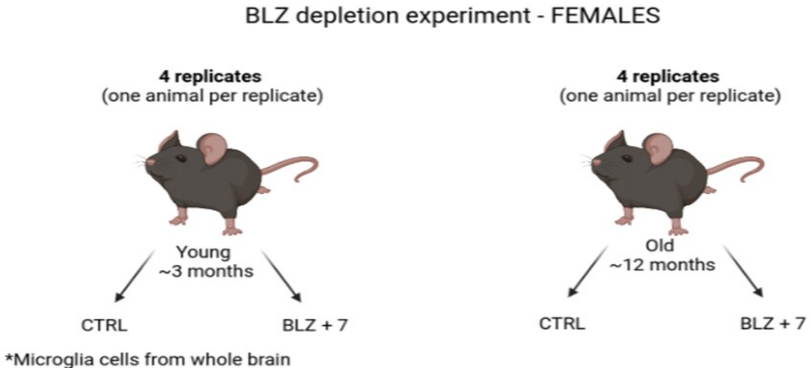

Figure 5.1 | Experimental design for BLZ-945–induced microglial depletion and repopulation in female mice. Schematic overview of the experimental setup. Young (~3-month-old) and old (~12-month-old) female mice were assigned to control (CTRL) or repopulated (BLZ + 7) groups, with four biological replicates per condition (one animal per replicate). Microglia were depleted using the CSF1R

inhibitor BLZ-945, and brains were collected 7 days after treatment withdrawal to capture early repopulated microglia. Cd11b^{+} cells were isolated from whole brains for downstream analyses.

5.2 scRNA-seq experiments

5.2.1 Tissue dissociation and isolation of CD11b^{+} by flow cytometry

The mice were anesthetized with 3% isoflurane (Iso-Vet), an overdose of ketamine (Biowet Pulawy), and xylazine (Sedazin, Biowet) (160 mg/kg and 20 mg/kg of body weight, respectively) via i.p. injection, followed by perfusion with cold PBS. The brains were collected and placed in cold HBSS (without Ca^{2+} and Mg^{2+}). In the first experiment, the whole hemisphere was isolated for flow cytometry experiments, and the remaining hemisphere was stored in cold PFA for 48 h. Subsequently, the brains were transferred to 30% sucrose (w/v) in PBS for 48 h and frozen in Tissue Freezing Medium (Leica) at -80 °C.

For flow cytometry, tissue was minced, transferred onto c-tubes containing 1950 µL DMEM supplemented with 50 µL of Deoxyribonuclease I (Sigma Aldrich). Dissociation was performed with the MACS dissociator with heaters (Militenyi Biotec) for 22 min and later the samples were passed through 70 nm and 40 nm strainers into 50 mL cold HBSS with ions to stop the enzymatic reaction (EasyStrainer™, BioOne). The cell suspension was centrifuged (10 min, 4 ºC, 300×*g*), the supernatant was removed and the pellet was resuspended in 25 mL of Myelin Gradient Buffer with 5 mL of cold PBS overlayed, followed by centrifugation (950×*g*, 4 ºC, 20’ with acc. 0 and deacc. 0). The pellet was resuspended in 1 mL of BD buffer (Dulbecco’s Phosphate-Buffered, Stain Buffer, FBS, BD Pharmigen™). The cells were counted using the Nucleocounter (Chemometec). The cells were suspended in the Stain Buffer (BD Pharmingen) with anti-mouse CD16/CD32 Fc Block™ 1:200 (BD Pharmigen) for 10 min. Next, anti-mouse CD11b antibody 1:250 (M1/70, BD Pharmigen) was added and cells were incubated for 20 min at 4 °C, then washed with Stain Buffer. The cells were sorted using purity precision mode on FACS Aria flow cytometer (BD FACSAria Cell sorter BD-Biosciences) into 200 µL of sterile PBS. The sorted sample was mixed by inverting the Eppendorf tubes and placed on ice, for no longer than 30 min. The experiments were performed by Dr. Maria Banqueri Ph.D., Dr. Anna M. Lenkiewicz Ph.D., Dr. Natalia Ochocka Ph.D., and Zuzanna Łuczak-Sobotkowska M.D.

5.2.2 Total RNA isolation from CD11b+ cells

For RNA isolation, sorted $CD11b^+$ cells were stored in a − 80 °C freezer. The samples were thawed on ice and total RNA was isolated with the RNAeasy Plus Mini Kit (Qiagen) according to the manufacturer's instructions. The RNA concentration was immediately determined using a spectrophotometer NanoDrop2000 (ThermoScientific). The experiments were performed by Dr. Maria Banqueri Ph.D., Dr. Anna M. Lenkiewicz Ph.D., Dr. Natalia Ochocka Ph.D., and Zuzanna Łuczak-Sobotkowska M.D.

5.2.3 Single-cell RNA-seq experiments

Directly after sorting, the quantity and viability of $CD11b^+$ cells were determined, and a cell suspension containing 5,000 target cells was used for further processing. Preparation of gel beads in emulsion and libraries were performed with Chromium Controller and Single-Cell Gene Expression v2 Chemistry (10 × Genomics) according to the Chromium Single-Cell 3' Reagent Kits v2 User Guide provided by the manufacturer. Libraries' quality and quantity were verified with a High-Sensitivity DNA Kit (Agilent Technologies, USA) on a 2100 Bioanalyzer (Agilent Technologies, USA). Next, sequencing was performed in the rapid run flow cell and paired-end sequenced (read 1–26 bp, read 2–100 bp) on a HiSeq 1500 (Illumina, San Diego, CA 92122, USA). To minimize batch effects, four scRNA-seq libraries (Rep1 to Rep4) were constructed, each combining 4 animals across 4 experimental conditions (control young, control old, repopulated young, repopulated old, repopulated old). For each scRNA-seq library, samples from individual experimental conditions were tagged using TotalSeq™ anti-mouse hashtag antibodies. The hashtag assignment was as follows: control young - #Ab 1, control old - #Ab 2, repopulated young - #Ab 3, repopulated old - #Ab 4:

Table 5.1 | Antibodies used for sample hashing in scRNA-seq experiments. Summary of the hashtag oligonucleotide (HTO)-conjugated antibodies applied for sample multiplexing in the scRNA-seq experiment. Each biological condition was labeled with a unique HTO antibody prior to pooling and encapsulation. The listed antibodies (Hashtag 1-4) contain distinct DNA barcodes that enable unambiguous sample demultiplexing.

Antibody	Barcode	Source	Type
TotalSeq™-B0301 anti-mouse Hashtag 1 Antibody (Ab #1)	ACCCACCAGTAAGAC	Biolegend	HTO
TotalSeq™-B0302 anti-mouse Hashtag 2 Antibody (Ab #2)	GGTCGAGAGCATTCA	Biolegend	HTO
TotalSeq™-A0303 anti-mouse Hashtag 3 Antibody (Ab #3)	CTTGCCGCATGTCAT	Biolegend	HTO
TotalSeq™-B0304 anti-mouse Hashtag 4 Antibody (Ab #4)	AAAGCATTCTTCACG	Biolegend	HTO

The target yield for each library was 11,000 (~2,750 per sample). After FACS sorting, the number and viability of $CD11b^+$ cells were measured, and a suspension with 5,000 cells was prepared for single-cell capture. GEM generation and library preparation were performed on the 10x Genomics Chromium Controller using the Single-Cell 3' v2 chemistry, following the manufacturer's protocol. Library quality and concentration were assessed with a High-Sensitivity DNA Kit on a Agilent 2100 Bioanalyzer.

Sequencing was conducted on an Illumina HiSeq 1500 using paired-end reads (26 bp for read 1, 100 bp for read 2). To minimize batch effects, four scRNA-seq libraries (Rep1–Rep4) were generated, each containing cells pooled from four animals: control young (~3 months), control old (~12 months), repopulated young (~3 months), and repopulated old (~12 months). Samples were distinguished using TotalSeq™ anti-mouse hashtag antibodies (#1–#4). Library preparation was performed by Dr. Natalia Ochocka Ph.D. (Laboratory of Molecular Neurobiology).

5.3 Bulk RNA sequencing

To ensure the generation of high-quality transcriptomic data, both single-cell and bulk RNA-seq workflows included rigorous quality control steps. All procedures were carried out in accordance with best practices for RNA integrity and library preparation.

For both single-cell and bulk RNA-seq experiments, the quality and integrity of total RNA were assessed using an Agilent 2100 Bioanalyzer with an RNA 6000 Nano Kit (Agilent Technologies, Ltd.). Library quality was subsequently verified using the Agilent 2100 Bioanalyzer together with the Agilent DNA High Sensitivity chip (Agilent Technologies Ltd.), confirming a mean library size of approximately 300 bp. The entire process of sample preparation and library amplification was overseen by Dr. Anna M. Lenkiewicz Ph.D. from the Laboratory of Molecular Neurobiology.

For sequencing, libraries were run on a rapid-run flow cell and paired-end sequenced as follows: 2×76 bp on the HiSeq 1500 (Illumina, San Diego, USA) for scRNA-seq and 2×151 bp on the NovaSeq 6000 (Illumina, San Diego, USA) for bulk RNA-seq. Sequencing was performed by Dr. Bartosz Wojtaś Ph.D., D.Sc., from the Laboratory of Sequencing and Dr. Paulina Szadkowska Ph.D. from the Laboratory of Molecular Neurobiology.

5.4 Single-cell RNA-seq data preprocessing and normalization

5.4.1 Raw data preprocessing

To provide robust downstream analysis, the raw scRNA-seq data underwent a standardized bioinformatics processing pipeline. The raw sequencing output, comprising 1,671 million reads in binary base call (BCL) files, was demultiplexed into four libraries (Rep1 to Rep4) and converted to FASTQ format using CellRanger v3.0.1 from 10X Genomics and bcl2fastq tool v2.20.0.422 developed by Illumina. FASTQ format stores a biological sequence in their sequencing order, along with quality scores, in text format. Each entry begins with a @ character followed by an identifier and sometimes sample description. The next line contains sequence letters, + character, and finally quality values of the raw sequence. The quality values, known as Phred quality scores, are assigned to each nucleotide base call, and are proportional to logarithm of the probability that a given base is incorrectly called.

The sequencing results were mapped and quantified using CellRanger pipeline. The total number of cells identified was 30,904. On average, the median number of genes detected per cell was 2,310, and the median UMIs per cell was 68,228. Subsequent analyses were performed in R using Seurat v4.2.0[134].

5.4.2 Demultiplexing samples

The data were split into two matrices: one containing RNA counts for each sample and another one containing HTO counts. Gene annotations from ENSEMBL were applied to the gene matrix, and HTO annotations were used for hashtag data. The HTO matrices were normalized using the NormalizeData() function with the normalization method selected as "CLR", which applied centered log-ratio transformation. Demultiplexing was performed based on the HTOs to assign cells to their respective experimental conditions (control young, control old, repopulated young, repopulated old), yielding 16 samples for further analysis. The hashtag oligonucleotides allowed for the identification of duplicates (two cells in one droplet) and negatives (empty droplets), which were filtered out. The MULTIseqDemux() function was used to identify and filter out doublets and negative droplets, with individual thresholds set for each hashtag to account for variability in cell numbers across samples[135]. This demultiplexing method is preferable when the expected number of cells varies among samples, as opposed to the standard HTODemux() function, which classifies cells based on a uniform threshold across all samples.

5.4.3 Quality control metrics

Each library was processed independently following a standard Seurat workflow, which included filtering based on quality control (QC) metrics, normalization, scaling, and identification of highly variable features. Cells with more than 7.5% mitochondrial gene content, fewer than 200 detected features, or more than 2,500 features were excluded to remove potential debris, dead cells, and doublets. After filtering, 20,058 high-quality cells remained for analysis.

5.4.4 Normalization, scaling and merging datasets

Gene expression values were normalized using the global-scaling method *LogNormalize*. In this method, the raw UMI counts for each gene are divided by the total counts for the corresponding cell, multiplied by a default scale factor of 10,000, and subsequently transformed using *log1p*. This procedure yields expression values that are comparable across cells and suitable for downstream analyses.

Seurat provides several alternative normalization strategies that can be adapted depending on dataset characteristics and research objectives. The CLR method, which was described previously, is often used for normalizing barcode data (e.g., cell hashing). Another available method is *Relative Counts* (RT), which is a simple scaling approach, in which raw counts for each gene are divided by the total UMI count of the corresponding cell, without any log-transformation. The newest implemented method is *SCTransform* (SCT), which is regularized negative binomial regression-based method, that models gene expression while accounting for sequencing depth and other technical factors. This method also performs variance stabilization, effectively reducing technical noise and improving downstream integration and differential expression analysis. This method has been increasingly favored for datasets with high technical variability or when integrative analysis across multiple batches is required[136,137].

For each library, the 2,000 most highly variable genes were identified using a variance stabilizing transformation (vst)[138]. This technique fits a local polynomial regression to the relationship between mean and variance[139]. The feature values were then standardized based on the observed mean and expected variance, which is determined by the fitted line. The variance for each feature was calculated using the standardized values, with a maximum limit applied to avoid outliers. After identifying highly variable genes for each library, the datasets were combined into a single Seurat object using the merge() function rather than the standard Seurat integration workflow. This approach was appropriate because the use of HTO barcoding allowed us to pool and multiplex samples within each sequencing run, thereby minimizing potential batch effects. Since each experimental condition was demultiplexed based on unique HTOs, additional integration steps to correct for batch variation were unnecessary. The normalized counts were scaled and centered using the Seurat function ScaleData(), where all genes were included as the “features” argument. This function regressed out the effects of specified variables and then scaled the residuals accordingly.

5.5 Dimensionality reduction and clustering

5.5.1 Principal Component Analysis

To cluster cells effectively and visualize the data in an interpretable way, it is essential to reduce this dimensionality while preserving the most informative variation. Dimensionality reduction

was performed using Principal Component Analysis (PCA), which is an unsupervised machine learning method useful for dimensionality reduction [140,141]. This approach allows to identify the cell types associated with each data point by uncovering axes that correspond to the largest variations in high-dimensional space. The first principal component is selected based on maximizing the variance of the positions of the analyzed cells, while the subsequent principal components are determined to be orthogonal to the first one. PCA allows for the selection of factors that contribute to the heterogeneity within the dataset. At this stage, biological conditions are expected to influence the data, particularly as significant variance is observed in relation to the expression correlations of multiple genes. In this study, PCA was run to obtain the first 30 principal components, as determined by the elbow plot results (Fig. 5.2). The elbow plot visually represents the standard deviation of the principal components to identify the threshold at which adding more components introduces mostly noise rather than informative signal, which obscures relevant biological data.

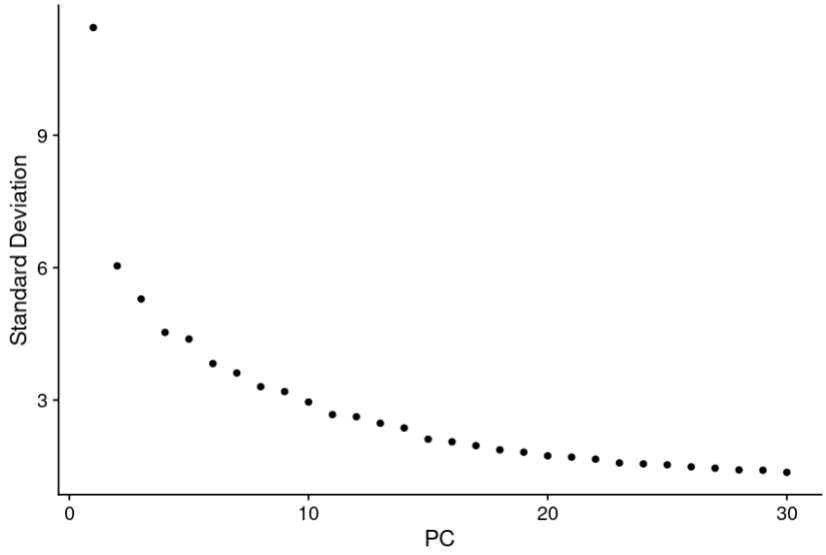

Figure 5.2 | Elbow plot of scRNA-seq data on PCA dimension reduction.

5.5.2 Uniform Manifold Approximation and Projection

Data visualization in 2D space was conducted using the Uniform Manifold Approximation and Projection (UMAP) for dimension reduction[142,143]. UMAP is a non-linear method that distributes data uniformly on Riemannian manifold with a locally constant metric. Manifolds are characterized by their local connectivity. It creates a low-dimensional representation that retains the fuzzy topological structure of the high-dimensional data.

UMAP offers several advantages: it is suitable for large-scale data, operates quickly, and tends to visually capture global data structures more effectively than other non-linear methods. In the analyzed dataset, UMAP was applied using 30 nearest neighbors, which helped in approximating the local manifold structure. This number reflects a balance between preserving the global structure with a larger number of neighbors and retaining detailed structure.

5.5.3 Clustering

Following dimensionality reduction, clustering was performed to identify groups of similar cells. Clustering was performed using Leiden algorithm that constructs a shared nearest neighbor (sNN) graph[144]. This method calculates the neighborhood overlap between each cell and its *k*-nearest neighbors. In this graph, each cell is represented as a node, and an edge connects two cells if they share a common nearest neighbor from the *k*-nearest neighbor graph. Neighbors are ranked from 1 (when the cells are the same) to *k* (when they are farther apart). The edges are weighted based on these rankings, with higher weights assigned to edges connecting cells that are closer together[145,146].

To detect clusters, the FindClusters() function employed an improved version of the sNN modularity optimization-based clustering algorithm, known as the Louvain method[147]. The chosen resolution of 0.4 provided a moderate granularity, appropriate for analyzed dataset that focused exclusively on the $CD11b^+$ cell population, and produces 16 distinct cell clusters. This balance allowed to resolve biologically meaningful subpopulations without excessive over-clustering, ensuring that each cluster could be assigned a plausible functional identity.

5.6 Single-cell RNA-seq downstream analysis

5.6.1 Cell type identification

For the downstream analysis, we identified the cell populations present in the dataset. To assist in this process, the ProjecTILs-3.0 R library was used[148], which facilitates the projection of scRNA-seq data onto well-characterized reference atlases[149]. This approach leverages existing datasets to predict cell identities and uncover gene programs that differentiate experimental conditions or tissue types. It is widely regarded as a robust

method for interpreting complex single-cell data and can be adapted to both published reference atlases and custom-built datasets. In our study, we used a CITE-seq reference dataset from Ochocka, Segit et al., Cell Rep. 2023[149], which we projected on query data derived from repopulation microglia processes.

5.6.2 Differential gene expression analysis

Differential gene expression analysis allows finding genes, whose activity signal level (expression) is significantly different when comparing different conditions or experimental groups. We took the normalized read count data and performed statistical analysis to find quantitative changes in expression levels between experimental groups. A differential gene expression test usually returns the log2 fold-change and the adjusted *p*-value per compared genes per compared conditions. We employed methods originally designed for bulk expression samples such as edgeR[150,151].

To further explore transcriptional changes across experimental conditions, we identified differentially expressed genes (DGE) using the FindMarkers() function applying a negative binomial regression model, which is particularly suitable for scRNA-seq data. This function allows flexible specification of statistical tests. We used tests which compute gene-wise differences in expression between defined groups of cells, correcting for multiple hypothesis testing using Benjamini-Hochberg procedure. Only genes surpassing predefined thresholds for adjusted *p*-value and log fold change were considered significantly differentially expressed.

The negative binomial regression model was used for differential expression analysis because it accurately captures the characteristics of single-cell RNA-seq data. Gene expression counts in scRNA-seq are highly variable and often show greater variance than expected from simple count models. The negative binomial distribution includes a dispersion parameter, allowing the variance the exceed the mean, which makes it well suited for modeling this over dispersed data.

Within this framework, gene counts are modeled as a function of experimental conditions, enabling the estimation of expression differences while accounting for cell-to-cell variability. The model also allows inclusion of covariates, such as sequencing depth or batch effects, ensuring that differential expression reflects biological rather than technical variation. Statistical significance is evaluated within the regression framework and corrected for multiple testing to control the false discovery rate[152].

Differential expression analyses were performed separately for each experimental condition and within each microglial cluster to identify changes associated with repopulation. A log fold-change cutoff of 0.25 was applied.

5.6.3 Pathway enrichment analysis

To have an insight into the biological processes underlying the observed transcriptional changes, we performed functional enrichment analysis on the differentially expressed genes (DEGs) identified using the negative binomial regression model. These DEGs were utilized to identify enriched Gene Ontology terms and pathways from the Kyoto Encyclopedia of Genes and Genomes (KEGG) and the Reactome Pathway Database. This analysis aimed to reveal which cellular processes were activated or suppressed between the compared cell populations.

Enrichment analysis and visualizations were performed using the pathfindR library (v.2.3.1)[153], which employs a protein-protein interaction networks to improve the detection of biologically meaningful pathways. This method is one of the third-generation pathway enrichment methods, which take not only information about the ranking scores, but also the gene interaction network. To build an interaction network, genes and their associated *p*-values were mapped into a subnetwork space and ranked based on their significance scores and the number of significant genes they connected. These ranked gene lists were used to identify enrichment analysis. Terms with adjusted *p*-values above a predefined threshold were discarded, while those with the lowest adjusted *p*-values for each term were retained for further analysis. The entire process was repeated multiple times in parallel to enhance result stability. Finally, distances between the retained enriched terms were calculated, and hierarchical clustering was performed to group related pathways, providing a clearer overview of the functional themes associated with microglial repopulation.

5.6.4 Trajectory inference

To gain deeper insight into the dynamics of microglial repopulation and to characterize potential cell differentiation trajectories, we leveraged RNA velocity analysis[154], which represent quantitative measure of future transcriptional state of individual cells, offering valuable information about cellular maturation and lineage progression. This analysis was performed using the scVelo library (v.0.3.2)[155], which estimates velocities by comparing

the ratio of un-spliced pre-mRNA fragments to mature, spliced mRNA, as indicated by the presence or absence of introns in the sequencing data.

We applied a likelihood-based dynamical model implemented in scVelo, which generalizes RNA velocity estimation to capture complex transcriptional dynamics across various cellular systems, including transient states that often arise during development or in response to perturbations. Initially, velocyto (v.1.0) was used to generate spliced and un-spliced count matrices from the raw sequencing data, while relevant metadata were extracted from the processed Seurat object. Gene-specific rates of transcription, splicing, and degradation were inferred, enabling the reconstruction of the latent temporal progression of microglial states. Finally, RNA velocity vectors were estimated using a deterministic model and visualized on a UMAP embedding, providing an interpretable two-dimensional representation of the inferred cellular trajectories during microglial repopulation.

5.6.5 Identification of significant ligand–receptor pairs

To investigate the intercellular communication during the microglial repopulation, we employed the CellChat R package (v.1.5.0)[156]. CellChat infers cell–cell communication networks by integrating known ligand–receptor interactions with single-cell transcriptomic data, leveraging social network analysis and pattern recognition methods. This approach identifies how different cell populations act as signal senders, receivers, or mediators within a complex tissue microenvironment.

In our workflow, we used the cluster identities obtained from the Seurat analysis as input for CellChat. First, CellChat constructed a probability matrix based on the expression levels of ligands and their corresponding receptors across cell clusters, estimating the likelihood of interaction between all cluster pairs. Next, the tool grouped these interactions into major signaling pathways, quantified the overall communication probability for each pathway, and evaluated the strength and directionality of signaling flows within the network.

We then applied pattern recognition analysis to identify dominant incoming and outgoing signaling patterns for each microglial cluster, allowing us to pinpoint which clusters act as primary information senders, receivers, or coordinators in the repopulating microglial niche. To visualize and interpret these complex intercellular relationships, we generated hierarchical network diagrams, circle plots, and heatmaps, which clearly illustrate the functional signaling architecture and the putative roles of each cluster within the reconstructed intercellular communication network.

5.7 Bulk RNA-seq analysis

After bulk RNA-seq of CD11b+ cells, we obtained FASTQ files containing raw read counts for each sample. We assessed the quality of the raw data using FastQC, which generated detailed metrics on base quality, sequence duplication levels, adapter content, and other quality indicators. The individual reports were then aggregated with MultiQC, providing a comprehensive overview across all samples to identify consistent issues. Because the quality check revealed significant adapter contamination, we performed adapter trimming using Trimmomatic[157], to ensure that downstream alignment and quantification would not be biased by residual adapter sequences. The cleaned reads were then aligned to the mouse reference genome mm10/GRCm38 using the STAR aligner[158], implemented through the RNA-seq-STARdeseq2 pipeline v2.0.0.

In the preprocessing stage, genes with zero counts across all samples were removed to avoid skewing normalization. The data were normalized using the calcNormFactors() function from the edgeR package[151], applying the Trimmed Mean of M-values (TMM) method[159]. TMM normalization adjusts for compositional differences between libraries by removing genes with extreme expression ratios (which could be due to technical or biological factors) to better estimate relative RNA output levels. After normalization, pseudo-counts were scaled to counts per million (CPM) to account for differences in sequencing depth. PCA was then performed to visualize sample variation and detect potential outliers. Based on this, one sample (sample2) from the control group was excluded due to its unusually high variance, which was manifested by it not clustering consistently with other biological replicates. To gather more information about the genes, biomaRt library (v.3.16) was used to map ENSEMBL gene IDs to gene names and functional descriptions, enriching our interpretation of downstream results[160].

DEG analysis was conducted using the limma package[161], which fits a linear model for each gene, estimating expression differences between experimental groups while borrowing information across all genes to stabilize variance estimates - a method known as empirical Bayes moderation. This approach improves the reliability of differential expression estimates, especially when sample sizes are moderate or small. After fitting the model, we applied false discovery rate (FDR) correction to the resulting *p*-values to control for multiple testing. Genes were considered significantly differentially expressed if they had an absolute log2 fold change ($|\log2FC| > 1$) and an adjusted *p*-value ≤ 0.05. This analysis

yielded 736 differentially expressed genes, with 453 upregulated and 283 downregulated in the repopulated group compared to controls.

Finally, the list of DEGs was input into pathfindR for pathway enrichment analysis[153]. By leveraging the KEGG, Reactome, and Gene Ontology (Biological Process) databases, we identified key pathways and biological processes that were significantly activated or suppressed in the repopulating microglia populations.

5.8 scRNA-seq data integration

To investigate the hypothesis that gliomas can recapitulate the microglia repopulation program to reprogram microglial functionality into a tumor-supportive state, we performed an integrative scRNA-seq analysis combining data on microglia from glioma and repopulation groups. Specifically, we employed the Reciprocal PCA (RPCA) method - a robust strategy for integrating datasets where batch effects and biological differences coexist, and especially effective for smaller datasets[162].

This method was implemented using the Seurat function *FindIntegrationAnchors()[163], which identifies a set of 'anchors' by pairing cells from the reference and query datasets that are mutual nearest neighbors in PCA-reduced space. Low-confidence anchors are filtered out by maximizing anchor feature values, ensuring that the final anchors define a consistent low-dimensional space that reflects the true high-dimensional structure. The algorithm then scores each anchor pair and builds a shared neighbor graph, calculating overlaps between anchors and query cells to produce an integrated dataset that aligns shared biological signals.

For this study, we selected microglia populations from an unpublished glioma dataset (Jacek, Lenkiewicz, Cyranowski et al., in preparation) representing distinct tumor microenvironments and integrated these data with selected clusters from repopulated microglia in young mice. Annotated clusters were compared to identify shared transcriptional programs that might indicate functional reprogramming.

Finally, to strengthen these findings, we performed pseudotime trajectory analysis using the Monocle library. This approach reconstructs cellular trajectories based on gene expression dynamics, allowing us to visualize lineage progression and fate decisions within the integrated data. By examining the expression of key genes along these pseudotime branches, we could infer the likely progenitor states and trace the continuum from immature to more differentiated

microglial phenotypes, supporting the notion that glioma-associated microglia may partially mirror a repopulation-like program[164–166].

6. Results

6.1 Assessment of single-cell transcriptomics data integrity

We conducted a systematic investigation to determine whether repopulated microglia can effectively restore the functional diversity typically observed in intact brains, and whether this restoration differs between young and aging mice. To address these questions, we performed single-cell RNA sequencing on CD11b+ cells isolated from the brains of both young and aging mice, comparing control versus repopulated microglia. The sorting of CD11b+ cells was performed according to previously established protocols[67], ensuring consistency and reliability of microglial populations across experiments.

For each sample, we aimed to capture approximately 10,000 cells, which were subsequently partitioned into nanoliter-scale gel bead-in-emulsion (GEM) droplets. This cell recovery target was chosen to provide sufficient depth for detecting cellular heterogeneity while minimizing the likelihood of multiplets, thereby preserving the resolution required for accurate single-cell transcriptomic profiling[167]. Cell viability was assessed prior to GEM loading to ensure a survival rate exceeding 80%, a prerequisite for generating reliable transcriptomic data.

To assess data quality, we generated “knee” plots, which visualize the distribution of unique RNA reads, quantified by UMIs across individual GEMs. These plots clearly differentiate GEMs containing intact cells from empty droplets that capture ambient RNA. A distinct inflection point, marked by a sharp decline in UMI counts, reflects the separation between cell-containing GEMs and empty ones (Fig. 6.1). This method demonstrates the high efficiency of the achieved cell encapsulation.

The generation of high-quality scRNA-seq libraries was confirmed by examining library complexity, sequencing saturation, and transcript alignment rates. Only samples passing these quality thresholds were retained for downstream analysis, ensuring that the resulting transcriptomics profiles accurately reflect the biological variability between microglial populations. Collectively, these measures provide strong confidence in the robustness of the scRNA-seq dataset and enable a reliable comparison of transcriptional states across experimental conditions.

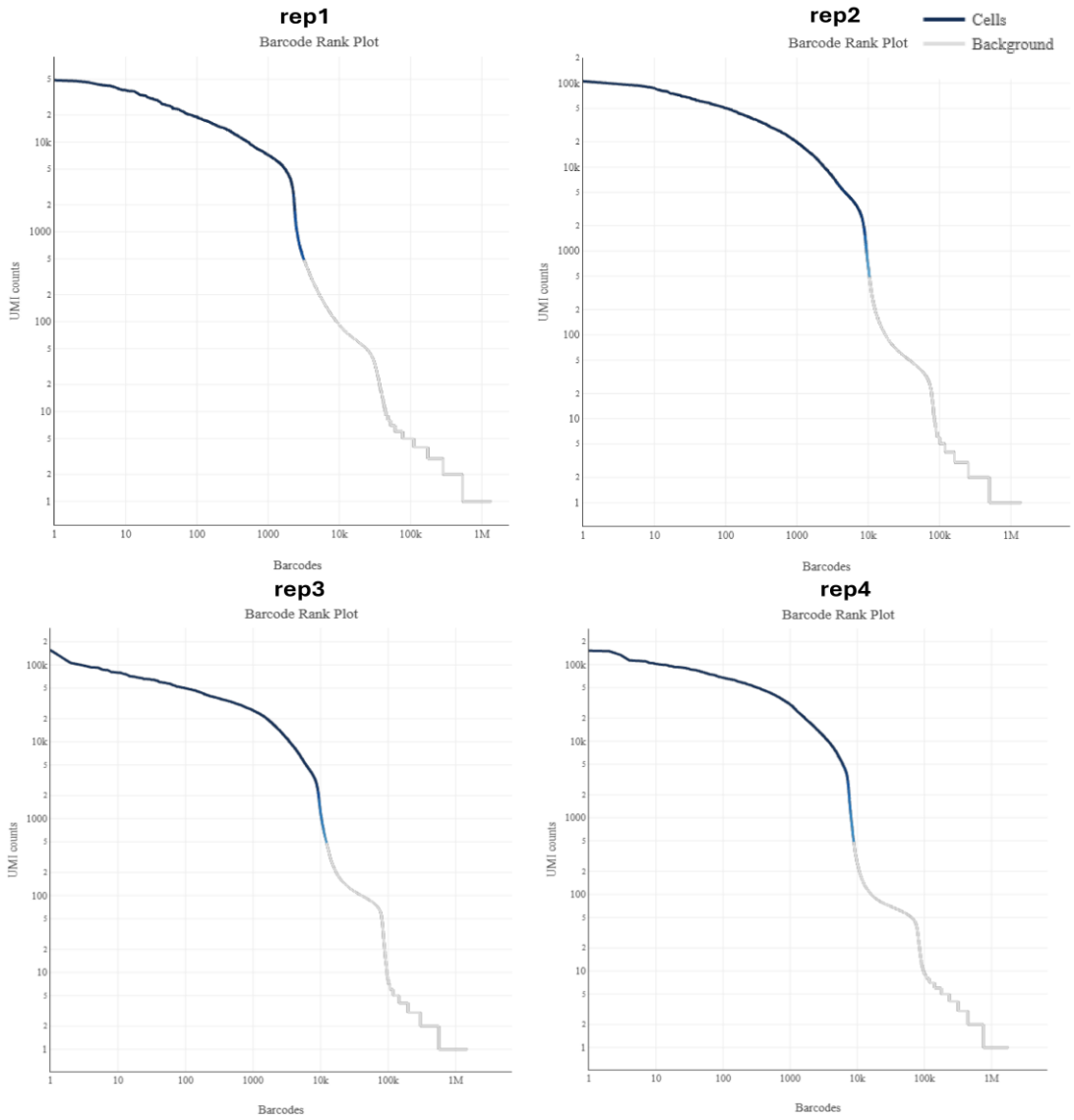

Figure 6.1 | Quality control of scRNA-seq libraries: identification of cell-containing GEMs. Knee plots illustrate the separation between true cell-containing GEMs and background signal. Barcodes corresponding to background reads were excluded from downstream analyses to ensure high-quality single-cell transcriptomic profiling.

6.2 Sample demultiplexing using Hashtag Oligonucleotides

HTO-based cell hashing was used to multiplex biological replicates within a single sequencing run, allowing accurate sample assignment while reducing batch effects. This approach increases a number of cells loaded per well without increasing multiplets rates, as droplets containing cells from different samples can be identified by the presence of multiple HTO barcodes.

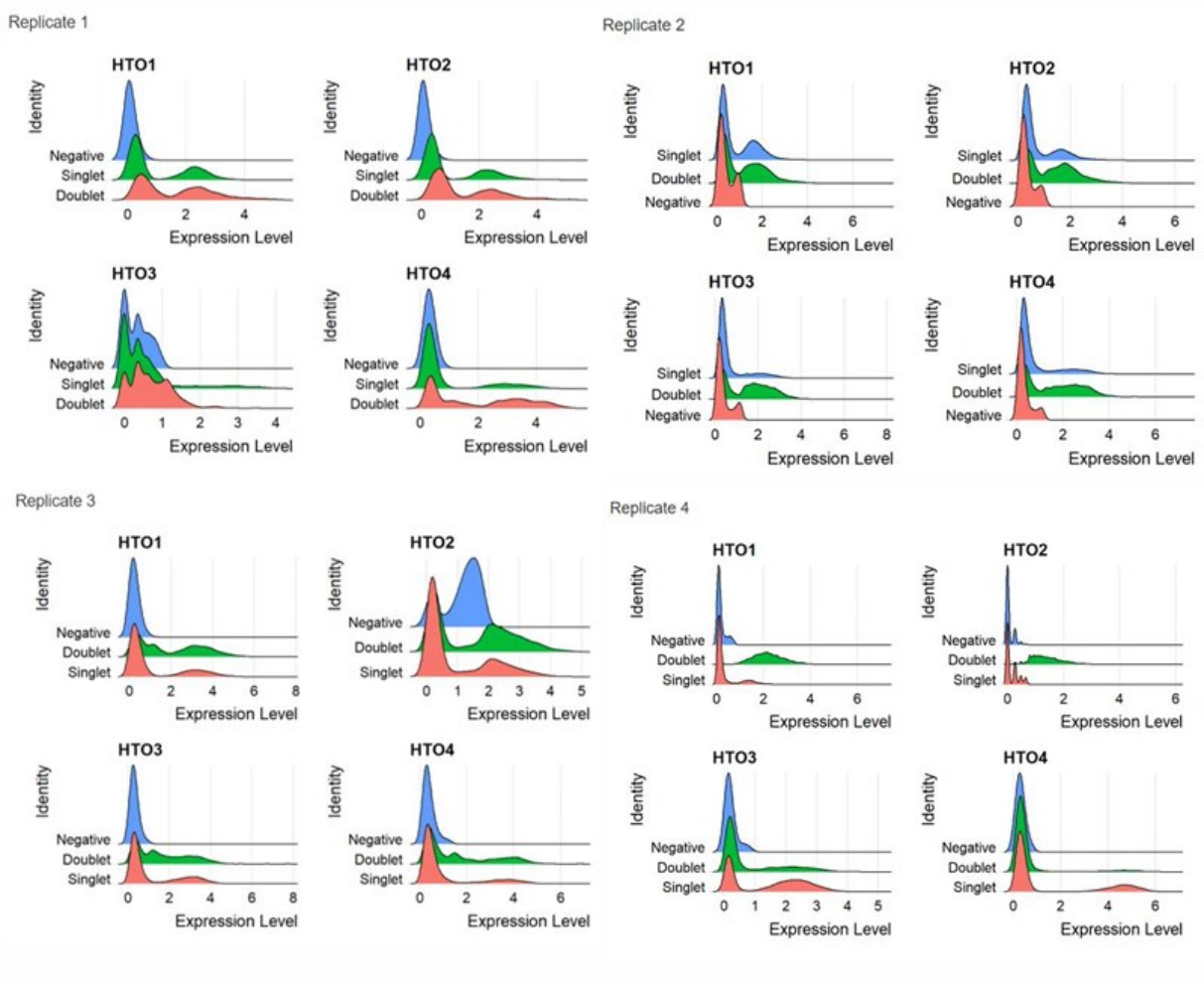

Figure 6.2 | Classification of Gel Bead-in-Emulsions (GEMs) based on hashtag oligonucleotide expression. Ridge plots depicting the distribution of hashtag oligonucleotide level across individual replicate prior to filtering. Cells were classified into three groups: **negatives (blue)**, representing background GEMs without detectable HTO signal; **doublets (green)**, containing mixed HTO signals from more than one sample; and **singlets (red)**, corresponding to uniquely labeled cell-containing GEMs. This classification was used to filter out background and doublets, retaining only singlets for downstream analysis.

Within the generated GEMs, multiplets containing cells from different samples were identifiable by the presence of multiple HTO barcodes and were classified as doublets. Droplets lacking detectable hashtag signal were distinctly categorized as negatives. To assess the quality of sample demultiplexing and multiplets detection, we analyzed the distribution of expression levels of HTOs across all replicates.

The density plots generated for each replicate (HTO1–HTO4) clearly demonstrate three distinct populations: negative, singlet, and doublet cells. Cells classified as negative (blue) exhibit expression levels near zero, indicating the absence of specific hashtag labeling.

The singlet population (green) displays a pronounced peak at intermediate expression levels, confirming the presence of a single, dominant hashtag per cell. In contrast, the doublet population (red) is represented by a broader distribution at higher expression levels, reflecting cells with significant reads for multiple hashtags, consistent with multiplets events. Notably, we detected a bimodal distribution in the HTO2 replicate of replicate 3, which was attributed to the accidental loading of HTO2 cells from replicates 3 and 4. This oversight necessitated the implementation of a refined method for separating negatives and doublets, allowing us to adjust thresholds according to the cell concentration observed in each sequenced well. This clear separation of negative, singlet and doublet populations across all replicates highlights the reliability of the cell hashing approach and demonstrates the robustness of demultiplexing strategy, ensuring high-confidence downstream analysis (Fig. 6.2).

Following stringent demultiplexing and filtering steps, we further examined the distribution of HTO expression levels across all replicates to confirm the effectiveness of the approach. As shown in the Fig. 6.2, each replicate (HTO1–HTO4) demonstrates well-defined populations with clear separation of negative cells, singlets for each individual hashtag, and doublets. The distinct peaks corresponding to each unique HTO confirm the successful recovery of high-confidence singlet cells, while doublets and ambiguous multiplets are clearly delineated and minimized. This refined classification ensures that only robustly labeled single cells are retained for downstream single-cell transcriptomic analysis, enhancing the accuracy of sample assignment across replicates. Importantly, the consistent patterns observed across all four replicates demonstrate the reproducibility of our cell hashing strategy and the reliability of the filtering thresholds applied.

6.3 Reconstitution of microglia heterogeneity after repopulation in brains of young mice

After demultiplexing, we initially recovered a total of **30,904 cells** across all experimental conditions and replicates, which after removing negatives and doublets has yield 21,223 high-confidence singlet cells for downstream analysis. To further ensure the integrity of the dataset, additional quality control criteria were applied, focused on filtering cells with suboptimal characteristics. Specifically, cells with abnormally dwindling numbers of detected genes or unique molecular identifiers (UMIs) were removed, as these represent poor-quality or dying cells. We also excluded cells with an elevated percentage of mitochondrial gene expression

(>10%), a hallmark of stressed or apoptotic cells. After applying these stringent filters, **20,058 cells** remained across four samples for each experimental condition, providing a robust dataset for subsequent analyses.

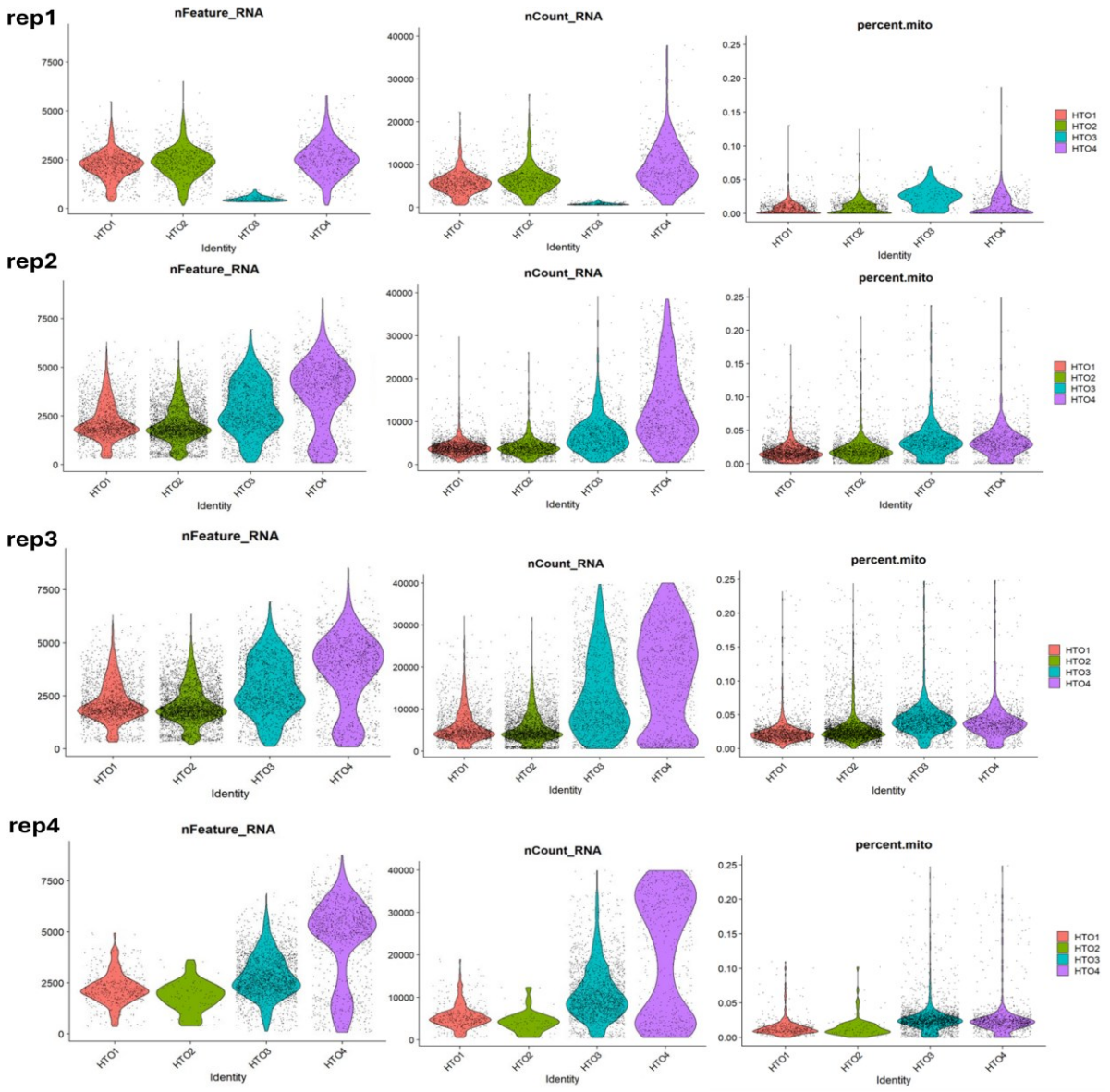

Figure 6.3 | Quality control of demultiplexed single-cell RNA-seq samples. Violin plots displaying the distributon of detected features (genes), total UMI counts, and the percentage of mitochondrial gene expression across analyzed sample repilcates. These quality control metrics were used to assess cell integrity and exclude low-quality cells from downstream analysis.

Notably, replicate 3 HTO1 exhibited lower total features and UMI counts compared to other hashtags and replicates. This reduction may reflect a lower initial cell capture efficiency for this barcode or sample loss during library preparation. Importantly, inspection

of the HTO expression plots for Replicate 3 and Replicate 4 revealed a subtle bimodal distribution of counts for certain hashtags. This pattern suggests the presence of actively dividing cells with asynchronous cell cycle phases, which can cause variability in total RNA content and lead to a distinct subpopulation with slightly lower gene or UMI counts.

To account for this, we carefully balanced the filtering thresholds to retain biologically meaningful dividing cells while removing low-quality droplets. Additionally, we verified that the ratio of mitochondrial genes within these bimodal populations did not exceed the established threshold, ensuring that these cells represent genuine biological states rather than dying or lysed cells.

Table 6.1 | Summary of sequenced cells recovery before and after quality control and filtering steps. The table presents a number of cells retained at successive stages of processing across four replicates. Cell barcodes were first demultiplexed using either HTODemux or MULTIseqDemux, yielding a comparable initial cell count (30,904 in total). Subsequent removal of negative droplets and doublets reduced the dataset to 19,546 (HTODemux) or 21,223 (MULTIseqDemux) high-confidence singlets. Finally, exclusion of cells with a high proportion of mitochondrial transcripts resulted in 20,058 high-quality single-cell transcriptomes that were used for downstream analysis.

	Replicate 1	**Replicate 2**	**Replicate 3**	**Replicate 4**	**All cells**
Demultiplexing with HTODemux	2,970	9,245	10,717	7,972	30,904
Demultiplexing with MULTIseqDemux	2,970	9,245	10,717	7,972	30,904
Removing negatives and doublets using HTODemux	2,131	6,192	7,031	4,192	19,546
Removing negatives and doublets using MULTIseqDemux	2,405	6,227	8,689	3,902	21,223
Number of cells after filtering out cells with high number of mitochondrial genes	2,383	5,971	8,022	3,682	20,058

6.4 Microglia subtype profiling and cluster validation

We successfully identified clusters through our analysis (Fig. 6.4A) and consolidated them into 8 distinct cell subtypes. These subtypes were meticulously annotated using the most significant differentially expressed genes alongside canonical markers previously established in the literature, which greatly enhances the accuracy and interpretability of our findings[67,149]. To ensure a focused analysis of microglia-specific states, we rigorously examined all clusters and excluded rare populations corresponding to contaminating monocytes, CNS-associated macrophages, T cells, NK cells, and Cd24a+ cells. This refinement step enabled us to delineate a clearer microglia landscape (Fig. 6.4B).

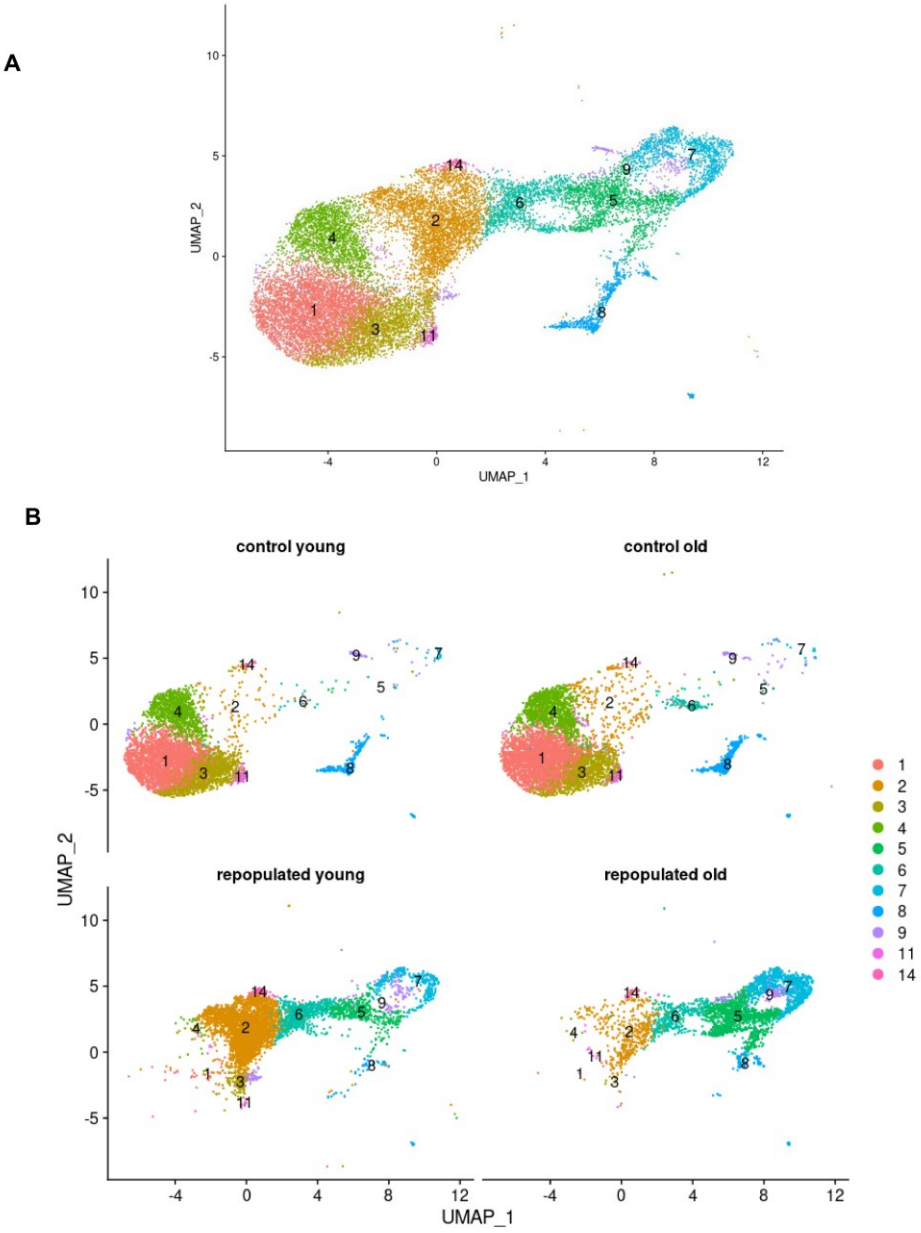

Figure 6.4 | Clustering of single-cell transcriptomics data visualized by UMAP. (A) Global clustering of all cells projected on UMAP embedding, illustrating the overall structure of the dataset. (B) The same UMAP projection, with cells divided according to the four experimental conditions, highlighting condition-specific distribution across clusters.

The final clusters - MG1, MG2, MG3, Act-MG1, Act-MG2, and Act-MG3 – demonstrate a direct correspondence with the previously characterized Hom-MG1, Hom-MG2, Hom-MG3, Act-MG1, Act-MG2, and Act-MG3 subtypes identified by scRNA-seq and CITE-seq analyses in glioma-associated microglia (Table 6.2).

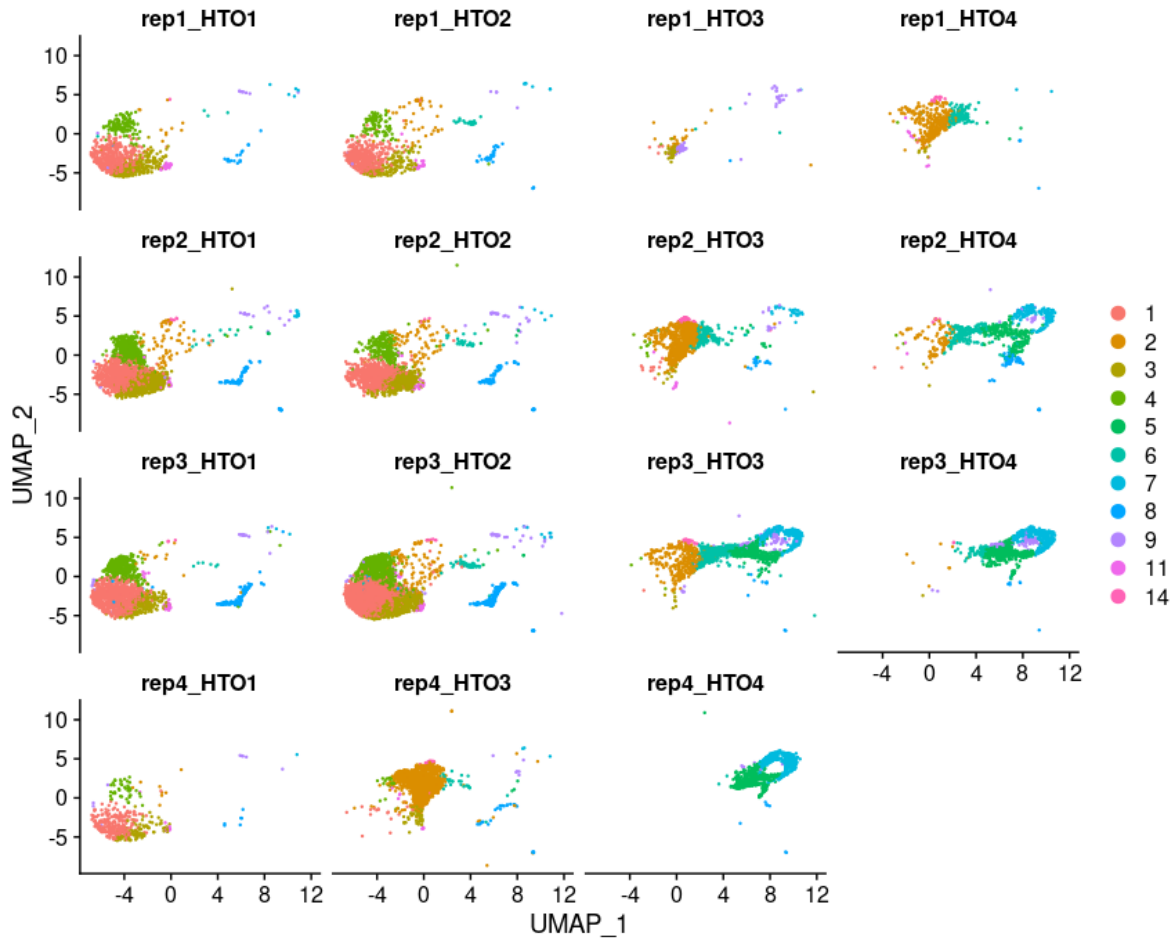

Figure 6.5 | Clustering of single-cell transcriptomics data across all sequenced samples. UMAP embedding with cells separated by the 16 individual samples, allowing assessment of batch contribution and sample-specific variability within clusters.

Table 6.2 | Comparison of microglial cell clustering across studies and annotation strategies. Mapping of cell clusters identified in *Ochocka et al., Nat. Comm. 2021* and *Ochocka et al., Cell Rep 2023* with the Surat-based clustering performed in this study. Subtypes were assigned based on transcriptional signatures and marker gene expression. Clusters corresponding to microglial activation states (Act-MG), proliferating microglia (prolif-MG) and homeostatic subtypes (Hom-MG1, Hom-MG2, Hom-MG3) were consistently reproduced, while additional clusters (e.g. T/NK cells, monocytes, macrophages) represent minor non-microglial populations. Some clusters identified in previous studies (MG4, MG5, MG6) were not detected in the present dataset.

Ochocka et al., 2021 cluster	Ochocka et al., 2023 cluster	Seurat cluster (this study)	Subtype (this study)
MG1	Hom-MG1	1	MG1
N/A	Act-MG1	2	Act-MG1
MG1	Hom-MG1	3	MG1
MG2	Hom-MG2	4	MG2
N/A	Act-MG3	5	Act-MG3
N/A	Act-MG2	6	Act-MG2
prolif-MG	Act-MG4	7	prolif-MG
MG3	Hom-MG3	8	MG3
N/A	Act-MG3	9	Act-MG3
T-cells/NK cells	T-cells/NK cells	10	N/A
MG1	Hom-MG1	11	MG1
Mo	Mo	12	N/A
pre-MG	N/A	13	pre-MG
N/A	Act-MG1	14	Act-MG1
N/A	Cd24a+	15	N/A
MΦ	MΦ	16	N/A
MG4	N/A	N/A	N/A
MG5	N/A	N/A	N/A

MG6	N/A	N/A	N/A

Cluster annotations were robustly assigned using the automatic classification framework implemented in the ProjecTILs library[148], as detailed in the *Materials and Methods* section. The clear expression of canonical markers across these clusters further validates annotations and highlights the reliability of the employed integrative approach. Collectively, the robust cluster identification and annotation provide a critical foundation for downstream analyses and underscore the broader significance of our findings within the context of microglia heterogeneity (Fig. 6.6)[149,168].

6.5 Repopulated microglia reconstitute transcriptional heterogeneity but exhibit elevated inflammatory signatures

The analysis revealed the appearance of distinct "active" microglia states that were absent in control brains. Specifically, three clusters of active microglia (Act-MG1, Act-MG2, and Act-MG3) emerged predominantly in repopulated samples, resembling microglia states previously described in tumor-bearing brains (Fig. 6.7A,B)[149]. These Act-MG clusters exhibited transcriptional programs associated with phagocytosis, migration, and extracellular matrix remodeling, reflecting their heightened functional engagement during the repopulation process.

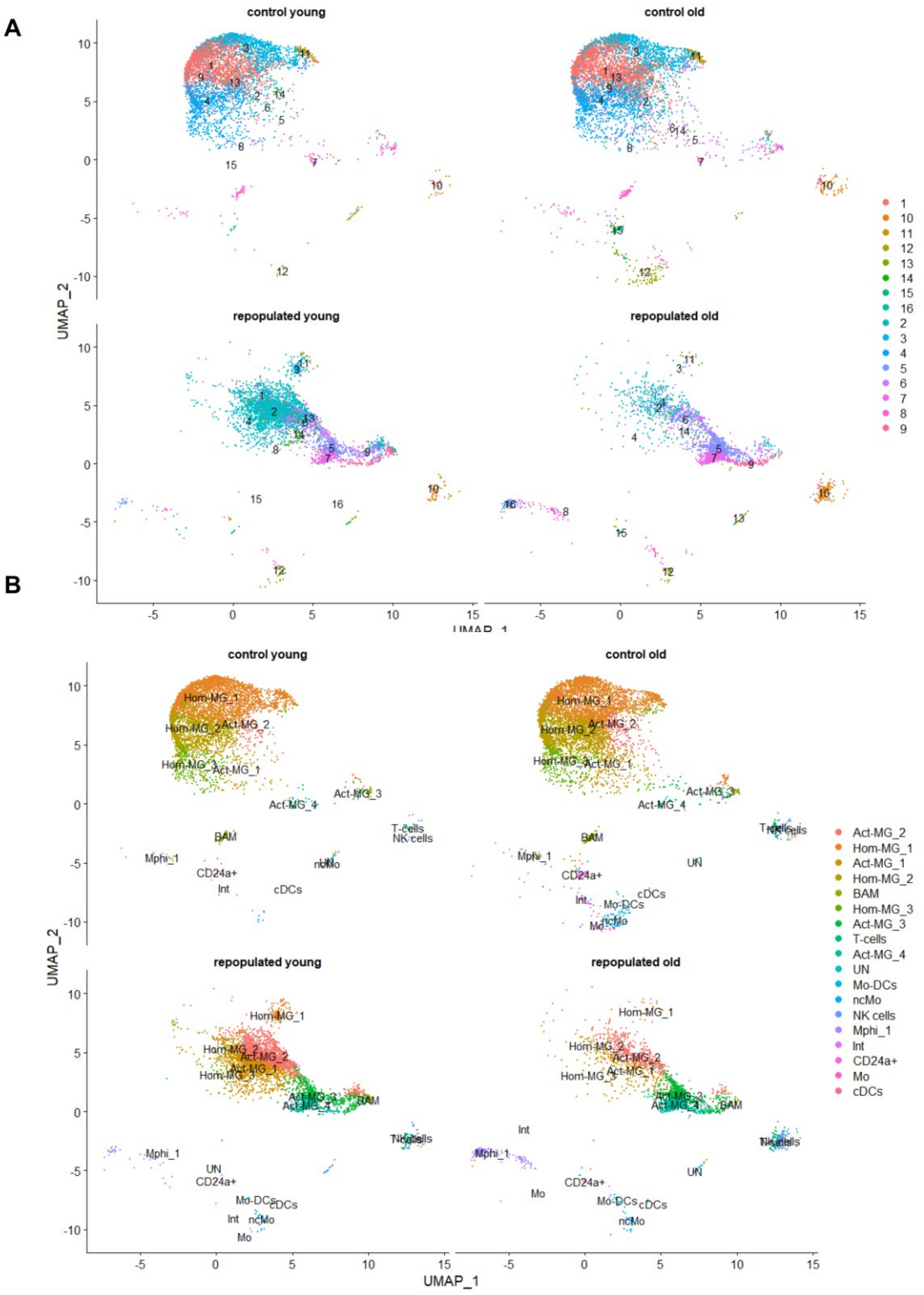

Figure 6.6 | Single-cell transcriptomics annotation of microglial clusters. (A) Projection of Seurat-derived clusters onto a reference data from Ochocka et al., Cell Rep. 2023. (B) UMAP visualization of the annotated clusters, with cell type labels transferred from the reference dataset, enabling identification of homeostatic, activated, proliferating microglia and non-microglial populations.

In addition to these active states, two further clusters were uniquely identified in repopulated brains: a proliferating microglia cluster (prolif-MG) and a premature microglia cluster (pre-MG). The prolif-MG subpopulation was characterized by high expression of canonical cell cycle genes, including *Ki-67*, *Esco1/2*, *Cdk1*, and *H2afx* (Fig. 6.7F)[169], consistent with ongoing self-renewal and expansion within the repopulated niche. In contrast, the pre-MG cluster demonstrated marked enrichment of inflammation-related genes - including *Mcm5*, *Ifitm3*, *Irf7*, *Isg15*, *Usp18*, and *Mif*[170], alongside cytokine-encoding genes including *Tnf, Ccl2, Ccl3, Ccl4, Ccl7, and Ccl12*[171]. These transcriptional features suggest a role for pre-MG cluster in directing cell migration and inflammatory signaling during repopulation (Fig. 6.9 A-D).

Trajectory inference analysis provided further insight into the dynamics of these states. Pseudotime ordering revealed a continuous trajectory, beginning with proliferating microglia, transitioning through active states, and converging on mature homeostatic microglia (Fig. 6.7E). This continuous trajectory underscores the dynamic plasticity of repopulated microglia and suggests that the pre-MG cluster represents an intermediate inflammatory state poised for further differentiation. KEGG pathway enrichment supported this interpretation, highlighting elevated activity of interferon, Toll-like receptor (TLR), and NF-κB signaling pathways within the pre-MG population, consistent with their role in directing cell migration and inflammatory responses during repopulation.

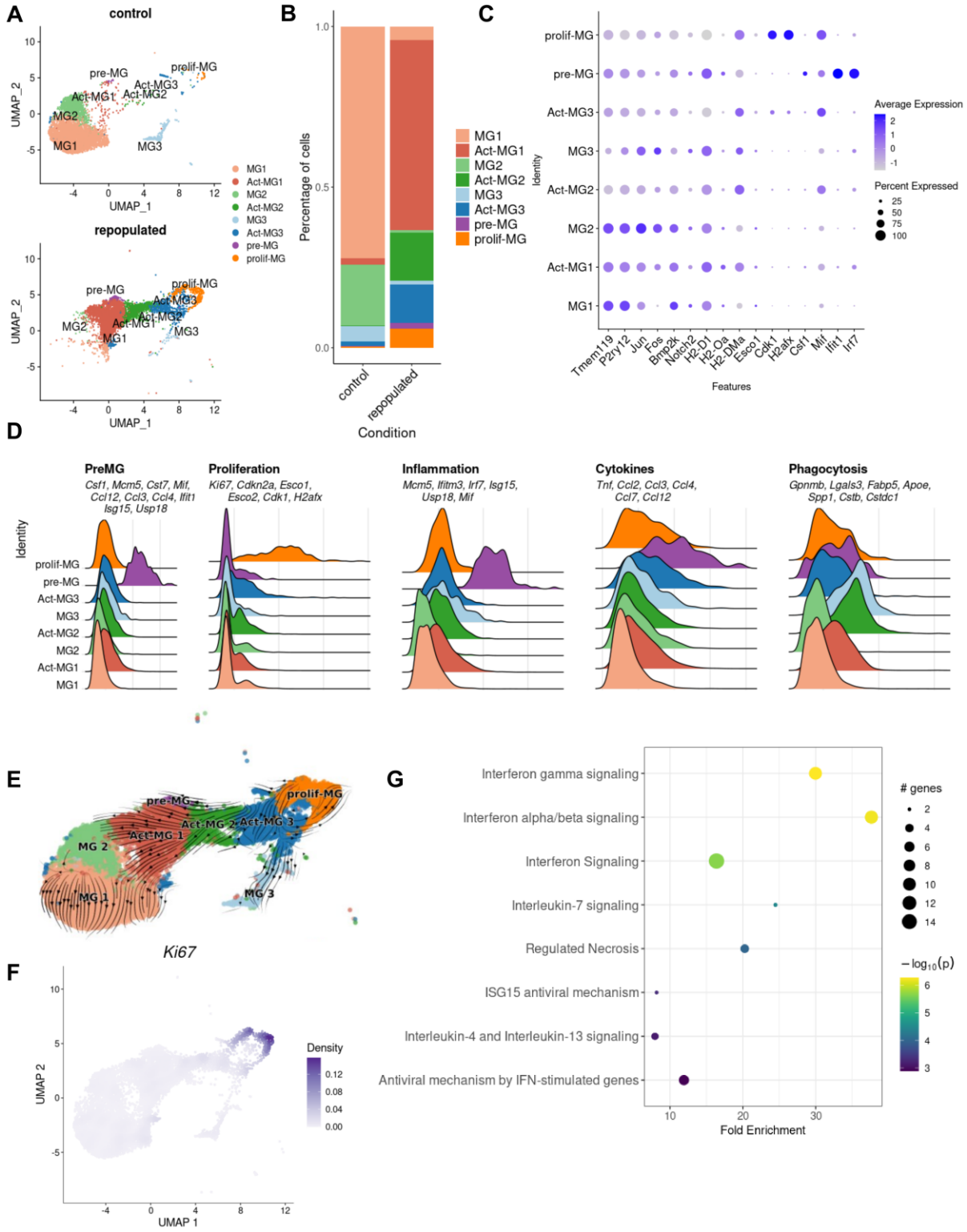

Figure 6.7 | Functional heterogeneity of repopulated microglia revealed by single-cell transcriptomics. (A) UMAP visualization of scRNA-seq data from control and repopulated MG. Four scRNA-seq replicates were pooled per condition. Clusters were annotated based on the reference datasets (*Ochocka, Segit et al. 2021, Ochocka et al., 2023)*, and included: MG1 (homeostatic microglia), Act-MG1 (activated microglia), MG2 (transcriptionally active cells), Act-MG2 (activated transcriptionally active cells), MG3 (signaling inhibitors and transcriptional repressors), Act-MG3

(activated signaling inhibitors and transcriptional repressors), pre-MG (premature microglia) and prolif-MG (proliferating microglia). (B) Relative proportions of cells assigned to each cell cluster in young control versus repopulated mouse brains. (C) Dot plot showing average expression levels of established microglial signature genes (*Ochocka et al., 2021*) across annotated clusters. (D) Ridge plots depicting gene signature scores associated pre- MG, proliferation, inflammation, cytokine signaling, and phagocytosis across clusters. (E) UMAP projection overlaid with RNA velocity vectors (scVelo), illustrating transcriptional dynamics and cluster transitions. All clusters originated from prolif-MG. (F) Weighted kernel density UMAP plot of *Mki67* expression, highlighting proliferative activity. (G) Reactome pathway enrichment analysis of differentially expressed genes in the pre-MG cluster compared with other clusters shown in (A).

These findings indicate that while repopulated microglia successfully re-establish the transcriptional diversity observed in intact brains, they also transiently acquire proliferative and inflammatory states, not typically observed under homeostatic conditions. These unique states reflect the dynamic plasticity of the microglia compartment and the active remodeling of the niche during the repopulation process.

6.6 Defective reconstitution of the homeostatic phenotype by repopulated microglia from older mice

A comprehensive comparison of the cellular composition and transcriptional heterogeneity of repopulated microglia (MG) in young (3 months old) and aging (12 months old) mice was conducted. ScRNA-seq analysis revealed that the previously identified MG clusters were consistently detected across both age groups, with naïve mice showing similar contributions of each cluster regardless of age (Fig. 6.10A). However, notable differences emerged in the distribution of repopulated MG subtypes between young and older mice (Fig. 6.10B).

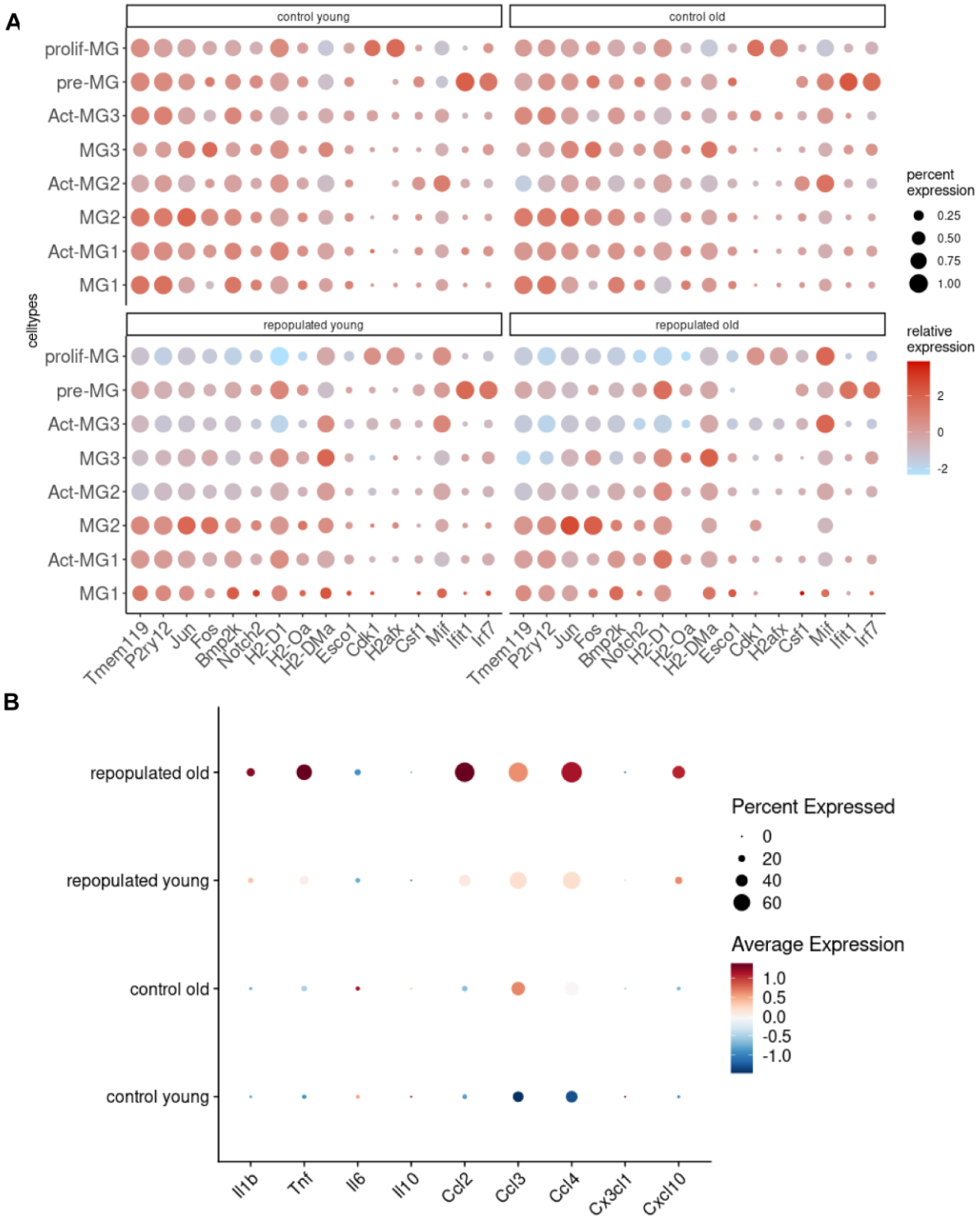

Figure 6.8 | Differential gene expression of microglia across experimental conditions. (A) Dot plot showing the average expression levels of selected microglial marker genes across experimental conditions. (B) Dot plot illustrating the average expression levels of selected cytokine-related marker genes across experimental conditions.

Specifically, there was observed a marked increase in the prevalence of active cell states (Act-MG1, Act-MG2, Act-MG3) within the repopulated MG of older mice. Compared to their younger counterparts, older mice exhibited significant enrichment in the Act-MG3 and prolif-MG clusters, while repopulated MG from young mice showed a higher representation of Act-MG1 cells. Trajectory analysis further demonstrated that repopulated MG in older mice accumulate in proliferating and intermediate active states, with delayed transition towards reconstituted homeostatic clusters compared to young mice (Fig. 6.10A–C).

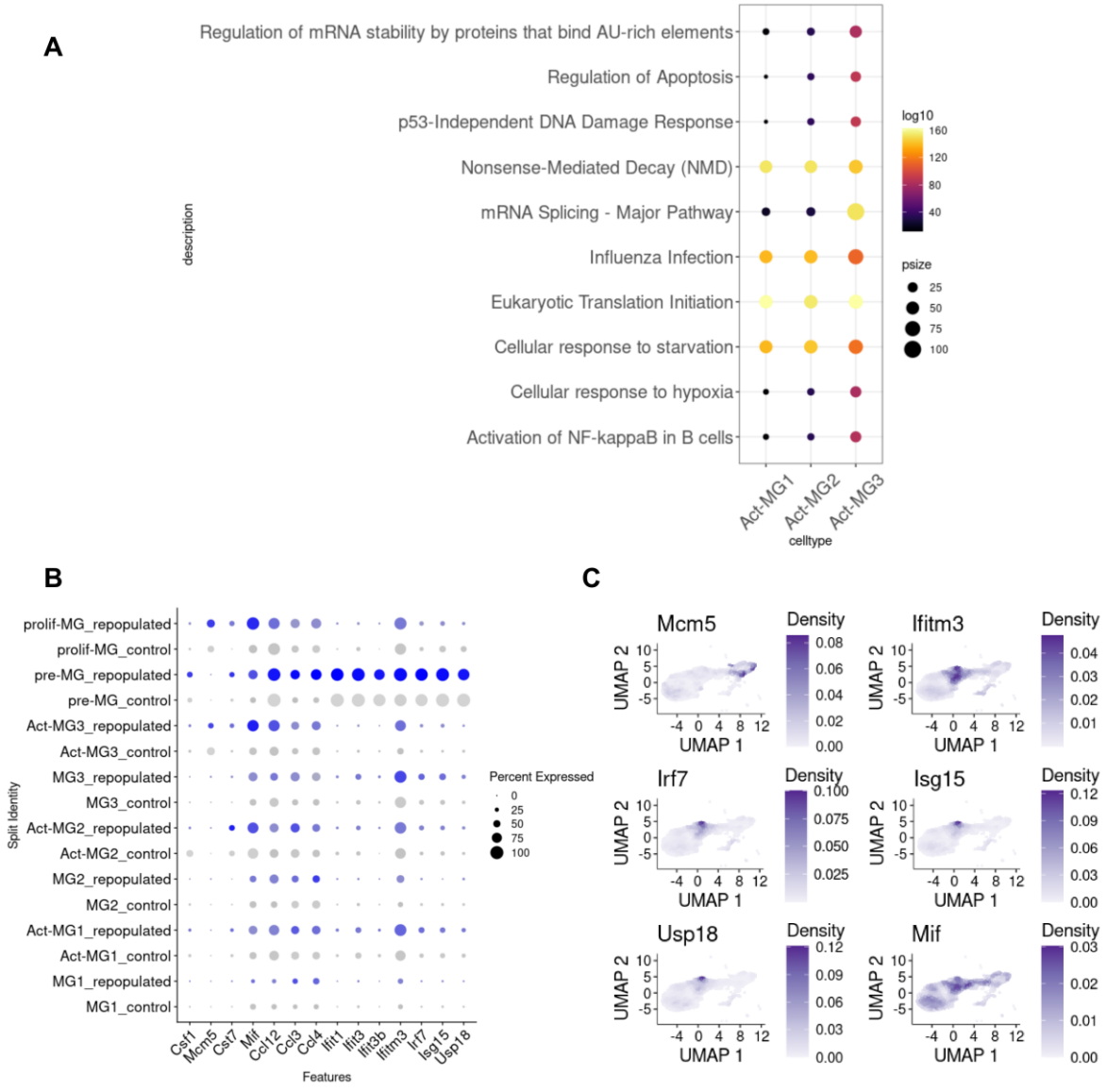

Figure 6.9 | Functional and transcriptional characterization of premature and activated microglia. (A) Dot plot showing the average expression of selected marker genes associated with premature microglia in young mice, stratified by cell type and experimental condition. (B) Dot plot summarizing the top enriched KEGG pathways identified in three transcriptionally distinct activated

microglial subsets. (C) Feature plots displaying the expression of representative genes related to inflammatory processes, projected on the UMAP embedding.

To validate these findings, the expression patterns of selected marker genes across all four experimental conditions were compared. The normalized expression levels and fractions of cells expressing these markers within each of the eight identified clusters confirm consistent, robust expression profiles, supporting their reliability as cell-type-defining features (Fig. 6.8A).

Furthermore, KEGG pathway enrichment analysis of upregulated genes in the prolif-MG clusters revealed significant associations with proliferation-related processes, including mRNA splicing, DNA replication, and chromatin remodeling (Fig. 6.10D). The accompanying heatmaps illustrate the expression profiles of these differentially expressed genes, highlighting key pathways involved in the impaired resolution of proliferative and inflammatory states (Fig. 6.8B, Fig. 6.10.E).

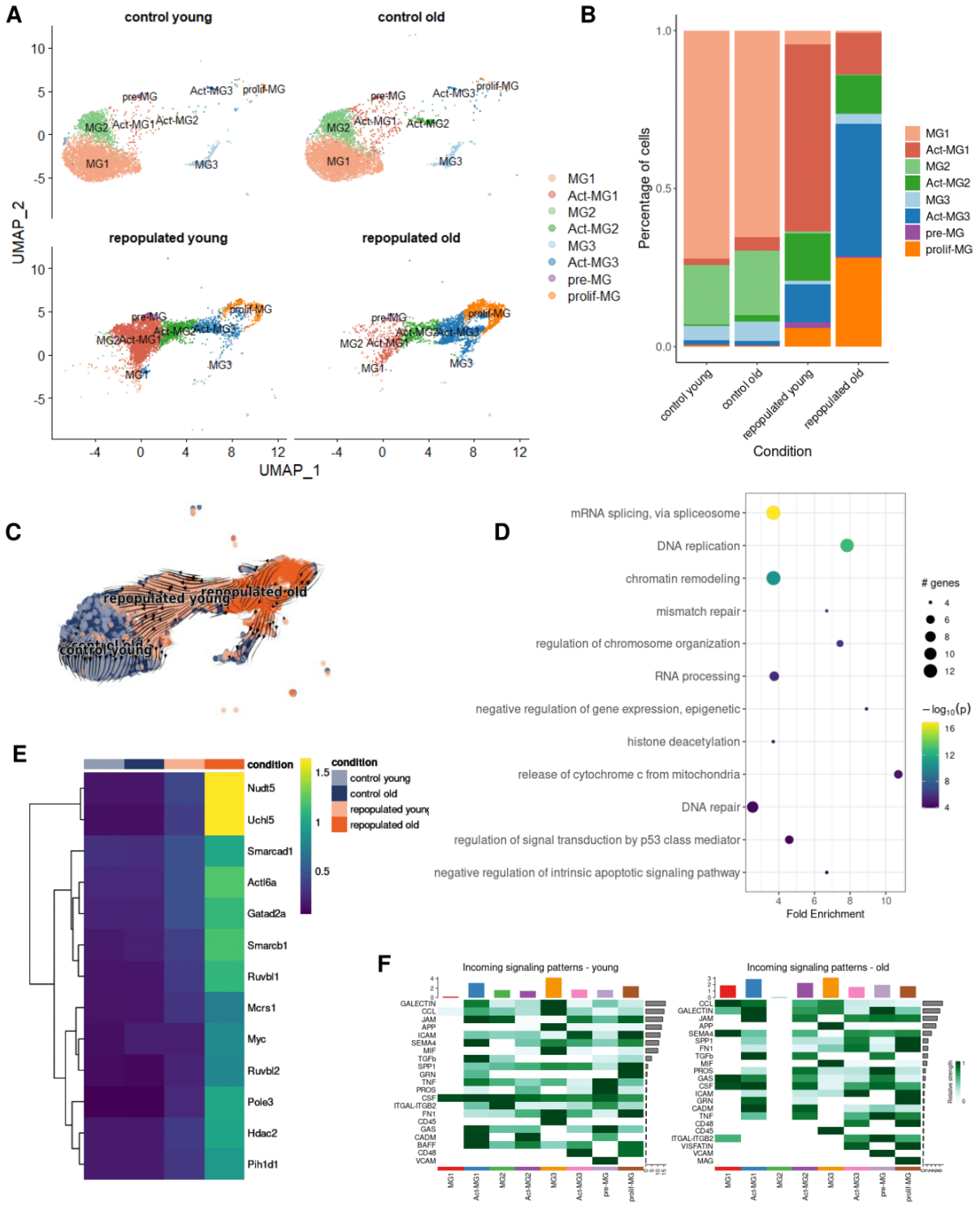

Figure 6.10 | Dysfunctional microglial repopulation in aging mice. (A) UMAP plot of scRNA-seq data showing clustering of control and repopulated microglia (MG) from young and aged mouse brains. For each condition, four replicates were combined, with cluster annotations corresponding to those shown in Fig. 6.7A. (B) Bar plots showing the fraction of cells assigned to each cluster, separated by the four experimental conditions. (C) UMAP embedding overlaid with RNA velocity vectors

(scVelo), illustrating transcriptional dynamics across conditions. (D) Dot plot of selected enriched KEGG pathways among differentially expressed genes within the activated MG3 (Act-MG3) cluster, compared to other clusters. (E) Heatmap displaying average expression of upregulated genes from the chromatin remodeling KEGG pathway enriched in Act-MG3, stratified by experimental condition. (F) Predicted intercellular communication networks showing communication probability via selected ligand–receptor pairs (y-axis) for each directed cluster–cluster interaction (x-axis).

To further dissect the functional implications of these transcriptional differences, potential intercellular communication networks within the repopulated MG populations were explored. A rich landscape of ligand-receptor (L-R) interactions across MG subtypes was identified using CellPhoneDB v 2.0[172]. Notably, extensive incoming and outgoing interactions involving premature microglia (pre-MG) and Act-MG1 clusters were detected. These interactions prominently featured genes encoding galectins, C-C motif chemokine ligands (CCLs), intercellular adhesion molecules (ICAM), semaphorin 4, and macrophage migration inhibitory factor (MIF). CCLs are well-known mediators of chemotaxis in myeloid and lymphoid cells[173], while galectins and ICAM-1 play critical roles in orchestrating immune cell migration within the brain during inflammation[174]. MIF, a multifunctional cytokine, further underscores the sustained inflammatory and immune signaling observed in aging repopulated MG (Fig. 6.10F, Fig.6.8B)[175].

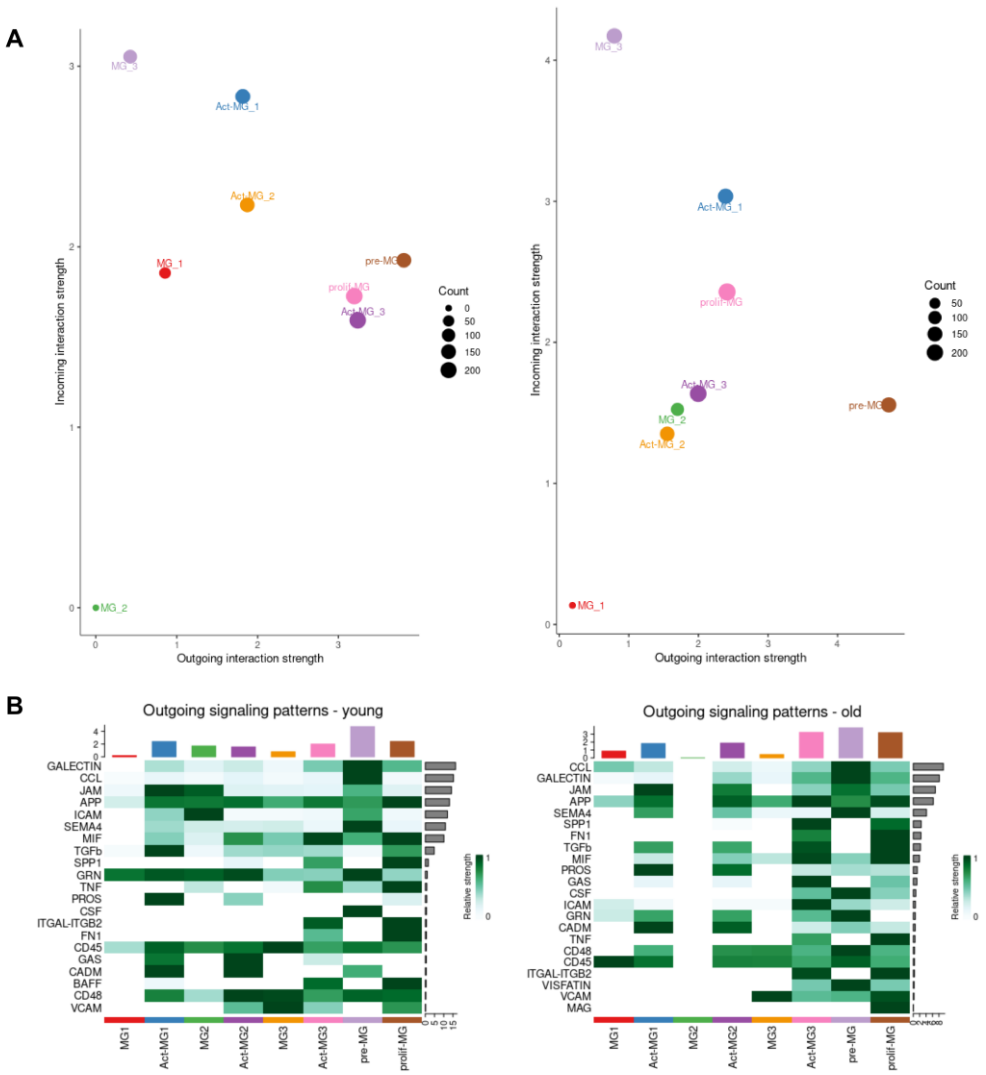

Figure 6.11 | Altered intercellular communication of repopulated microglia in young and aged mice.(A) CellChat analysis showing the enriched ratio of outgoing versus incoming interactions in repopulated microglia, presented separately for young (left) and aged (right) mice. (B) Predicted outgoing communication patterns of repopulated microglia inferred by CellChat, shown for young (left) and aged (right) mice.

These results suggest that while repopulated microglia from older mice partially restore their homeostatic phenotype, they maintain elevated proliferating and inflammatory states, which may contribute to impaired microglial function and increase susceptibility to age-associated neuroinflammation.

6.7 Distinct gene expression profiles in repopulated microglia from brains of aged mice

The distinct dynamics of repopulated microglia from aging mice prompted us to further investigate their transcriptional patterns by interrogating bulk RNA-seq and scRNA-seq datasets. Bulk RNA-seq was performed CD11b+ cells were immunosorted from both control and repopulated brains of aged mice (18-22 months). This approach offered a cost-effective generating high-resolution datasets with greater statistical power to detect differentially expressed genes (DEGs) and enriched pathways that might otherwise be overlooked in scRNA-seq due to its limited coverage.

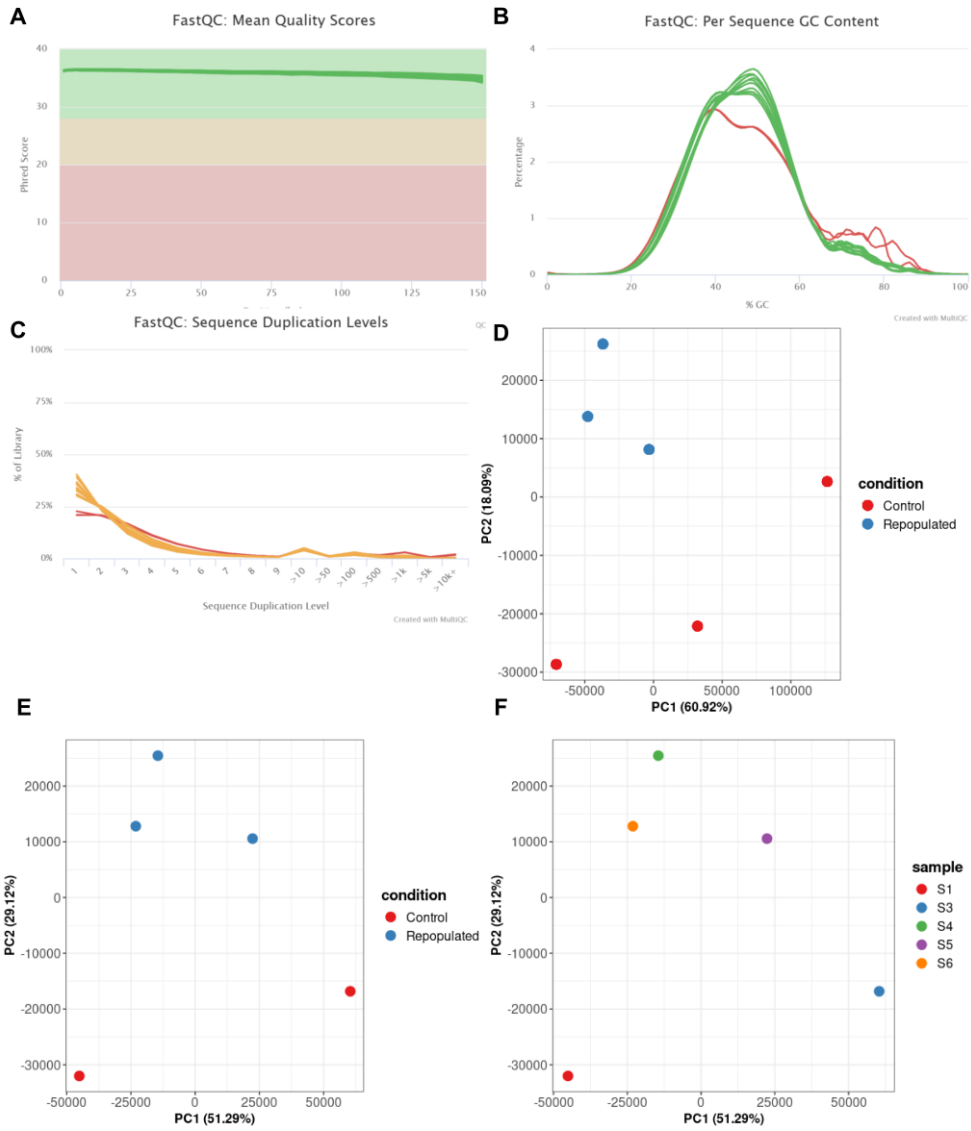

Figure 6.12 | Quality control of bulk RNA-seq data. (A–C) FastQC quality metrics for bulk RNA-seq libraries, including mean quality scores, per-sequence GC content, and sequence duplication levels.

(D–F) Principal component analysis (PCA) of bulk RNA-seq data, showing sample clustering by experimental condition (control vs. repopulated) and replicate identity.

Bulk RNA-seq analysis was carried out using linear regression models, with sample variance assessed via Principal Component Analysis (PCA). A significant outlier was excluded to preserve data integrity (Fig. 6.12).

DEG analysis revealed substantial transcriptional differences between control and repopulated microglia. As illustrated in the volcano plot (Fig. 6.13A), numerous DEGs were identified, many of which were functionally linked to cell death, apoptosis, and cellular senescence. KEGG pathway enrichment of upregulated genes in repopulated MG revealed significant enrichment of pathways linked to cell death, apoptosis, and cellular senescence, as well as HIF1, Ca^{2+}, and FoxO signaling pathways (Fig. 6.13B). Notably, *Bax*, a key pro-apoptotic gene, was markedly elevated in MG from aged mice, and showed similar upregulation in clusters of repopulated MG identified in the scRNA-seq dataset (Figure 6.14A,B). Furthermore, the expression of various apoptotic genes was higher in clusters of repopulated MG from aging mice.

The heatmap of the top 50 DEGs further demonstrated consistent downregulation of genes associated with homeostatic MG state in repopulated MG in aged mice indicating that those cells do not fully regain their mature transcriptional profile (Fig. 6.13C). Cross-validation with scRNA-seq data reinforced this finding, highlighting increased expression of additional pro-apoptotic genes, including *Lmnb1, Casp8, Psmd3* and *Bak1*, in repopulated MG from brains of older mice (Fig. 6.13D). Importantly, the enrichment of apoptotic genes expression and markers of cell death appeared restricted to the Act-MG3 cluster in aged mice (Fig. 6.13E) suggesting that cells in this cluster may be particularly susceptible to apoptotic processes.

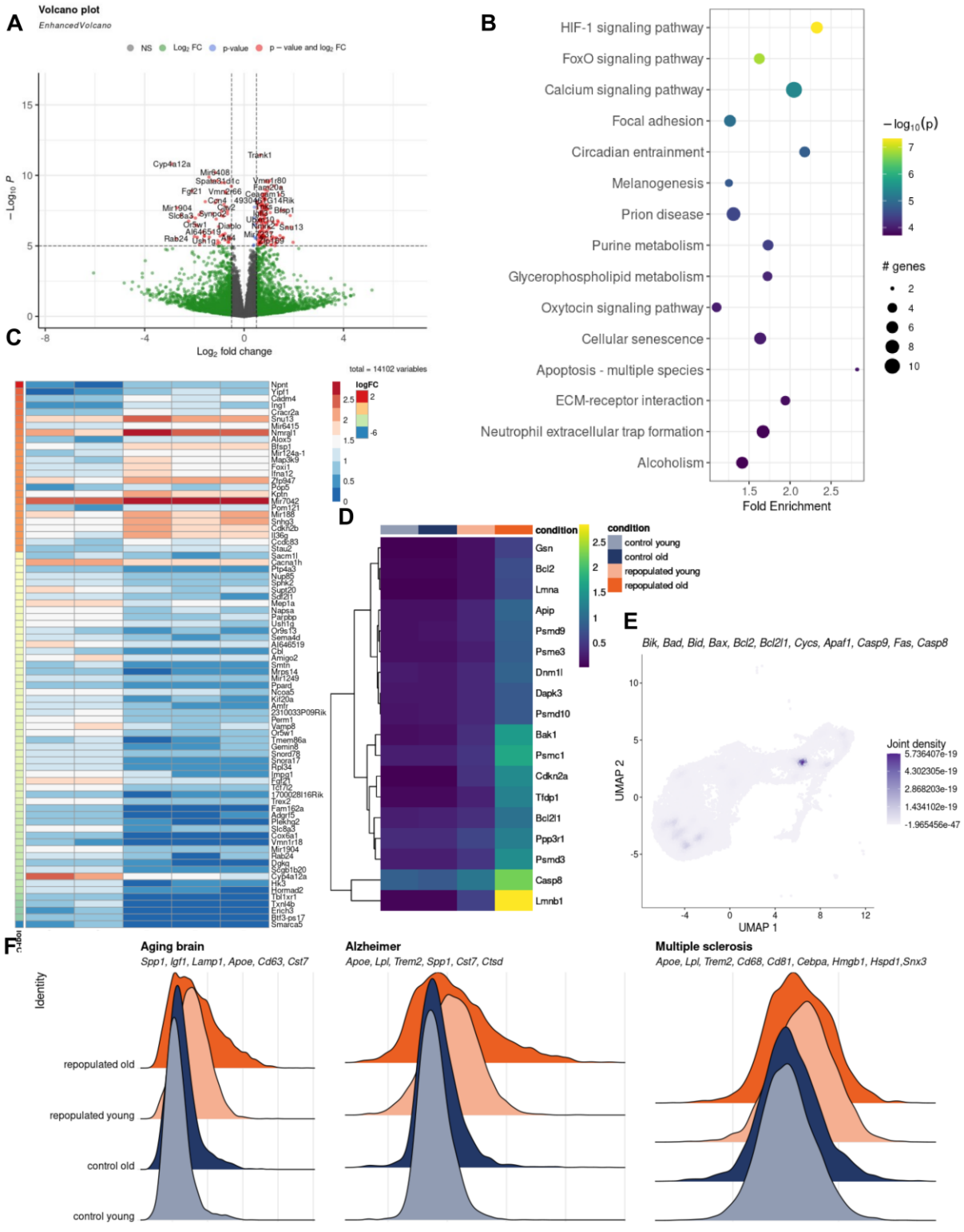

Figure 6.13 | Repopulated microglia from aged mice exhibit transcriptional signatures associated with apoptosis and neurodegenerative disease. (A) Volcano plot showing fold-change expression and significance (–log10 p-value) for all genes in control and repopulated microglia from aged mice (18–22 months). Mice received PB or BLZ-945 (200 mg/kg) orally for 21 days, followed by a 7-day recovery. Brains were perfused with PBS, enzymatically digested, and CD11b^{+} cells were FACS-sorted

for bulk RNA-seq (n = 4 per group). (B) Top 15 enriched KEGG pathways identified among differentially expressed genes (based on log_2FC and adjusted p-value thresholds) from (A). (C) Heatmap of the 50 most upregulated genes ranked by log_2FC and adjusted *p*-value < 0.05 in the bulk RNA-seq dataset. (D) Heatmap of average expression of upregulated genes from the "Apoptosis - multiple species" KEGG pathway in the scRNA-seq dataset. (E) UMAP plot showing weighted kernel density of scaled expression for selected apoptosis marker genes in the scRNA-seq dataset (related to Fig. 6.10 (A). (F) Ridge plots displaying expression scores of microglial neurodegeneration-associated gene signatures characteristic of the aging brain, Alzheimer's disease, and multiple sclerosis in scRNA-seq data.

Finally, examination of broader transcriptional signatures defined previously in different public datasets of neurological diseases revealed that repopulated microglia in aged brains expressed elevated levels of genes linked to aging, neurodegeneration, and neuroinflammation (Fig. 6.13F). Taken together, these data indicate that while repopulated MG can partially re-establish cellular microglia diversity in aging brains, they adopt a transient inflammatory phenotype characterized by persistent upregulation of pro-apoptotic pathways. This increased expression of cell-death related genes suggests that a subset of repopulated MG in aged brains may be predisposed to cell death, potentially limiting their capacity to restore and maintain long-term homeostasis.

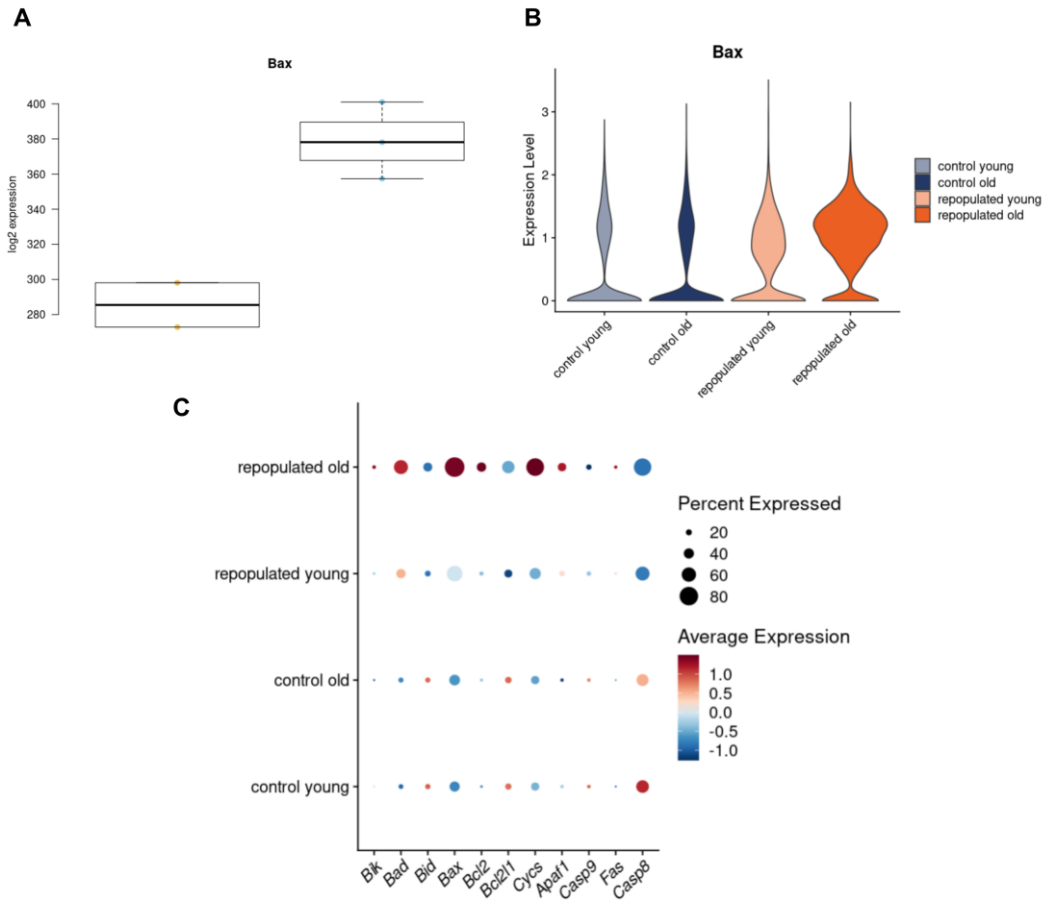

Figure 6.14 | Integration of bulk and single-cell RNA-seq reveals apoptosis gene signatures in repopulated microglia. (A) Box plot of *Bax* gene expression in bulk RNA-seq data across experimental conditions. (B) Violin plot of *Bax* gene expression in scRNA-seq data, stratified by condition (control young, control old, repopulated young, repopulated old). (C) Dot plot of selected apoptosis-related marker genes (*Bik, Bad, Bid, Bax, Bcl2, Bcl2l1, Cycs, Apaf1, Casp9, Fas, Casp8*) in experimental groups, showing average expression and percentage of cells expressing each gene.

6.8 Transcriptional signatures of migration and motility in aged repopulated microglia

In older mice, repopulated microglia displayed marked alterations in the expression of genes regulating motility and migratory function. Notably, expression of *P2ry12* and *Trem2* was significantly reduced following repopulation. The *P2ry12* receptor plays a critical role in guiding microglial migration and motility, and contributes to the initiation of neuroinflammatory responses[176]. Consistent with previous reports, we observed diminished *P2ry12* expression in aged microglia under control conditions. However, repopulated microglia

from aged mice exhibited an even more pronounced downregulation of *P2ry12*, suggesting further impairment of this functional axis (Fig. 6.15).

Microglial migration is governed by a tightly regulated balance between *P2ry12* and related purinergic receptors, such as *P2rx4* and *P2ry6*. Examination of gene expression patterns along the inferred trajectory, from prolif-MG, through activated states, and culminating in homeostatic microglia clusters, revealed dynamic shifts in the expression of these genes (Fig. 6.15C). These findings highlight the progressive adaptation of migratory signaling pathways during repopulation and emphasize their dysregulation in the aged mouse brains.

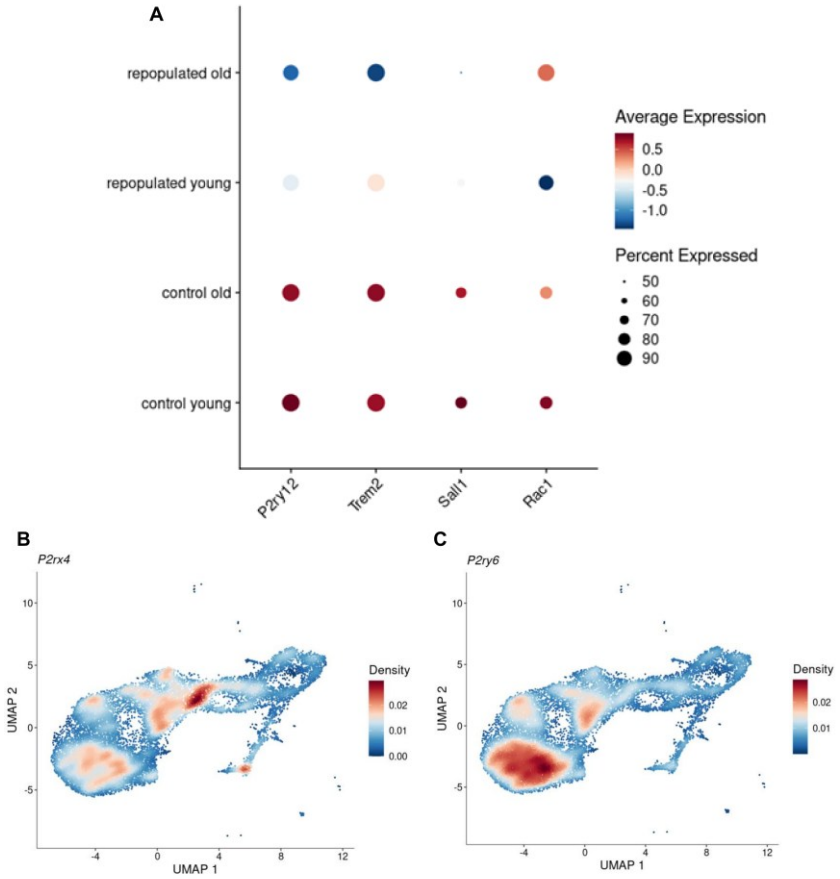

Figure 6.15 | Transcriptional programs of migration and motility in aged repopulated microglia. (A) Dot plot showing expression levels and percent expression of *P2ry12, Trem2, Sall1,* and *Rac1* across control and repopulated microglia from young and aged mice. Expression of *P2ry12*, a homeostatic and migration-associated receptor, is markedly reduced in aged control microglia and further diminished in repopulated aged groups, highlighting impaired migratory potential with aging. *Trem2* expression follows a similar trend, whereas *Rac1* expression is increased in repopulated aged microglia, suggesting partial restoration of motility pathways despite overall age-related decline. (B) (C) UMAP feature density plots illustrate spatial distribution of *P2rx4* and *P2ry6* expression across

microglial clusters. These genes act downstream of *P2ry12* to regulate migratory activity, showing distinct patterns between control and repopulated groups.

In addition to altered purinergic signaling, we detected a notable increase in *Rac1* expression in repopulated microglia from aged mice. This result contrasts with the typical decline in Rac1 observed in the brains of aged animals. *Rac1* is a central regulator of cytoskeletal remodeling and directed migration, and its upregulation suggests that repopulated microglia retain, at least in part, the capacity for motile and regenerative behaviors. This finding implies that microglia repopulation in aged brains is not fully suppressed but may proceed along a delayed trajectory compared to younger mice (Fig. 6.15A).

Observations of increased apoptotic and senescence-related gene expression in aged repopulated microglia suggest that the aged microglia niche imposes both functional limitations and survival constraints on repopulated cells. The downregulation of *P2ry12* and *Trem2* highlights reduced responsiveness to migratory cues, while the sustained upregulation of apoptotic mediators reflects heightened vulnerability to cell death. The modest recovery of *Rac1* expression, however, suggests that partial compensatory mechanisms remain active, enabling some degree of motility and structural remodeling despite the aged environment.

Together, these data demonstrate that repopulated microglia in aged brains are in a fragile balance between delayed functional maturation and increased apoptotic susceptibility. This dual phenotype contributes to their incomplete restoration of homeostatic states and may underline their limited ability to sustain long-term brain health during aging.

6.9 Dysregulation of ROCK signaling pathway in repopulated old microglia

Differential expression analysis of distinct cell clusters revealed a compelling enrichment of Reactome pathway within the Act-MG3 cluster, encompassing genes associated with Interleukin-33 (*Il-33*) and the ROCK-1 family[177]. *Il-33* is a critical regulator of microglial functional states, and its activity within Act-MG3 suggests that this cluster contains a transcriptional program directing microglia toward specialized functional roles. Genes related to *Il-33* signaling emerged as a particularly relevant pathway, with upregulation of *Il1rl1* (the ST2 receptor), *Nfkb1*, and *Mapk14*, indicating a transcriptional program favoring

pro-inflammatory activation. In particular, the reduction of expression of RHO family factors in Act-MG3 may represent an important indicator of impaired signaling processes that contribute to age-associated neurodegeneration. Such changes reflect the diminished functional competence of microglia during repopulation in aged mice. This line of inquiry underscores the significance of these genetic interactions in understanding microglial behavior in aging and neurodegeneration[178].

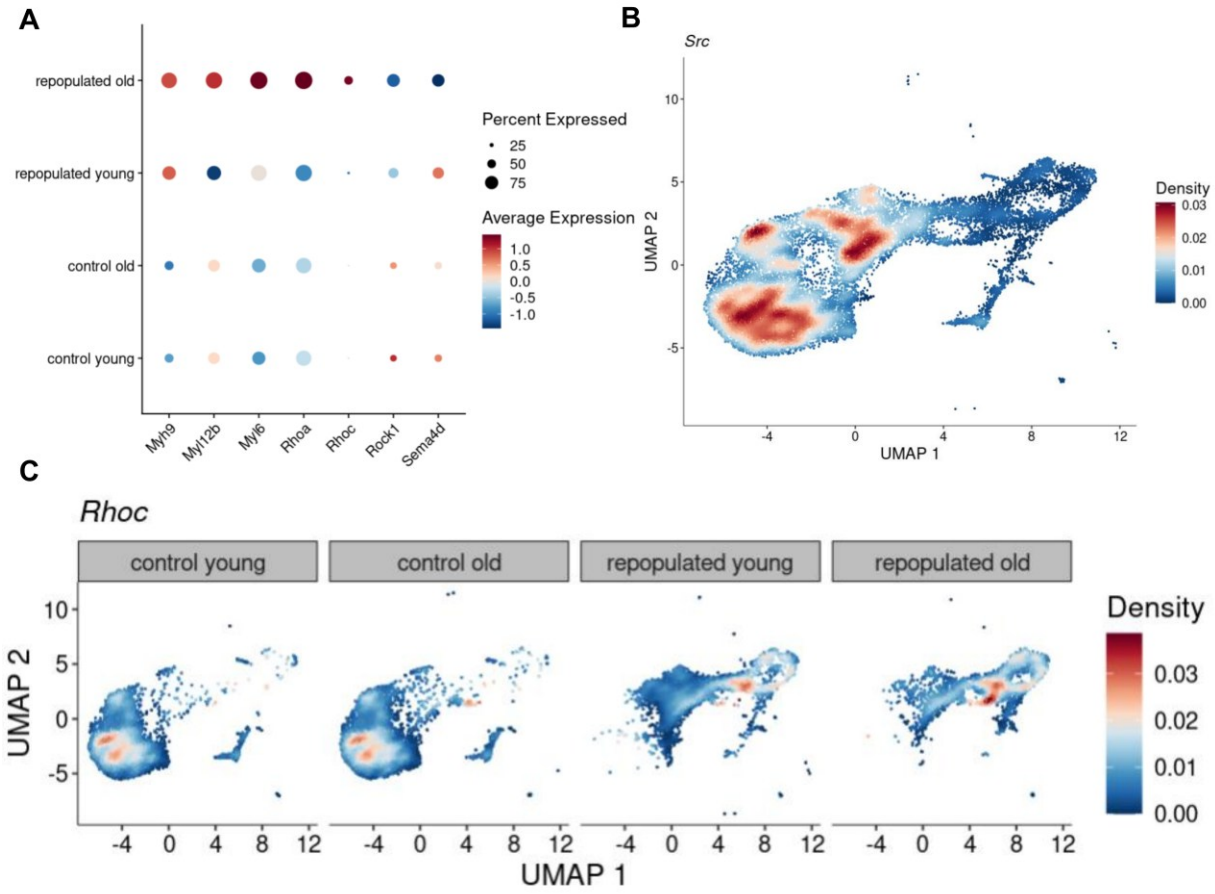

Figure 6.16 | Altered expression of ROCK-pathway genes in repopulated microglia. (A) Dot plot showing expression patterns of ROCK-pathway–associated genes (*Myl9, Myl12b, Myh9, Rhoa, Rhoc, Rock1, Stmn4d*) across microglia from experimental groups. Repopulated old microglia exhibit reduced expression of several *Rho* family genes compared to controls. (B) (C) UMAP density plots visualize the distribution of *Src* and *Rhoc* expression across microglial subsets. Rhoc expression is markedly reduced in repopulated microglia from old mice, whereas *Src* shows broad distribution across active microglial states.

In parallel, genes linked to the RHO/ROCK axis displayed marked alterations. Specifically, reduced expression of *Rock1*, and downstream effectors such as *Sema4d* (Fig. 6.16A) was observed in aged repopulated microglia, coinciding with upregulation

of stress-responsive genes, including *RhoA, Myh9, Myl6*. All of these processes were accompanied by elevation of expression of pro-inflammatory state markers. These transcriptional changes might affect cytoskeletal dynamics, suggesting impaired motility and remodeling capacity. These data identify the Il-33-ROCK signaling axis as a potential regulator of microglia functionality in aging, which disruptions correlate with enhanced inflammatory gene expression and reduced migratory potential.

6.10 Similarities in transcriptional programs of repopulated and glioma-associated microglia

The striking similarities between activated states of repopulated microglia and those described in published datasets of glioma-associated microglia from Ochocka et al. (2023) were observed[149]. In both contexts, activated microglia (Act-MG) displayed transcriptional programs enriched for pathways linked to cell motility, proliferation, inflammation, extracellular matrix (ECM) degradation, and apoptosis. These similarities suggest that molecular circuits active in GAMs and the glioma microenvironment are reminiscent of those driving repopulation

Table 6.3 | Marker genes characteristic for activated microglia (Act-MG). Representative gene signatures of Act-MG1, Act-MG2, and Act-MG3 clusters, as defined by *Ochocka et al., Cell Reports (2023)*.

Subtype	Representative marker genes
Act-MG1	MHCII protein, *Cd74, Stat1, Ifitm3, Ccl12, C4b, Tnf, Ccl2, Ccl3, Ccl4, Ccl7, Ccl2, Klf2, Klf4, Egr1, Cited2, Atf3, Fos, Fosb, Ier2*
Act-MG2	MHCII protein, *Cd74, Stat1, Ifitm3, Ccl12, C4b*
Act-MG3	MHCII protein, *Cd74, Stat1, Ifitm3, Ccl12, C4b, Gpnmb, Lglas3, Fabp5, Apoe, Spp1, Cstb, Ctsd*

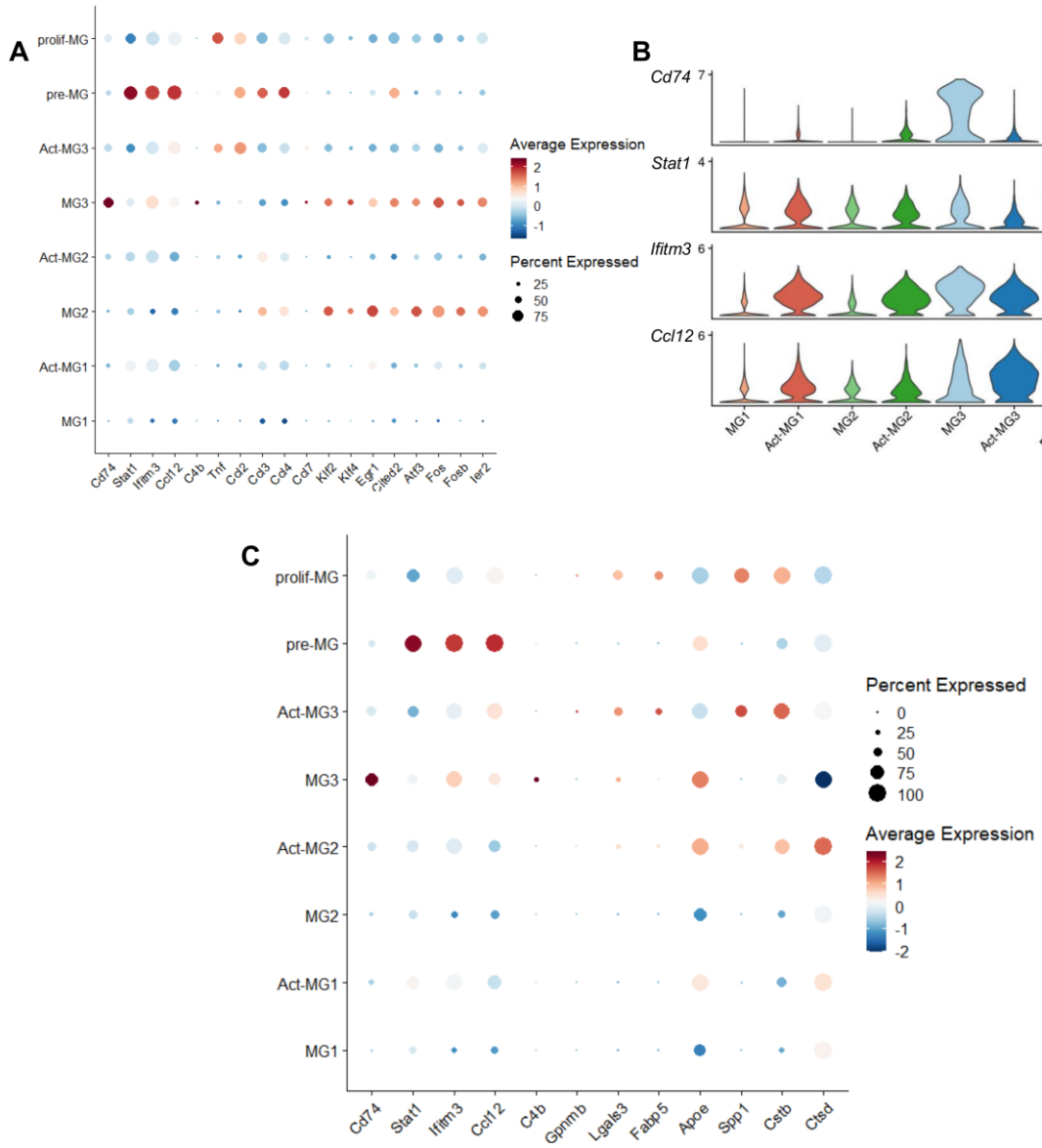

Figure 6.17 | Subtype-specific validation of activated microglia marker genes reveals distinct transcriptional signatures. (A) Dot plot showing the expression of selected marker genes for Act-MG1 across microglial subtypes. Marker selection was based on annotations from Ochocka et al., 2023. Dot size represents the percentage of cells expressing a gene, while color intensity reflects average expression level. (B) Violin plots depicting the distribution of expression levels of representative Act-MG2 marker genes (*Cd74, Stat1, Ifitm3, Ccl12,* and *C4b*) across all identified cell subtypes. These plots highlight both the presence and variability of Act-MG2 gene expression within distinct microglial populations. (C) Dot plot illustrating the expression of selected Act-MG3 marker genes across microglial subtypes. Similar to the panel (A), dot size corresponds to the proportion of cells expressing each gene, and color represents average expression intensity.

To further explore potential similarities between the transcriptomic programs of microglial subsets during repopulation and those in gliomas, we compared two datasets: scRNA-seq of immunosorted CD11b+ cells after repopulation and the dataset based on Cellular Indexing of Transcriptomes and Epitopes (CITE-seq) of CD45++ cells isolated from various murine experimental gliomas. For this comparative analysis, the focus was on the microglial subpopulations present in both datasets (Fig. 6.18A-C).

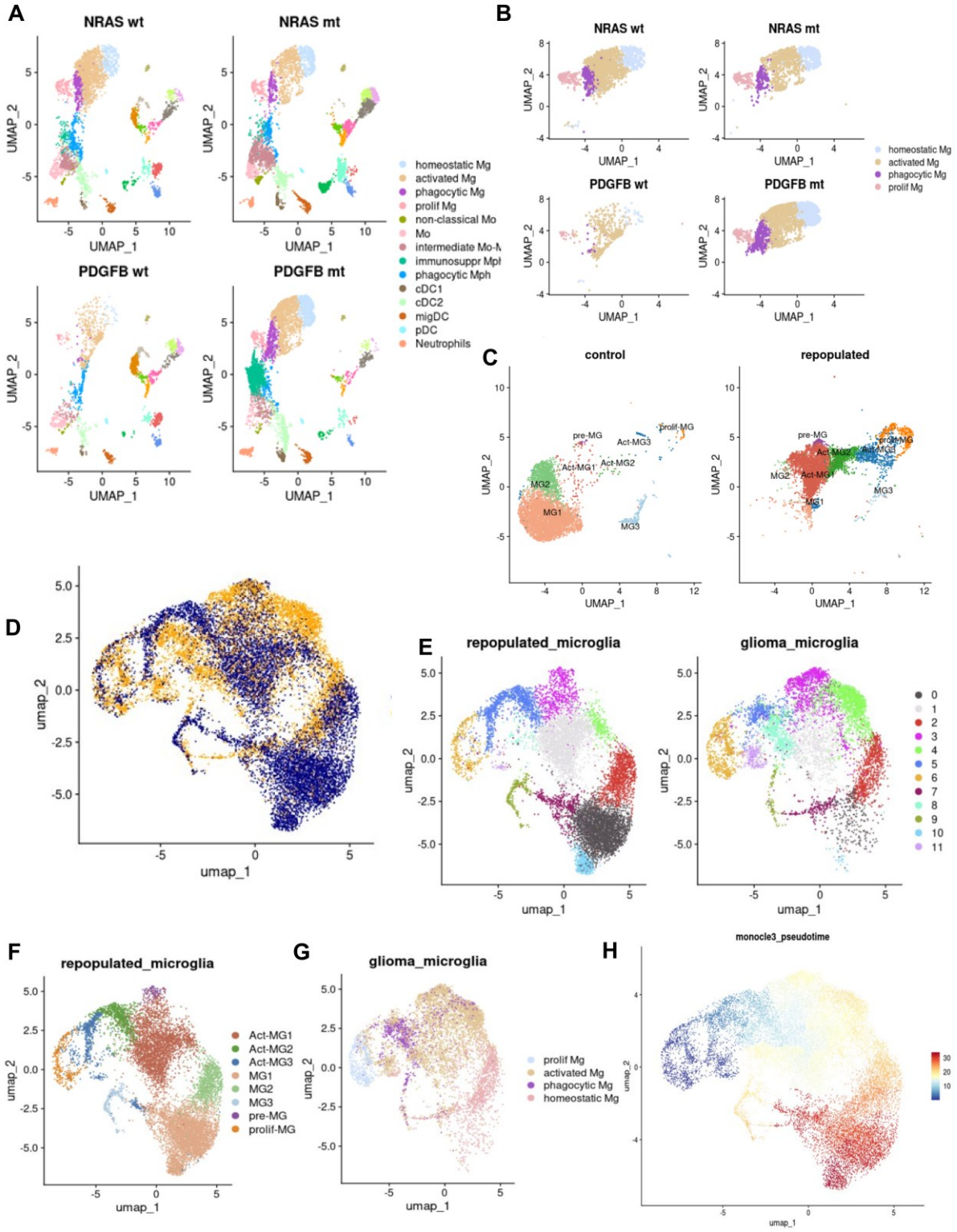

Figure 6.18 | Comparative analysis of repopulated and glioma-associated microglia. (A-C) UMAP plots showing scRNA-seq of microglia from repopulated brains compared with glioma datasets (NRAS and PDGFB gliomas). Microglial subsets are annotated according to their transcriptional state (homeostatic, activated, proliferating, phagocytic). (D-G) Integration of repopulated and glioma microglia using RPCA reveals 11 shared clusters, with differential enrichment of clusters between the two conditions. Clusters 8 and 11 correspond to phagocytic microglia enriched in gliomas, whereas

clusters 0 and 10 are enriched in repopulated microglia.(H) Trajectory analysis illustrates a shared progression from proliferating microglia through activated states toward homeostatic microglia in repopulated brains. In contrast, glioma-associated microglia are biased toward persistent activated and phagocytic states, indicating an arrested maturation trajectory in the tumor microenvironment.

Using RPCA integration (see Methods), a joint reference comprising 11 distinct clusters shared between repopulated and glioma-associated microglia was generated. Within this integrated dataset, certain clusters were preferentially enriched in one condition. For example, clusters 8 and 11 (Fig. 6.18E, F), corresponding to phagocytic microglia, were predominantly associated with gliomas and showed minimal representation in the repopulated group. Conversely, clusters 0 and 10 were enriched in repopulated microglia but nearly absent in the glioma dataset. Notably, homeostatic microglia were confined to repopulated brains, consistent with their capacity to reacquire mature signatures, whereas glioma-associated microglia demonstrated reduced representation of homeostatic states (Fig. 6.18F-H).

Trajectory inference further revealed that proliferating microglia constitute the earliest progenitor-like population in both conditions, giving rise to activated states characterized by heightened migration, differentiation, and inflammatory activity (Fig. 6.18H). From these activated states, microglia gradually transitioned toward more homeostatic profiles in repopulated brains. By contrast, in gliomas, the persistence of phagocytic and activated states suggested an arrested or maladaptive maturation trajectory.

Together, these results demonstrate that repopulated and glioma-associated microglia share a common transcriptional framework of activation but diverge in their terminal states: repopulated microglia progress toward homeostasis, whereas glioma-associated microglia are skewed toward persistent activation and phagocytosis, reflecting the pathological demands of the tumor microenvironment.

7. Discussion

7.1 Restoration of microglia functional heterogeneity after repopulation in young mice.

In the present study, we employed scRNA-seq to dissect the cellular heterogeneity of microglia following pharmacological depletion and endogenous repopulation. This paradigm of the microglia self-renewal has gained an increasing attention and emerged as a powerful model for studying microglial turnover, resilience, and regenerative capacity. It has been proposed as a path to therapeutically reset dysfunctional microglial states.

Our findings demonstrate that newly repopulated microglia arise from proliferating residual cells rather than infiltrating peripheral macrophages and that these cells are capable of re-establishing the major canonical microglial states present in the intact brain within one week after the inhibitor withdrawal. Such restoration emphasizes that microglia maintain an intrinsic transcriptional program that enables self-renewal and niche reconstruction when the resident compartment is removed[95,99,179].

However, thanks to the application of scRNA-seq our data also reveal novel transient states and age-dependent alterations. In brains of young mice, repopulation followed a structured, temporally ordered course. Within seven days after CSF1R inhibitor withdrawal, repopulating microglia recapitulated the principal homeostatic transcriptional signatures defined by markers such as *P2ry12*, *Tmem119*, and *Sall1*[10,65,180], and other core regulatory genes that enforce microglial identity and maintain neuron-supportive function[181]. The re-emergence of these states indicates that microglial replacement in the young brain is not merely repopulation in a number, but true restoration of identity. This process likely reflects preserved chromatin accessibility landscapes and TF networks (*Sall1-Mefc2-Sox9* axis) that re-establish homeostasis once inflammatory and proliferative cues subside[181,182].

However, repopulation was not a direct return to the baseline, Instead, we identified three transient activation states (Act-MG1, Act-MG2, Act-MG3) unique to the repopulating populations. These states shared molecular features associated with proliferation, phagocytosis, and migration. Activation of processes associated with cell cycling, cytoskeletal rearrangements, extracellular matrix (ECM) remodeling, chemotaxis, and phagocytic clearance, suggests that prior to stabilizing into homeostasis identities, nascent microglia pass through a functional activation phase required for a niche acquisition.

The enrichment of *Cstb* and *Ctsd*, associated with lysosomal activities, and *Spp1* and *Apoe*, linked to lipid metabolism and ECM remodeling supports the notion that microglia replacement is coupled to matrix degradation and tissue remodeling[183]. These functions may enable microglia to displace astrocytic processes, tunnel through dense neuropil, and re-establish territorial tiling, and are critical for microglia traversing the brain parenchyma, clearing debris, and remodeling their environment during repopulation[24,68,184]. These processes involve cytoskeletal reorganization, extension of motile processes, migration toward vacant niches, reminding responses seen in tumor and injury contexts[44,95,101,185].

The inflammatory-repair transcriptional signature we identified resembles activation sates reported in development, acute injury and tumor-associated microglia, suggesting a conserved regeneration program[68,81]. Upregulation of genes coding for cytokines (*Il-1β*, *Tnf*, *Il-6*) and chemokines (*Ccl2*, *Ccl3*, *Ccl4*, *Cxcl10*), implies a role for inflammatory signaling as a part of the development-like maturation program [68,81,99]. In this context, cytokines likely act as drivers of proliferation, survival and motility, while chemokine gradients guide microglial colonization of vacant spatial domains[95,186]. The fact that similar transcriptomic states emerge in microglia in glioma, traumatic injury, demyelination, and monocyte infiltration models supports the hypothesis that microglial activation is not solely a marker of disease, but also a physiological component of regenerative expansion[33,67,187].

Ligand-receptor interaction analysis further emphasizes the significant role of precursor microglia (pre-MG) in orchestrating repopulation. Pre-MG cells send strong putative signals to cells in other clusters, including those in proliferative and activated states, highlighting their decisive role in initiating the repopulation cascade. Importantly, interferon-related pathways are upregulated in these cells, which may provide both protective and detrimental effects: protective in mobilizing rapid recolonization, but detrimental in perpetuating low-level inflammatory activation that could impair long-term maturation[104,188,189]. The newly generated microglia undergo a transient “activation phase” as they migrate into the parenchyma, remodel the extracellular matrix, and integrate into neural circuits[95,101]. Importantly, the upregulation of cytokines such as *Il-1β*, *Tnf*, and *Il-6*, alongside chemokines including *Ccl2* and *Cxcl10*, highlights a transient but coordinated inflammatory response that may be necessary to support effective colonization and maturation[101]. Process of returning to homeostasis indicates that the transient activation program is neither pathological nor permanent in young animals, but rather a necessary intermediate step to restore microglial density, morphologic coverage, and functional competence. Thus microglial turnover in young brain can be seen

as a regenerative process combining proliferation, transient activation, local remodeling, and eventual normalization.

The transcriptional activation observed during early repopulation is accompanied by pronounced morphological remodeling, reflecting the dynamic structural adaptations required for microglia to reoccupy depleted brain niches[33,95,101]. In the first days following CSF1R inhibitor withdrawal, newly generated microglia adopt a hypertrophic, amoeboid-like morphology characterized by enlarged soma, thickened primary branches, and reduced arbor complexity[95,190,191]. This phenotype closely parallels the Act-Mg states detected transcriptionally, particularly those enriched for cytoskeletal reorganization, lysosomal activity, and ECM remodeling[129]. These morphological features are not static but appear to represent a transitional proliferative- migratory phase during which cells detach from their stationary niches and adopt a motile phenotype optimized for tissue colonization[44,192].

As repopulation progresses, a gradual re-establishment of highly ramified morphology is observed, corresponding to the maturation of homeostatic clusters in young brains[3,192]. Fine terminal branches reappear, territorial fields expand, and surveillance morphology is restored in parallel with the reacquisition of *P2ry12*, *Tmem119*, and *Sall1* expression[193].
This outcome suggests that structural remodeling is not merely a consequence of transcriptional change, but an active component of the repopulation program: newly formed microglia must temporarily abandon the branched structure optimized for scanning in order to divide, migrate, and populate empty parenchymal domains[101]. Following territory saturation and stabilization of cell density, morphological complexity increases, reflecting a mechanistic shift from colonization to maintenance and surveying phenotype[101,192,194].

7.2 Defective restoration of homeostatic microglia after repopulation in old mice.

A key finding of the present study is the demonstration that aging significantly alters the trajectory of microglia repopulation. While microglia after repopulation from young and aged control brains show similar transcriptomic patterns (as visualized by the appearance of similar clusters), repopulated MG from aged brains diverge substantially by exhibition fundamental defects in post-repopulation recovery[1]. Specifically, we observed a marked increase in proliferating MG alongside a reduction in homeostatic clusters, suggesting a failure to fully mature into stable, supportive phenotypes. As the transcriptional patterns were studied in one time point (7 days after cessation of CSF1R inhibitor treatment), the additional

experiments are required to define if the observed patterns are due to the delay or more permanent defect of microglia differentiation to homeostatic microglia.

Bulk RNA-seq of repopulated CD11b+ cells from brains of aged mice (18-22 months old) favors the latter interpretation. The analysis revealed downregulation of canonical homeostatic genes (*P2ry12*, *Tmem119*, *Sall1*) and upregulation of genes associated with apoptosis, inflammation and stress responses in microglia from old mice brains. The scRNA-seq data supports the notion of defective repopulation showing that repopulated MG from old mice brains display transcriptional signatures enriched in neurodegenerative and neuroinflammatory pathologies, while young repopulated MG retain a greater proportion of homeostatic subsets.

These findings align with previous findings documenting age-related shifts of MG toward dystrophic or senescent phenotypes[7,195]. Such cells are characterized by fragmented processes, impaired motility, and aberrant expression of immune molecules including MHC II, CD86, CD68, and CR3, as well as pattern recognition receptors such as TLRs and *Clec7a*[196]. In the context of repopulation, our data suggest that aging restricts the ability of MG to return to a fully homeostatic state, leaving them trapped in a partially activated, pro-inflammatory phenotype.

The impaired differentiation of aged repopulated MG can be linked to disruptions in several key pathways. First, we observed alterations in genes associated with RhoA/ROCK signaling, a pathway critical for cytoskeletal organization, motility, and survival[103,197]. Downregulation of *Rho* family genes and ROCK-dependent effectors likely compromises the structural plasticity required for effective migration, remodeling capacity and re-establishment of surveillance morphology of aged MG, impairing their ability to efficiently colonize and integrate into the brain parenchyma[198,199]. Second, purinergic signaling through *P2ry12* and *P2ry6* is markedly reduced in aged repopulated MG[180,200,201]. Given the crucial role of ATP/ADP sensing in chemotaxis, injury surveillance and neuron-microglia communication, reduction in this receptors diminishes the ability of MG to respond to subtle physiological disturbances and to engage in dynamic process extension, further compromising their functional integration and homeostatic functions[48,180,201].

Third, genes associated with interferon-related pathways remain persistently elevated, particularly in precursor and activated MG. While interferon-dependent signals might accelerate initial proliferation and colonization and are beneficial for rapid immune activation, chronic interferon signaling can promote inflammatory responses, prime MG toward neurodegeneration-associated phenotypes, and impair their return to a homeostatic state[202–204].

This finding may explain why aged repopulated MG adopt transcriptional signatures that overlap with those found in Alzheimer's disease and other neuroinflammatory conditions[204,205].

Our bulk and single-cell analyses revealed a pronounced apoptotic signature in repopulated microglia from aged brains, a finding that meaningfully complements the transcriptional patterns of impaired maturation and chronic activation. In MG from aged repopulated brains we observed upregulation of canonical pro-apoptotic genes (e.g., *Bax*, *Casp8*, *Bak1* and additional members of the intrinsic and extrinsic apoptotic cascades) and enrichment of apoptosis-related KEGG/Reactome terms in bulk RNA-seq.

At single-cell resolution these programs were not uniformly expressed but were concentrated within distinct subpopulations - most notably the transient Act-MG3 cluster - suggesting that apoptosis is a cell-state–specific outcome rather than a global feature of all repopulated microglia. The coexistence of proliferation and apoptosis within the same repopulation event implies a tightly coupled homeostatic regulatory circuit: proliferation expands the niche, while apoptosis prunes cells that fail to integrate or that are maladaptively activated[89,192]. In young animals this balance appears to favor successful integration and survival of a majority of progeny, with a controlled removal of excess or mis-specified cells. In aged brains, however, transcriptional evidence points to a shift in the set-point of this circuit: greater proportions of nascent cells express apoptotic effectors while fewer cells achieve the transcriptional hallmarks of homeostasis. This shift could reflect intrinsic defects in survival signaling, increased cellular stress (oxidative, metabolic or ER stress), impaired trophic support from the aging parenchyma, or sustained inflammatory cues that sensitize cells to programmed cell death[206,207].

Mechanistically, several observations from our data can be tied to an apoptosis-prone phenotype. Reduced expression of pro-survival and homeostatic factors interferes with transcriptional programs that normally bolster microglial fitness[208,209]. Concurrent downregulation of cytoskeletal and motility pathways (*RhoA*/ROCK axis) may limit access to trophic niches or synaptic contacts that provide survival signals[117,210]. Persistent interferon and inflammatory signaling can engage death receptors and sensitize mitochondria to dysfunction, increasing *Bax*/*Bak* activity and caspase activation[33,211]. Dysregulated proteostasis and lysosomal overload suggested by the lysosomal gene signatures may render repopulated microglia more susceptible to cell-intrinsic stress pathways and to phagoptosis by neighboring cells[212,213]. Functionally, a higher rate of apoptosis among repopulated cells will reduce the effective yield of new, functional microglia and may preferentially remove cells

that were attempting to mature, thereby biasing the surviving population toward more resilient but potentially dysfunctional phenotypes[89,98].

These apoptotic gene expression have several experimental and conceptual implications. First, apoptosis may be a major contributor to the reduced representation of homeostatic clusters in the aged repopulated MG: not only do fewer cells transit to homeostatic states, but those that do may be lost before stabilization. Second, apoptosis could release additional danger signals and cellular debris, perpetuating local inflammation and creating a feed-forward loop that further impairs maturation[30,214,215]. Third, because apoptosis was enriched in specific clusters, targeted rescue of vulnerable subpopulations – by augmenting pro-survival signaling or by transiently attenuating interferon responses during the repopulation window - might increase the fraction of repopulated cells that achieve homeostasis.

The interplay between proliferation, apoptosis, and impaired maturation reflects a delicate balance disrupted by aging[216,217]. As a result of these combined defects - impaired motility, reduced sensory responsiveness, and chronic inflammatory priming - MG in brains of young mice successfully balance the expansion with restoration of homeostasis, while MG in brains of old mice remain trapped in a proliferative and inflammatory states that may contribute to their functional decline[1,218].

Taken together, the presented findings suggest that while microglial repopulation is a robust process in brains of young mice, it is compromised with aging, leaving the CNS more vulnerable to dysregulated immunity and neurodegeneration. The inability of aged MG to reestablish homeostatic phenotypes may reduce their capacity to support neuronal survival, synaptic functions and plasticity, and overall brain homeostasis[219,220]. Furthermore, the persistence of activated and inflammatory states may exacerbate tissue vulnerability, and may further aggravate neurotoxicity or dampen microglial survival over time[54]. Consequently, repopulation in the aged brain does not result in rejuvenation, but rather is contributing to maladaptive states, such as chronic neuroinflammation observed in aging and neurodegenerative diseases[110,221,222].

The presented results highlight several potential therapeutic avenues. Targeting ROCK signaling may enhance cytoskeletal remodeling and migration in aged MG, restoring their motility and potential for tissue integration[178,198,223]. Modulating purinergic pathways could improve ATP/ADP sensing and enhance microglial surveillance capacity[115,180,200,224]. Moreover, interventions aimed at dampening chronic interferon signaling or reestablishing homeostatic transcriptional programs (*P2ry12*, *Sall1*, *Tmem119*) may rejuvenate MG function

in aging brains[202–204]. These findings emphasize that microglial repopulation is not a simple replacement process, but a dynamic sequence of events shaped by both intrinsic programs and environmental cues.

More broadly, strategies to manipulate microglial turnover, through controlled depletion and repopulation, hold promise as regenerative approaches. However, our findings caution that such strategies may have limited efficacy in aged brains unless combined with interventions that restore signaling balance and support maturation[95,194].

In summary, our study reveals that repopulated MG recapitulates the major states of control MG in young brains, but display profound deficiencies in aged brains, including impaired maturation, dysregulated ROCK and purinergic signaling, and persistent inflammatory activation. These findings underscore the significant role of age in shaping microglial resilience and highlight potential molecular targets for enhancing microglial regenerative capacity and preserving CNS homeostasis in aging and disease[13,225].

In young animals, repopulated microglia were able to recapitulate the diversity of transcriptional states found in controls. Core homeostatic clusters such as MG1 and MG2 were restored, indicating that microglial turnover is, in brains of young mice, a robust regenerative process. Yet, we also uncovered transitional populations (Act-MG1, Act-MG2, and Act-MG3), that displayed proliferative, phagocytic, migratory, and inflammatory gene programs. These states mirrored those observed in tumor-associated or injury-responsive microglia in other published datasets[67,149]. Their presence suggests that newly generated microglia undergo a transient “activation phase” as they migrate into the parenchyma, remodel the extracellular matrix, and integrate into neural circuits[95,226]. Importantly, the upregulation of cytokines such as *Il-1β*, *Tnf*, and *Il-6*, alongside chemokines including *Ccl2* and *Cxcl10*, highlights a transient but coordinated inflammatory response that may be necessary to support effective colonization and maturation[104].

The restorative trajectory observed in young mice stands in striking contrast to aged repopulation. While newly formed microglia in aged brains also enter an activated, motile phase, the transition into a highly ramified state is incomplete. Instead, aged repopulated MG retain thicker processes, reduced tip complexity, truncated branching patterns, and uneven territory distribution[30,227,228]. These cells frequently display dystrophic features (bead-like varicosities, fragmented processes, and shortened arbor length) resembling senescence-associated microglia morphotypes reported in naturally aged cortex[227,229]. The molecular correlates of this failure are reflected in persistent suppression of RhoA/ROCK-dependent cytoskeletal remodeling, reduced expression of purinergic receptors required for directional

outgrowth, and continued IFN-I pathway activation, which is known to reduce process motility and branch extension[180,183,230].

Aging alters not only the transcriptional outcome of repopulation but also its physical architecture. In young brains, morphology follows amoeboid into transitional into highly ramified transition returning microglia to full surveillance capacity[231]. In aged tissue, this trajectory appears truncated. Cells enter the amoeboid proliferative phase, but their return to a fully branched state is delayed or entirely arrested[227,232]. This aligns with our transcriptional findings showing persistent activated MG clusters and reduced representation of homeostatic subsets. Morphology thus serves as a visible proxy for deeper failures in maturation: where structure does not recover, neither do molecular programs of synaptic support, phagocytic regulation, or neuronal homeostasis.

7.3. Glioma-associated microglia may recapitulate some pathways associated with repopulation.

Integration of the microglial repopulation transcriptional program with the transcriptomes of glioma-associated microglia (GAMs) yields additional insights. A comparative analysis gene expression in clusters of active, repopulated microglia showed paralleling gene expression profiles in GAMs[149]. This reflects activation of genes related to microglia proliferation, migration, ECM reorganization, and metabolic activation[95,225]. In both cases proliferation and survival is driven by CSF1R signaling[232].

There are meaningful differences: during the repopulation the activation phase is transient and is followed by restoration of homeostatic microglia, consistent with their capacity to reacquire mature signatures[1], whereas in GAMs reduced representation of homeostatic states is observed, while activated and phagocytic states persists[67,233]. The phagocytic microglia were associated with gliomas, where its presence is prominent[67,234], while this type of microglia is underrepresented in the repopulated group, indicating that the tumor niche imposes additional instructive signals that amplify phagocytic functions[235]. Clusters 0 and 10 were enriched in repopulated microglia but nearly absent in the GAMs dataset. The persistence of activated GAM states may reflect the continuous exposure of microglia to tumor-derived growth factors, altered ECM cues, hypoxia, and metabolic reprogramming that stabilize an activation program and block resolution[235,236]. GAMs exhibit persistent expression of *Spp1*, *ApoE*, *Trem2*, *Clec7a*, *Gpnmb*, *Ctsb*, and cathepsin-associated lysosomal genes[67,237] - a transcriptional module that is also observed in repopulating Act-MG

clusters, yet becomes attenuated during successful maturation. This suggests that the repopulation program intrinsically contains the machinery for resolution and return to homeostasis, but glioma-derived cues override this trajectory.

Proliferating microglia create the earliest progenitor-like population in both conditions, giving rise to activated states. From these activated states, microglia gradually transition toward more homeostatic states during repopulation but in gliomas, the phagocytic and activated states persist suggesting an arrest or maladaptive differentiation[235,238].

One compelling mechanistic link is lipid metabolism. Both repopulating MG and GAMs express lipid metabolism related transcripts associated with phagocytosis and cholesterol efflux (*ApoE*, *Lpl*, *Fabp5*)[95,235]. During repopulation, these pathways likely support membrane synthesis for process extension and clearance of apoptotic remnants left after depletion[99,207]. In glioma, however, tumor-derived lipids accumulate faster than they can be processed, driving lysosomal stress and sustaining a Trem2-ApoE microglial state that suppresses antigen presentation and promotes tumor growth[67,239]. This recapitulates the beneficial-pathological duality of microglial plasticity: a metabolic program necessary for regeneration can be applied into a tumor-supportive phenotype when resolution signals are absent[238].

ECM remodeling represents a second axis of convergence. Early repopulating MG express genes encoding MMPs, integrins, and ECM-interacting molecules required to populate parenchyma, degrade extracellular matrix and restore network architecture[240,241]. GAMs similarly rely on ECM remodeling to facilitate tumor invasion, angiogenesis, and matrix loosening[242]. Yet in contrast to repopulation, where ECM remodeling is transiently expressed and then silenced upon stabilization[99], GAMs persistently express *Spp1*, *Fn1*, *Mmp14*, *ItgaV*, and osteopontin-associated remodeling genes[239,243]. This suggests that the glioma niche actively prevents downregulation of ECM programs, stabilizing a migratory, plastic, and structurally permissive microglial state[239].

Inflammatory signaling further highlights divergence. Both repopulating MG and GAMs upregulate *Il-1β*, *Tnf*, *Cxcl10*, and interferon-response genes, yet their functional consequences differ. In repopulation, cytokine waves may serve to recruit additional microglia, facilitate migration, and expand precursor pools[95,192]. In glioma, sustained interferon and *Il-1* signaling drives chronic activation, immunosuppression and tumor tolerance[236]. A key distinction is the absence of homeostatic repressive cues - neuronal CX3CL1 signaling – which in tumors are downregulated or physically shielded by tumor tissue[244]. Without these axes, GAMs cannot leave activation state, reinforcing the idea that repopulation and glioma

states share an early trajectory but diverge based on the presence or absence of homeostatic resolution signals[244].

Apoptosis also connects these systems. In aging, a failure to exit an activation phase leads to apoptotic elimination of repopulating MG[30]. In glioma, despite persistent activation, GAMs do not undergo equivalent apoptotic pruning - suggesting that tumors may provide survival signals (*Csf1*, *Tgf-β*, *Il-10*, lactate-driven HIF signaling) that protect activated microglia from death and thereby amplify the activated compartment[236,245]. In this view, gliomas hijack the natural regenerative program by blocking the maturation and apoptotic checkpoints that normally ensure transient activation.

The similarities between the programs of repopulated microglia in old mice and GAMs, are striking. In both context, microglia exhibit proliferative and inflammatory gene signatures, elevated expression of lipid metabolism and lysosomal genes, and reduced representation of homeostatic markers[235,238]. The data presented in this study suggests that GAMs may recapitulate some of the mechanisms underlying microglia repopulation driven by the CSF1R signaling[185,246,247]. If so, insights gained from the repair process in healthy tissue could inform strategies to redirect or terminate maladaptive activation in disease.

These links have translational implications. Interventions that shift the balance away from apoptotic loss and chronic activation during repopulation - for example transient inhibition of type-I interferon signaling, enhancement of trophic support, modulation of ROCK to restore plasticity and motility, or enhancing P2RY12 agonism to reinstate neuron-derived survival cues - may both increase the efficacy of repopulation in aged brains and reduce the utility of this program in tumors.

Collectively, these comparisons establish that repopulated microglia and GAMs exploit similar transcriptional machinery, but differ in whether the activation phase resolves or becomes permanently stabilized. Repopulation is a regenerative event that - under physiological conditions - self-terminates. Gliomas transform the same program into a chronic state, sustaining the expansion of activated, phagocytic, lipid-loaded microglia that remodel the microenvironment in favor of tumor progression. Understanding how gliomas stabilize repopulation-like programs without permitting homeostatic resolution may identify tumor-specific ligands or metabolic niches that could be therapeutically targeted to reawaken differentiation and reduce tumor support.

7.4. Limitations of the study

The differences in the morphology of microglia from brains of young and old mice have been described, and these features might be consistent with computationally predicted defects in microglia maturation and vulnerability to cell death[1]. Most of the presented findings and predictions regarding MG functional states are based on transcriptomic profiles. Gene scores were derived from literature-curated markers, many of which were validated at the protein level or in non-CNS contexts. However, discrepancies between RNA and protein expression, tissue-specific marker variability, may reduce the precision of functional annotations. Key findings regarding the phagocytic and migratory capacities rely solely on transcriptional profiles. Experimental validation (e.g., phagocytosis assays, ECM degradation studies) is essential to confirm functional relevance of the findings. However, maintaining MG from old mice in long term cultures remains difficult, limiting experimental studies in the context of aging.

8. Conclusions

1. Repopulated microglia in young mice reconstitutes the functional heterogeneity of microglia observed in control mice.
2. Repopulated microglia arise from precursor microglia and differentiate to homeostatic microglia.
3. Repopulated microglia from old mice brains remain proliferating and do not reach homeostatic microglia states.
4. Transcriptional and functional analyses show the enrichment in cell death and neurodegeneration related genes in microglia from old mice.
5. Activated microglia in glioma microenvironment show transcriptomic similarities into repopulated active microglia suggesting common gene network underlying certain processes.

References

1. Luczak-Sobotkowska, Z. M. *et al.* Tracking changes in functionality and morphology of repopulated microglia in young and old mice. *J. Neuroinflammation* **21**, 248 (2024).
2. Ajami, B., Bennett, J. L., Krieger, C., Tetzlaff, W. & Rossi, F. M. V. Local self-renewal can sustain CNS microglia maintenance and function throughout adult life. *Nat. Neurosci.* **10**, 1538–1543 (2007).
3. Tay, T. L. *et al.* A new fate mapping system reveals context-dependent random or clonal expansion of microglia. *Nat. Neurosci.* **20**, 793–803 (2017).
4. Ginhoux, F. *et al.* Fate Mapping Analysis Reveals That Adult Microglia Derive from Primitive Macrophages. *Science* **330**, 841–845 (2010).
5. Kettenmann, H., Kirchhoff, F. & Verkhratsky, A. Microglia: New Roles for the Synaptic Stripper. *Neuron* **77**, 10–18 (2013).
6. Li, Q. & Barres, B. A. Microglia and macrophages in brain homeostasis and disease. *Nat. Rev. Immunol.* **18**, 225–242 (2018).
7. Angelova, D. M. & Brown, D. R. Microglia and the aging brain: are senescent microglia the key to neurodegeneration? *J. Neurochem.* **151**, 676–688 (2019).
8. Paolicelli, R. C. *et al.* Microglia states and nomenclature: A field at its crossroads. *Neuron* **110**, 3458–3483 (2022).
9. Lawson, L. J., Perry, V. H., Dri, P. & Gordon, S. Heterogeneity in the distribution and morphology of microglia in the normal adult mouse brain. *Neuroscience* **39**, 151–170 (1990).
10. Greter, M., Lelios, I. & Croxford, A. L. Microglia Versus Myeloid Cell Nomenclature during Brain Inflammation. *Front. Immunol.* **6**, (2015).
11. Borst, K., Dumas, A. A. & Prinz, M. Microglia: Immune and non-immune functions. *Immunity* **54**, 2194–2208 (2021).
12. Vidal-Itriago, A. *et al.* Microglia morphophysiological diversity and its implications for the CNS. *Front. Immunol.* **13**, 997786 (2022).
13. Roh, J. S. & Sohn, D. H. Damage-Associated Molecular Patterns in Inflammatory Diseases. *Immune Netw.* **18**, e27 (2018).
14. Green, K. N., Crapser, J. D. & Hohsfield, L. A. To Kill a Microglia: A Case for CSF1R Inhibitors. *Trends Immunol.* **41**, 771–784 (2020).
15. Nott, A. *et al.* Brain cell type–specific enhancer–promoter interactome maps and disease - risk association. *Science* **366**, 1134–1139 (2019).
16. Mathys, H. *et al.* Single-cell transcriptomic analysis of Alzheimer's disease. *Nature* **570**, 332–337 (2019).
17. Ueno, M. *et al.* Layer V cortical neurons require microglial support for survival during postnatal development. *Nat. Neurosci.* **16**, 543–551 (2013).
18. European Alzheimer's Disease Initiative (EADI) *et al.* Meta-analysis of 74,046 individuals identifies 11 new susceptibility loci for Alzheimer's disease. *Nat. Genet.* **45**, 1452–1458 (2013).
19. Cuyvers, E. *et al.* Investigating the role of rare heterozygous TREM2 variants in Alzheimer's disease and frontotemporal dementia. *Neurobiol. Aging* **35**, 726.e11-726.e19 (2014).
20. Rayaprolu, S. *et al.* TREM2 in neurodegeneration: evidence for association of the p.R47H variant with frontotemporal dementia and Parkinson's disease. *Mol. Neurodegener.* **8**, 19 (2013).
21. Cady, J. *et al. TREM2* Variant p.R47H as a Risk Factor for Sporadic Amyotrophic Lateral Sclerosis. *JAMA Neurol.* **71**, 449 (2014).

22. Mattiace, L. A., Davies, P., Yen, S.-H. & Dickson, D. W. Microglia in cerebellar plaques in Alzheimer's disease. *Acta Neuropathol. (Berl.)* **80**, 493–498 (1990).
23. Griciuc, A. *et al.* TREM2 Acts Downstream of CD33 in Modulating Microglial Pathology in Alzheimer's Disease. *Neuron* **103**, 820-835.e7 (2019).
24. Krasemann, S. *et al.* The TREM2-APOE Pathway Drives the Transcriptional Phenotype of Dysfunctional Microglia in Neurodegenerative Diseases. *Immunity* **47**, 566-581.e9 (2017).
25. Nguyen, P. T. *et al.* Microglial Remodeling of the Extracellular Matrix Promotes Synapse Plasticity. *Cell* **182**, 388-403.e15 (2020).
26. Yoo, H.-J. & Kwon, M.-S. Aged Microglia in Neurodegenerative Diseases: Microglia Lifespan and Culture Methods. *Front. Aging Neurosci.* **13**, 766267 (2022).
27. Fan, H. *et al.* Microglia in brain aging: An overview of recent basic science and clinical research developments. *J. Biomed. Res.* **38**, 122 (2024).
28. Malvaso, A. *et al.* Microglial Senescence and Activation in Healthy Aging and Alzheimer's Disease: Systematic Review and Neuropathological Scoring. *Cells* **12**, 2824 (2023).
29. Franco-Bocanegra, D. K., McAuley, C., Nicoll, J. A. R. & Boche, D. Molecular Mechanisms of Microglial Motility: Changes in Ageing and Alzheimer's Disease. *Cells* **8**, 639 (2019).
30. Damani, M. R. *et al.* Age-related alterations in the dynamic behavior of microglia. *Aging Cell* **10**, 263–276 (2011).
31. Koellhoffer, E., McCullough, L. & Ritzel, R. Old Maids: Aging and Its Impact on Microglia Function. *Int. J. Mol. Sci.* **18**, 769 (2017).
32. Orre, M. *et al.* Isolation of glia from Alzheimer's mice reveals inflammation and dysfunction. *Neurobiol. Aging* **35**, 2746–2760 (2014).
33. Gao, C., Jiang, J., Tan, Y. & Chen, S. Microglia in neurodegenerative diseases: mechanism and potential therapeutic targets. *Signal Transduct. Target. Ther.* **8**, 359 (2023).
34. Costa, J. *et al.* The old guard: Age-related changes in microglia and their consequences. *Mech. Ageing Dev.* **197**, 111512 (2021).
35. Holtman, I. R. *et al.* Induction of a common microglia gene expression signature by aging and neurodegenerative conditions: a co-expression meta-analysis. *Acta Neuropathol. Commun.* **3**, 31 (2015).
36. Javanmehr, N., Saleki, K., Alijanizadeh, P. & Rezaei, N. Microglia dynamics in aging-related neurobehavioral and neuroinflammatory diseases. *J. Neuroinflammation* **19**, 273 (2022).
37. Kierdorf, K. & Prinz, M. Microglia in steady state. *J. Clin. Invest.* **127**, 3201–3209 (2017).
38. Paolicelli, R. C. *et al.* Synaptic Pruning by Microglia Is Necessary for Normal Brain Development. *Science* **333**, 1456–1458 (2011).
39. Woodburn, S. C., Bollinger, J. L. & Wohleb, E. S. The semantics of microglia activation: neuroinflammation, homeostasis, and stress. *J. Neuroinflammation* **18**, 258 (2021).
40. Kiraly, M., Foss, J. F. & Giordano, T. Neuroinflammation, Its Role in Alzheimer's Disease and Therapeutic Strategies. *J. Prev. Alzheimers Dis.* **10**, 686–698 (2023).
41. Keren-Shaul, H. *et al.* A Unique Microglia Type Associated with Restricting Development of Alzheimer's Disease. *Cell* **169**, 1276-1290.e17 (2017).
42. Masuda, T. *et al.* Spatial and temporal heterogeneity of mouse and human microglia at single-cell resolution. *Nature* **566**, 388–392 (2019).
43. Wake, H., Moorhouse, A. J., Jinno, S., Kohsaka, S. & Nabekura, J. Resting Microglia Directly Monitor the Functional State of Synapses *In Vivo* and Determine the Fate of Ischemic Terminals. *J. Neurosci.* **29**, 3974–3980 (2009).

44. Davalos, D. *et al.* ATP mediates rapid microglial response to local brain injury in vivo. *Nat. Neurosci.* **8**, 752–758 (2005).
45. Stevens, B. *et al.* The Classical Complement Cascade Mediates CNS Synapse Elimination. *Cell* **131**, 1164–1178 (2007).
46. Weinhard, L. *et al.* Microglia remodel synapses by presynaptic trogocytosis and spine head filopodia induction. *Nat. Commun.* **9**, 1228 (2018).
47. Nimmerjahn, A., Kirchhoff, F. & Helmchen, F. Resting Microglial Cells Are Highly Dynamic Surveillants of Brain Parenchyma in Vivo. *Science* **308**, 1314–1318 (2005).
48. Honda, S. *et al.* Extracellular ATP or ADP Induce Chemotaxis of Cultured Microglia through $G_{i/o}$ -Coupled P2Y Receptors. *J. Neurosci.* **21**, 1975–1982 (2001).
49. Mazaheri, F. *et al.* TREM 2 deficiency impairs chemotaxis and microglial responses to neuronal injury. *EMBO Rep.* **18**, 1186–1198 (2017).
50. Paolicelli, R. C. & Ferretti, M. T. Function and Dysfunction of Microglia during Brain Development: Consequences for Synapses and Neural Circuits. *Front. Synaptic Neurosci.* **9**, 9 (2017).
51. Elkabes, S., Peng, L. & Black, I. B. Lipopolysaccharide differentially regulates microglial trk receptor and neurotrophin expression. *J. Neurosci. Res.* **54**, 117–122 (1998).
52. Welser-Alves, J. V. & Milner, R. Microglia are the major source of TNF-α and TGF-β1 in postnatal glial cultures; regulation by cytokines, lipopolysaccharide, and vitronectin. *Neurochem. Int.* **63**, 47–53 (2013).
53. Xie, Y. *et al.* Transforming growth factor-β1 protects against LPC-induced cognitive deficit by attenuating pyroptosis of microglia via NF-κB/ERK1/2 pathways. *J. Neuroinflammation* **19**, 194 (2022).
54. Lull, M. E. & Block, M. L. Microglial Activation and Chronic Neurodegeneration. *Neurotherapeutics* **7**, 354–365 (2010).
55. Li, J., Baud, O., Vartanian, T., Volpe, J. J. & Rosenberg, P. A. Peroxynitrite generated by inducible nitric oxide synthase and NADPH oxidase mediates microglial toxicity to oligodendrocytes. *Proc. Natl. Acad. Sci.* **102**, 9936–9941 (2005).
56. Vassileff, N. *et al.* Microglial activation induces nitric oxide signalling and alters protein S-nitrosylation patterns in extracellular vesicles. *J. Extracell. Vesicles* **13**, e12455 (2024).
57. Cardona, A. E. *et al.* Control of microglial neurotoxicity by the fractalkine receptor. *Nat. Neurosci.* **9**, 917–924 (2006).
58. Eyo, U. B. *et al.* Regulation of Physical Microglia–Neuron Interactions by Fractalkine Signaling after Status Epilepticus. *eneuro* **3**, ENEURO.0209-16.2016 (2016).
59. Hoek, R. M. *et al.* Down-Regulation of the Macrophage Lineage Through Interaction with OX2 (CD200). *Science* **290**, 1768–1771 (2000).
60. Sellner, S. *et al.* Microglial CX3CR1 promotes adult neurogenesis by inhibiting Sirt 1/p65 signaling independent of CX3CL1. *Acta Neuropathol. Commun.* **4**, 102 (2016).
61. Zhang, S. *et al.* CD200-CD200R dysfunction exacerbates microglial activation and dopaminergic neurodegeneration in a rat model of Parkinson's disease. *J. Neuroinflammation* **8**, 154 (2011).
62. Wright, G. J. *et al.* Characterization of the CD200 Receptor Family in Mice and Humans and Their Interactions with CD200. *J. Immunol.* **171**, 3034–3046 (2003).
63. Winter, A. N. *et al.* Two forms of CX3CL1 display differential activity and rescue cognitive deficits in CX3CL1 knockout mice. *J. Neuroinflammation* **17**, 157 (2020).
64. Walker, D. G., Dalsing-Hernandez, J. E., Campbell, N. A. & Lue, L.-F. Decreased expression of CD200 and CD200 receptor in Alzheimer's disease: A potential mechanism leading to chronic inflammation. *Exp. Neurol.* **215**, 5–19 (2009).
65. Butovsky, O. *et al.* Identification of a unique TGF-β–dependent molecular and functional signature in microglia. *Nat. Neurosci.* **17**, 131–143 (2014).

66. Goldmann, T. *et al.* Origin, fate and dynamics of macrophages at central nervous system interfaces. *Nat. Immunol.* **17**, 797–805 (2016).
67. Ochocka, N. *et al.* Single-cell RNA sequencing reveals functional heterogeneity of glioma-associated brain macrophages. *Nat. Commun.* **12**, 1151 (2021).
68. Hammond, T. R. *et al.* Single-Cell RNA Sequencing of Microglia throughout the Mouse Lifespan and in the Injured Brain Reveals Complex Cell-State Changes. *Immunity* **50**, 253-271.e6 (2019).
69. Zheng, J. *et al.* Single-cell RNA-seq analysis reveals compartment-specific heterogeneity and plasticity of microglia. *iScience* **24**, 102186 (2021).
70. Yaqubi, M. *et al.* Analysis of the microglia transcriptome across the human lifespan using single cell RNA sequencing. *J. Neuroinflammation* **20**, 132 (2023).
71. Guo, M. *et al.* Microglial exosomes facilitate α-synuclein transmission in Parkinson's disease. *Brain* **143**, 1476–1497 (2020).
72. Béraud, D. *et al.* Microglial Activation and Antioxidant Responses Induced by the Parkinson's Disease Protein α-Synuclein. *J. Neuroimmune Pharmacol.* **8**, 94–117 (2013).
73. Gehrmann, J., Matsumoto, Y. & Kreutzberg, G. W. Microglia: Intrinsic immuneffector cell of the brain. *Brain Res. Rev.* **20**, 269–287 (1995).
74. Ransohoff, R. M. How neuroinflammation contributes to neurodegeneration. *Science* **353**, 777–783 (2016).
75. Dubbelaar, M. L., Kracht, L., Eggen, B. J. L. & Boddeke, E. W. G. M. The Kaleidoscope of Microglial Phenotypes. *Front. Immunol.* **9**, 1753 (2018).
76. Howe, C. L., Mayoral, S. & Rodriguez, M. Activated microglia stimulate transcriptional changes in primary oligodendrocytes via IL-1β. *Neurobiol. Dis.* **23**, 731–739 (2006).
77. Wang, Y. *et al.* Single-cell RNA sequencing reveals roles of unique retinal microglia types in early diabetic retinopathy. *Diabetol. Metab. Syndr.* **16**, 49 (2024).
78. Zawadzka, M. *et al.* Early steps of microglial activation are directly affected by neuroprotectant FK506 in both in vitro inflammation and in rat model of stroke. *J. Mol. Med.* **90**, 1459–1471 (2012).
79. Rauschmeier, R. *et al.* Bhlhe40 and Bhlhe41 transcription factors regulate alveolar macrophage self-renewal and identity. *EMBO J.* **38**, e101233 (2019).
80. Rollins, D. A., Coppo, M. & Rogatsky, I. Minireview: Nuclear Receptor Coregulators of the p160 Family: Insights into Inflammation and Metabolism. *Mol. Endocrinol.* **29**, 502–517 (2015).
81. Matcovitch-Natan, O. *et al.* Microglia development follows a stepwise program to regulate brain homeostasis. *Science* **353**, aad8670 (2016).
82. Popova, G. *et al.* Human microglia states are conserved across experimental models and regulate neural stem cell responses in chimeric organoids. *Cell Stem Cell* **28**, 2153-2166.e6 (2021).
83. Marsh, S. E. *et al.* Dissection of artifactual and confounding glial signatures by single-cell sequencing of mouse and human brain. *Nat. Neurosci.* **25**, 306–316 (2022).
84. DePaula-Silva, A. B. *et al.* Differential transcriptional profiles identify microglial- and macrophage-specific gene markers expressed during virus-induced neuroinflammation. *J. Neuroinflammation* **16**, 152 (2019).
85. Gomez Perdiguero, E., Schulz, C. & Geissmann, F. Development and homeostasis of "resident" myeloid cells: The case of the microglia. *Glia* **61**, 112–120 (2013).
86. Lawson, L. J., Perry, V. H., Dri, P. & Gordon, S. Heterogeneity in the distribution and morphology of microglia in the normal adult mouse brain. *Neuroscience* **39**, 151–170 (1990).
87. Cadiz, M. P. *et al.* Culture shock: microglial heterogeneity, activation, and disrupted single-cell microglial networks in vitro. *Mol. Neurodegener.* **17**, 26 (2022).

88. Quarta, A. *et al.* Murine iPSC-derived microglia and macrophage cell culture models recapitulate distinct phenotypical and functional properties of classical and alternative neuro-immune polarisation. *Brain. Behav. Immun.* **82**, 406–421 (2019).
89. Askew, K. *et al.* Coupled Proliferation and Apoptosis Maintain the Rapid Turnover of Microglia in the Adult Brain. *Cell Rep.* **18**, 391–405 (2017).
90. Rademakers, R. *et al.* Mutations in the colony stimulating factor 1 receptor (CSF1R) gene cause hereditary diffuse leukoencephalopathy with spheroids. *Nat. Genet.* **44**, 200–205 (2012).
91. Lin, H. *et al.* Discovery of a Cytokine and Its Receptor by Functional Screening of the Extracellular Proteome. *Science* **320**, 807–811 (2008).
92. Sherr, C. J. *et al.* The c-fms proto-oncogene product is related to the receptor for the mononuclear phagocyte growth factor, CSF 1. *Cell* **41**, 665–676 (1985).
93. Hume, D. A., Monkley, S. J. & Wainwright, B. J. Detection of *c-fms* protooncogene in early mouse embryos by whole mount *in situ* hybridization indicates roles for macrophages in tissue remodelling. *Br. J. Haematol.* **90**, 939–942 (1995).
94. Erblich, B., Zhu, L., Etgen, A. M., Dobrenis, K. & Pollard, J. W. Absence of Colony Stimulation Factor-1 Receptor Results in Loss of Microglia, Disrupted Brain Development and Olfactory Deficits. *PLoS ONE* **6**, e26317 (2011).
95. Elmore, M. R. P. *et al.* Colony-Stimulating Factor 1 Receptor Signaling Is Necessary for Microglia Viability, Unmasking a Microglia Progenitor Cell in the Adult Brain. *Neuron* **82**, 380–397 (2014).
96. Hagemeyer, N. *et al.* Microglia contribute to normal myelinogenesis and to oligodendrocyte progenitor maintenance during adulthood. *Acta Neuropathol. (Berl.)* **134**, 441–458 (2017).
97. Coleman, L. G., Zou, J. & Crews, F. T. Microglial depletion and repopulation in brain slice culture normalizes sensitized proinflammatory signaling. *J. Neuroinflammation* **17**, 27 (2020).
98. Najafi, A. R. *et al.* A limited capacity for microglial repopulation in the adult brain. *Glia* **66**, 2385–2396 (2018).
99. Zhan, L. *et al.* Proximal recolonization by self-renewing microglia re-establishes microglial homeostasis in the adult mouse brain. *PLOS Biol.* **17**, e3000134 (2019).
100. Rice, R. A. *et al.* Elimination of Microglia Improves Functional Outcomes Following Extensive Neuronal Loss in the Hippocampus. *J. Neurosci.* **35**, 9977–9989 (2015).
101. Huang, Y. *et al.* Repopulated microglia are solely derived from the proliferation of residual microglia after acute depletion. *Nat. Neurosci.* **21**, 530–540 (2018).
102. Elmore, M. R. P., Lee, R. J., West, B. L. & Green, K. N. Characterizing Newly Repopulated Microglia in the Adult Mouse: Impacts on Animal Behavior, Cell Morphology, and Neuroinflammation. *PLOS ONE* **10**, e0122912 (2015).
103. Kierdorf, K. *et al.* Microglia emerge from erythromyeloid precursors via Pu.1- and Irf8-dependent pathways. *Nat. Neurosci.* **16**, 273–280 (2013).
104. León-Rodríguez, A., Grondona, J. M., Marín-Wong, S., López-Aranda, M. F. & López-Ávalos, M. D. Long-term reprogramming of primed microglia after moderate inhibition of CSF1R signaling. *Glia* **73**, 175–195 (2025).
105. Nakai, R., Kohyama, K., Nishito, Y. & Sakuma, H. CSF1R-Dependent Microglial Repopulation and Contact-Dependent Inhibition of Proliferation In Vitro. *Brain Sci.* **15**, 825 (2025).
106. Yao, Y. *et al.* Dynamics of spinal microglia repopulation following an acute depletion. *Sci. Rep.* **6**, 22839 (2016).
107. Panatier, A. & Robitaille, R. The Soothing Touch: Microglial Contact Influences Neuronal Excitability. *Dev. Cell* **23**, 1125–1126 (2012).

108. Morrison, H. W. & Filosa, J. A. A quantitative spatiotemporal analysis of microglia morphology during ischemic stroke and reperfusion. *J. Neuroinflammation* **10**, 782 (2013).
109. Parakalan, R. *et al.* Transcriptome analysis of amoeboid and ramified microglia isolated from the corpus callosum of rat brain. *BMC Neurosci.* **13**, 64 (2012).
110. Sierra, A. *et al.* Microglia Shape Adult Hippocampal Neurogenesis through Apoptosis-Coupled Phagocytosis. *Cell Stem Cell* **7**, 483–495 (2010).
111. Abiega, O. *et al.* Neuronal Hyperactivity Disturbs ATP Microgradients, Impairs Microglial Motility, and Reduces Phagocytic Receptor Expression Triggering Apoptosis/Microglial Phagocytosis Uncoupling. *PLOS Biol.* **14**, e1002466 (2016).
112. Ling, E. & Wong, W. The origin and nature of ramified and amoeboid microglia: A historical review and current concepts. *Glia* **7**, 9–18 (1993).
113. Bachstetter, A. D. *et al.* Rod-shaped microglia morphology is associated with aging in 2 human autopsy series. *Neurobiol. Aging* **52**, 98–105 (2017).
114. Zhu, H. *et al.* Noteworthy perspectives on microglia in neuropsychiatric disorders. *J. Neuroinflammation* **20**, 223 (2023).
115. Beaino, W. *et al.* Purinergic receptors P2Y12R and P2X7R: potential targets for PET imaging of microglia phenotypes in multiple sclerosis. *J. Neuroinflammation* **14**, 259 (2017).
116. Fekete, R. *et al.* Microglia control the spread of neurotropic virus infection via P2Y12 signalling and recruit monocytes through P2Y12-independent mechanisms. *Acta Neuropathol. (Berl.)* **136**, 461–482 (2018).
117. Madry, C. *et al.* Microglial Ramification, Surveillance, and Interleukin-1β Release Are Regulated by the Two-Pore Domain K+ Channel THIK-1. *Neuron* **97**, 299-312.e6 (2018).
118. Henry, C. J., Huang, Y., Wynne, A. M. & Godbout, J. P. Peripheral lipopolysaccharide (LPS) challenge promotes microglial hyperactivity in aged mice that is associated with exaggerated induction of both pro-inflammatory IL-1β and anti-inflammatory IL-10 cytokines. *Brain. Behav. Immun.* **23**, 309–317 (2009).
119. Yao, L. *et al.* Toll-like receptor 4 mediates microglial activation and production of inflammatory mediators in neonatal rat brain following hypoxia: role of TLR4 in hypoxic microglia. *J. Neuroinflammation* **10**, 785 (2013).
120. Henry, R. J. *et al.* Microglial Depletion with CSF1R Inhibitor During Chronic Phase of Experimental Traumatic Brain Injury Reduces Neurodegeneration and Neurological Deficits. *J. Neurosci.* **40**, 2960–2974 (2020).
121. O'Neil, S. M., Witcher, K. G., McKim, D. B. & Godbout, J. P. Forced turnover of aged microglia induces an intermediate phenotype but does not rebalance CNS environmental cues driving priming to immune challenge. *Acta Neuropathol. Commun.* **6**, 129 (2018).
122. Li, X. *et al.* Microglial replacement in the aged brain restricts neuroinflammation following intracerebral hemorrhage. *Cell Death Dis.* **13**, 33 (2022).
123. Goodwin, S., McPherson, J. D. & McCombie, W. R. Coming of age: ten years of next-generation sequencing technologies. *Nat. Rev. Genet.* **17**, 333–351 (2016).
124. Sanger, F., Nicklen, S. & Coulson, A. R. DNA sequencing with chain-terminating inhibitors. *Proc. Natl. Acad. Sci.* **74**, 5463–5467 (1977).
125. Glenn, T. C. Field guide to next-generation DNA sequencers. *Mol. Ecol. Resour.* **11**, 759–769 (2011).
126. Ronaghi, M. Pyrosequencing Sheds Light on DNA Sequencing. *Genome Res.* **11**, 3–11 (2001).
127. Jain, M., Olsen, H. E., Paten, B. & Akeson, M. The Oxford Nanopore MinION: delivery of nanopore sequencing to the genomics community. *Genome Biol.* **17**, 239 (2016).
128. Bentley, D. R. *et al.* Accurate whole human genome sequencing using reversible terminator chemistry. *Nature* **456**, 53–59 (2008).

129. Huang, J. *et al.* A reference human genome dataset of the BGISEQ-500 sequencer. *GigaScience* **6**, gix024 (2017).
130. Eid, J. *et al.* Real-Time DNA Sequencing from Single Polymerase Molecules. *Science* **323**, 133–138 (2009).
131. Jain, M. *et al.* Nanopore sequencing and assembly of a human genome with ultra-long reads. *Nat. Biotechnol.* **36**, 338–345 (2018).
132. Li, Z., Yin, L., Li, Y., Cao, Y. & Zeng, H. Single-Cell RNA-Sequencing Reveals the Cellular and Genetic Heterogeneity of Skin Scar to Verify the Therapeutic Effects and Mechanism of Action of Dispel-Scar Ointment in Hypertrophic Scar Inhibition. *Evid. Based Complement. Alternat. Med.* **2022**, 1–27 (2022).
133. Stoeckius, M. *et al.* Simultaneous epitope and transcriptome measurement in single cells. *Nat. Methods* **14**, 865–868 (2017).
134. Butler, A., Hoffman, P., Smibert, P., Papalexi, E. & Satija, R. Integrating single-cell transcriptomic data across different conditions, technologies, and species. *Nat. Biotechnol.* **36**, 411–420 (2018).
135. McGinnis, C. S. *et al.* MULTI-seq: sample multiplexing for single-cell RNA sequencing using lipid-tagged indices. *Nat. Methods* **16**, 619–626 (2019).
136. Lause, J., Berens, P. & Kobak, D. Analytic Pearson residuals for normalization of single-cell RNA-seq UMI data. *Genome Biol.* **22**, 258 (2021).
137. Choudhary, S. & Satija, R. Comparison and evaluation of statistical error models for scRNA-seq. *Genome Biol.* **23**, 27 (2022).
138. Hafemeister, C. & Satija, R. Normalization and variance stabilization of single-cell RNA-seq data using regularized negative binomial regression. *Genome Biol.* **20**, 296 (2019).
139. Jacoby, W. G. Loess: *Elect. Stud.* **19**, 577–613 (2000).
140. Townes, F. W., Hicks, S. C., Aryee, M. J. & Irizarry, R. A. Feature selection and dimension reduction for single-cell RNA-Seq based on a multinomial model. *Genome Biol.* **20**, 295 (2019).
141. Tsuyuzaki, K., Sato, H., Sato, K. & Nikaido, I. Benchmarking principal component analysis for large-scale single-cell RNA-sequencing. *Genome Biol.* **21**, 9 (2020).
142. McInnes, L., Healy, J. & Melville, J. UMAP: Uniform Manifold Approximation and Projection for Dimension Reduction. Preprint at https://doi.org/10.48550/arXiv.1802.03426 (2020).
143. Healy, J. & McInnes, L. Uniform manifold approximation and projection. *Nat. Rev. Methods Primer* **4**, 82 (2024).
144. Traag, V. A., Waltman, L. & Van Eck, N. J. From Louvain to Leiden: guaranteeing well-connected communities. *Sci. Rep.* **9**, 5233 (2019).
145. Zhu, X. *et al.* Single-Cell Clustering Based on Shared Nearest Neighbor and Graph Partitioning. *Interdiscip. Sci. Comput. Life Sci.* **12**, 117–130 (2020).
146. Baran, Y. *et al.* MetaCell: analysis of single-cell RNA-seq data using K-nn graph partitions. *Genome Biol.* **20**, 206 (2019).
147. Waltman, L. & Van Eck, N. J. A smart local moving algorithm for large-scale modularity-based community detection. *Eur. Phys. J. B* **86**, 471 (2013).
148. Andreatta, M. *et al.* Interpretation of T cell states from single-cell transcriptomics data using reference atlases. *Nat. Commun.* **12**, 2965 (2021).
149. Ochocka, N. *et al.* Specialized functions and sexual dimorphism explain the functional diversity of the myeloid populations during glioma progression. *Cell Rep.* **42**, 111971 (2023).
150. Robinson, M. D., McCarthy, D. J. & Smyth, G. K. edgeR : a Bioconductor package for differential expression analysis of digital gene expression data. *Bioinformatics* **26**, 139–140 (2010).

151. Chen, Y., Chen, L., Lun, A. T. L., Baldoni, P. L. & Smyth, G. K. edgeR v4: powerful differential analysis of sequencing data with expanded functionality and improved support for small counts and larger datasets. *Nucleic Acids Res.* **53**, gkaf018 (2025).
152. Holmes, S. & Huber, W. *Modern Statistics for Modern Biology*. (Cambridge university press, Cambridge, United Kingdom, 2019).
153. Ulgen, E., Ozisik, O. & Sezerman, O. U. pathfindR: An R Package for Comprehensive Identification of Enriched Pathways in Omics Data Through Active Subnetworks. *Front. Genet.* **10**, 858 (2019).
154. La Manno, G. *et al.* RNA velocity of single cells. *Nature* **560**, 494–498 (2018).
155. Bergen, V., Lange, M., Peidli, S., Wolf, F. A. & Theis, F. J. Generalizing RNA velocity to transient cell states through dynamical modeling. *Nat. Biotechnol.* **38**, 1408–1414 (2020).
156. Jin, S., Plikus, M. V. & Nie, Q. CellChat for systematic analysis of cell–cell communication from single-cell transcriptomics. *Nat. Protoc.* https://doi.org/10.1038/s41596-024-01045-4 (2024) doi:10.1038/s41596-024-01045-4.
157. Bolger, A. M., Lohse, M. & Usadel, B. Trimmomatic: a flexible trimmer for Illumina sequence data. *Bioinformatics* **30**, 2114–2120 (2014).
158. Dobin, A. *et al.* STAR: ultrafast universal RNA-seq aligner. *Bioinformatics* **29**, 15–21 (2013).
159. Robinson, M. D. & Oshlack, A. A scaling normalization method for differential expression analysis of RNA-seq data. *Genome Biol.* **11**, R25 (2010).
160. Durinck, S. *et al.* BioMart and Bioconductor: a powerful link between biological databases and microarray data analysis. *Bioinformatics* **21**, 3439–3440 (2005).
161. Ritchie, M. E. *et al.* limma powers differential expression analyses for RNA-sequencing and microarray studies. *Nucleic Acids Res.* **43**, e47–e47 (2015).
162. Luecken, M. D. *et al.* Benchmarking atlas-level data integration in single-cell genomics. *Nat. Methods* **19**, 41–50 (2022).
163. Stuart, T. *et al.* Comprehensive Integration of Single-Cell Data. *Cell* **177**, 1888-1902.e21 (2019).
164. Van Den Berge, K. *et al.* Trajectory-based differential expression analysis for single-cell sequencing data. *Nat. Commun.* **11**, 1201 (2020).
165. Trapnell, C. *et al.* The dynamics and regulators of cell fate decisions are revealed by pseudotemporal ordering of single cells. *Nat. Biotechnol.* **32**, 381–386 (2014).
166. Cao, J. *et al.* Comprehensive single-cell transcriptional profiling of a multicellular organism. *Science* **357**, 661–667 (2017).
167. Zheng, G. X. Y. *et al.* Massively parallel digital transcriptional profiling of single cells. *Nat. Commun.* **8**, 14049 (2017).
168. Andreatta, M. *et al.* Interpretation of T cell states from single-cell transcriptomics data using reference atlases. *Nat. Commun.* **12**, 2965 (2021).
169. Pepe, G. *et al.* Selective proliferative response of microglia to alternative polarization signals. *J. Neuroinflammation* **14**, 236 (2017).
170. Smith, J. A., Das, A., Ray, S. K. & Banik, N. L. Role of pro-inflammatory cytokines released from microglia in neurodegenerative diseases. *Brain Res. Bull.* **87**, 10–20 (2012).
171. Hanisch, U. Microglia as a source and target of cytokines. *Glia* **40**, 140–155 (2002).
172. Efremova, M., Vento-Tormo, M., Teichmann, S. A. & Vento-Tormo, R. CellPhoneDB: inferring cell–cell communication from combined expression of multi-subunit ligand–receptor complexes. *Nat. Protoc.* **15**, 1484–1506 (2020).
173. Gschwandtner, M., Derler, R. & Midwood, K. S. More Than Just Attractive: How CCL2 Influences Myeloid Cell Behavior Beyond Chemotaxis. *Front. Immunol.* **10**, 2759 (2019).
174. Lyck, R. & Enzmann, G. The physiological roles of ICAM-1 and ICAM-2 in neutrophil migration into tissues: *Curr. Opin. Hematol.* **22**, 53–59 (2015).

175. Nishihira, J. Macrophage Migration Inhibitory Factor (MIF): Its Essential Role in the Immune System and Cell Growth. *J. Interferon Cytokine Res.* **20**, 751–762 (2000).
176. Gómez Morillas, A., Besson, V. C. & Lerouet, D. Microglia and Neuroinflammation: What Place for P2RY12? *Int. J. Mol. Sci.* **22**, 1636 (2021).
177. Xiong, T., Wang, X., Zha, Y. & Wang, Y. Interleukin-33 regulates the functional state of microglia. *Front. Cell. Neurosci.* **16**, 1012968 (2022).
178. Socodato, R. *et al.* Microglia Dysfunction Caused by the Loss of Rhoa Disrupts Neuronal Physiology and Leads to Neurodegeneration. *Cell Rep.* **31**, 107796 (2020).
179. Elmore, M. R. P. *et al.* Replacement of microglia in the aged brain reverses cognitive, synaptic, and neuronal deficits in mice. *Aging Cell* **17**, e12832 (2018).
180. Haynes, S. E. *et al.* The P2Y12 receptor regulates microglial activation by extracellular nucleotides. *Nat. Neurosci.* **9**, 1512–1519 (2006).
181. Fixsen, B. R. *et al.* SALL1 enforces microglia-specific DNA binding and function of SMADs to establish microglia identity. *Nat. Immunol.* **24**, 1188–1199 (2023).
182. Nguyen, C. *et al.* Transcriptional and epigenetic targets of MEF2C in human microglia contribute to cellular functions related to autism risk and age-related disease. *Nat. Immunol.* **26**, 1989–2003 (2025).
183. Deczkowska, A. *et al.* Disease-Associated Microglia: A Universal Immune Sensor of Neurodegeneration. *Cell* **173**, 1073–1081 (2018).
184. Bernier, L.-P. *et al.* Nanoscale Surveillance of the Brain by Microglia via cAMP-Regulated Filopodia. *Cell Rep.* **27**, 2895-2908.e4 (2019).
185. De, I. *et al.* CSF1 Overexpression Promotes High-Grade Glioma Formation without Impacting the Polarization Status of Glioma-Associated Microglia and Macrophages. *Cancer Res.* **76**, 2552–2560 (2016).
186. Shi, L. *et al.* Repopulating Microglia Suppress Peripheral Immune Cell Infiltration to Promote Poststroke Recovery. *CNS Neurosci. Ther.* **31**, e70565 (2025).
187. Baaklini, C. S. *et al.* Microglia promote remyelination independent of their role in clearing myelin debris. *Cell Rep.* **42**, 113574 (2023).
188. Packer, J. M. *et al.* Diffuse traumatic brain injury induced stimulator of interferons (STING) signaling in microglia drives cortical neuroinflammation, neuronal dysfunction, and impaired cognition. *J. Neuroinflammation* **22**, 128 (2025).
189. Mendes, M. S. *et al.* The role of P2Y12 in the kinetics of microglial self-renewal and maturation in the adult visual cortex in vivo. *eLife* **10**, e61173 (2021).
190. Kettenmann, H., Hanisch, U.-K., Noda, M. & Verkhratsky, A. Physiology of Microglia. *Physiol. Rev.* **91**, 461–553 (2011).
191. Kreutzberg, G. W. Microglia: a sensor for pathological events in the CNS. *Trends Neurosci.* **19**, 312–318 (1996).
192. Bruttger, J. *et al.* Genetic Cell Ablation Reveals Clusters of Local Self-Renewing Microglia in the Mammalian Central Nervous System. *Immunity* **43**, 92–106 (2015).
193. Bennett, M. L., Song, H. & Ming, G. Microglia modulate neurodevelopment in human neuroimmune organoids. *Cell Stem Cell* **28**, 2035–2036 (2021).
194. Rice, R. A. *et al.* Microglial repopulation resolves inflammation and promotes brain recovery after injury: RICE et al. *Glia* **65**, 931–944 (2017).
195. Antignano, I., Liu, Y., Offermann, N. & Capasso, M. Aging microglia. *Cell. Mol. Life Sci.* **80**, 126 (2023).
196. Niraula, A., Sheridan, J. F. & Godbout, J. P. Microglia Priming with Aging and Stress. *Neuropsychopharmacology* **42**, 318–333 (2017).
197. Roser, A.-E., Tönges, L. & Lingor, P. Modulation of Microglial Activity by Rho-Kinase (ROCK) Inhibition as Therapeutic Strategy in Parkinson's Disease and Amyotrophic Lateral Sclerosis. *Front. Aging Neurosci.* **9**, (2017).

198. Glotfelty, E. J. *et al.* The RhoA-ROCK1/ROCK2 Pathway Exacerbates Inflammatory Signaling in Immortalized and Primary Microglia. *Cells* **12**, 1367 (2023).
199. Cai, J. *et al.* Loss of RhoA in microglia disables glycolytic adaptation and impairs spinal cord injury recovery through Arhgap25/HIF-1α pathway. *Cell Death Dis.* **16**, 636 (2025).
200. Stoessel, M. B. *et al.* The effects of P2Y12 loss on microglial gene expression, dynamics, and injury response in the cerebellum and cerebral cortex. Preprint at https://doi.org/10.1101/2024.09.25.614526 (2024).
201. Peng, J. *et al.* Microglial P2Y12 receptor regulates ventral hippocampal CA1 neuronal excitability and innate fear in mice. *Mol. Brain* **12**, 71 (2019).
202. Aw, E., Zhang, Y. & Carroll, M. Microglial responses to peripheral type 1 interferon. *J. Neuroinflammation* **17**, 340 (2020).
203. Nazmi, A. *et al.* Chronic neurodegeneration induces type I interferon synthesis via STING, shaping microglial phenotype and accelerating disease progression. *Glia* **67**, 1254–1276 (2019).
204. Roy, E. R., Li, S., Saroukhani, S., Wang, Y. & Cao, W. Fate-mapping and functional dissection reveal perilous influence of type I interferon signaling in mouse brain aging. *Mol. Neurodegener.* **19**, 48 (2024).
205. Joshi, R. *et al.* IRF3 regulates neuroinflammatory responses and the expression of genes associated with Alzheimer's disease. *J. Neuroinflammation* **21**, 212 (2024).
206. Hickman, S. E., Allison, E. K. & El Khoury, J. Microglial Dysfunction and Defective β-Amyloid Clearance Pathways in Aging Alzheimer's Disease Mice. *J. Neurosci.* **28**, 8354–8360 (2008).
207. Cantoni, C. *et al.* TREM2 regulates microglial cell activation in response to demyelination in vivo. *Acta Neuropathol. (Berl.)* **129**, 429–447 (2015).
208. Frosch, M. *et al.* Microglia–neuron crosstalk through Hex–GM2–MGL2 maintains brain homeostasis. *Nature* **646**, 913–924 (2025).
209. Hickman, S. E. *et al.* The microglial sensome revealed by direct RNA sequencing. *Nat. Neurosci.* **16**, 1896–1905 (2013).
210. Nobes, C. D. & Hall, A. Rho, Rac, and Cdc42 GTPases regulate the assembly of multimolecular focal complexes associated with actin stress fibers, lamellipodia, and filopodia. *Cell* **81**, 53–62 (1995).
211. Chen, X. *et al.* Bid-Independent Mitochondrial Activation in Tumor Necrosis Factor Alpha-Induced Apoptosis and Liver Injury. *Mol. Cell. Biol.* **27**, 541–553 (2007).
212. Maria, D. A. *et al.* A novel proteasome inhibitor acting in mitochondrial dysfunction, ER stress and ROS production. *Invest. New Drugs* **31**, 493–505 (2013).
213. Koenigsknecht, J. & Landreth, G. Microglial Phagocytosis of Fibrillar β-Amyloid through a β_1 Integrin-Dependent Mechanism. *J. Neurosci.* **24**, 9838–9846 (2004).
214. Elliott, M. R. *et al.* Nucleotides released by apoptotic cells act as a find-me signal to promote phagocytic clearance. *Nature* **461**, 282–286 (2009).
215. Butler, C. A. *et al.* Microglial phagocytosis of neurons in neurodegeneration, and its regulation. *J. Neurochem.* **158**, 621–639 (2021).
216. Nikodemova, M. *et al.* Microglial numbers attain adult levels after undergoing a rapid decrease in cell number in the third postnatal week. *J. Neuroimmunol.* **278**, 280–288 (2015).
217. Zöller, T. *et al.* Silencing of TGFβ signalling in microglia results in impaired homeostasis. *Nat. Commun.* **9**, 4011 (2018).
218. Moraga, A. *et al.* Aging increases microglial proliferation, delays cell migration, and decreases cortical neurogenesis after focal cerebral ischemia. *J. Neuroinflammation* **12**, 87 (2015).

219. Flowers, A., Bell-Temin, H., Jalloh, A., Stevens, S. M. & Bickford, P. C. Proteomic analysis of aged microglia: shifts in transcription, bioenergetics, and nutrient response. *J. Neuroinflammation* **14**, 96 (2017).
220. McCoy, M. K. & Tansey, M. G. TNF signaling inhibition in the CNS: implications for normal brain function and neurodegenerative disease. *J. Neuroinflammation* **5**, 45 (2008).
221. Sierra, A., Gottfried-Blackmore, A. C., McEwen, B. S. & Bulloch, K. Microglia derived from aging mice exhibit an altered inflammatory profile. *Glia* **55**, 412–424 (2007).
222. Ritzel, R. M. *et al.* Functional and transcriptional profiling of microglial activation during the chronic phase of TBI identifies an age-related driver of poor outcome in old mice. *GeroScience* **44**, 1407–1440 (2022).
223. Fu, P.-C. *et al.* The Rho-associated kinase inhibitors Y27632 and fasudil promote microglial migration in the spinal cord via the ERK signaling pathway. *Neural Regen. Res.* **13**, 677 (2018).
224. Ohsawa, K. *et al.* $P2Y_{12}$ receptor-mediated integrin-β1 activation regulates microglial process extension induced by ATP. *Glia* **58**, 790–801 (2010).
225. Huang, Y. *et al.* Microglia use TAM receptors to detect and engulf amyloid β plaques. *Nat. Immunol.* **22**, 586–594 (2021).
226. Lund, H. *et al.* Competitive repopulation of an empty microglial niche yields functionally distinct subsets of microglia-like cells. *Nat. Commun.* **9**, 4845 (2018).
227. Streit, W. J., Sammons, N. W., Kuhns, A. J. & Sparks, D. L. Dystrophic microglia in the aging human brain. *Glia* **45**, 208–212 (2004).
228. Hefendehl, J. K. *et al.* Homeostatic and injury-induced microglia behavior in the aging brain. *Aging Cell* **13**, 60–69 (2014).
229. Streit, W. J., Braak, H., Xue, Q.-S. & Bechmann, I. Dystrophic (senescent) rather than activated microglial cells are associated with tau pathology and likely precede neurodegeneration in Alzheimer's disease. *Acta Neuropathol. (Berl.)* **118**, 475–485 (2009).
230. Socodato, R. *et al.* RhoA balances microglial reactivity and survival during neuroinflammation. *Cell Death Dis.* **14**, 690 (2023).
231. Swinnen, N. *et al.* Complex invasion pattern of the cerebral cortex bymicroglial cells during development of the mouse embryo. *Glia* **61**, 150–163 (2013).
232. Tremblay, M., Zettel, M. L., Ison, J. R., Allen, P. D. & Majewska, A. K. Effects of aging and sensory loss on glial cells in mouse visual and auditory cortices. *Glia* **60**, 541–558 (2012).
233. Sankowski, R. *et al.* Mapping microglia states in the human brain through the integration of high-dimensional techniques. *Nat. Neurosci.* **22**, 2098–2110 (2019).
234. Ross, J. L. *et al.* Microglia and monocyte-derived macrophages drive progression of pediatric high-grade gliomas and are transcriptionally shaped by histone mutations. *Immunity* **57**, 2669-2687.e6 (2024).
235. Szulzewsky, F. *et al.* Glioma-Associated Microglia/Macrophages Display an Expression Profile Different from M1 and M2 Polarization and Highly Express Gpnmb and Spp1. *PLOS ONE* **10**, e0116644 (2015).
236. Pyonteck, S. M. *et al.* CSF-1R inhibition alters macrophage polarization and blocks glioma progression. *Nat. Med.* **19**, 1264–1272 (2013).
237. Darmanis, S. *et al.* Single-Cell RNA-Seq Analysis of Infiltrating Neoplastic Cells at the Migrating Front of Human Glioblastoma. *Cell Rep.* **21**, 1399–1410 (2017).
238. Bowman, R. L. *et al.* Macrophage Ontogeny Underlies Differences in Tumor-Specific Education in Brain Malignancies. *Cell Rep.* **17**, 2445–2459 (2016).
239. Pombo Antunes, A. R. *et al.* Single-cell profiling of myeloid cells in glioblastoma across species and disease stage reveals macrophage competition and specialization. *Nat. Neurosci.* **24**, 595–610 (2021).

240. Lalancette-Hébert, M., Gowing, G., Simard, A., Weng, Y. C. & Kriz, J. Selective Ablation of Proliferating Microglial Cells Exacerbates Ischemic Injury in the Brain. *J. Neurosci.* **27**, 2596–2605 (2007).
241. Oboki, K. *et al.* IL-33 is a crucial amplifier of innate rather than acquired immunity. *Proc. Natl. Acad. Sci.* **107**, 18581–18586 (2010).
242. Markovic, D. S. *et al.* Gliomas induce and exploit microglial MT1-MMP expression for tumor expansion. *Proc. Natl. Acad. Sci.* **106**, 12530–12535 (2009).
243. Hambardzumyan, D., Gutmann, D. H. & Kettenmann, H. The role of microglia and macrophages in glioma maintenance and progression. *Nat. Neurosci.* **19**, 20–27 (2016).
244. Erreni, M. *et al.* Human glioblastoma tumours and neural cancer stem cells express the chemokine CX3CL1 and its receptor CX3CR1. *Eur. J. Cancer* **46**, 3383–3392 (2010).
245. Friebel, E. *et al.* Single-Cell Mapping of Human Brain Cancer Reveals Tumor-Specific Instruction of Tissue-Invading Leukocytes. *Cell* **181**, 1626-1642.e20 (2020).
246. Foray, C. *et al.* Interrogating Glioma-Associated Microglia and Macrophage Dynamics Under CSF-1R Therapy with Multitracer In Vivo PET/MRI. *J. Nucl. Med.* **63**, 1386–1393 (2022).
247. Fermi, V. *et al.* Effective Reprogramming of Patient-Derived M2-Polarized Glioblastoma-Associated Microglia/Macrophages by Treatment with GW2580. *Clin. Cancer Res.* **29**, 4685–4697 (2023).

List of publications

Publications used in the following dissertation:

1. Luczak-Sobotkowska Z.*, **Rosa P**.*, Banqueri Lopez M., Ochocka N., Kiryk A., Lenkiewicz A. M., Fuhrman M., Jankowski A., Kaminska B. “Tracking changes in functionality and morphology of repopulated microglia in young and old mice” *Journal of Neuroinflammation* **21**, 248 (2024).

Other publications:

2. Dzwigonska M., **Rosa P.,** Lipiec Sz., Obrebski T., Smyk G., Kaza B., Cyranowski S., Ellert-Miklaszewska A., Kominek A., Malik A. R., Piwocka K., Mieczkowski J., Kaminska B., Leszczynska K.B. “Hypoxis stress dysregulates functions of glioma-associated myeloid cells through epigenomics and transcriptional programs” *Cell Reports* **9**,44 (2025)
3. Mohana G., Dorier J., Li X., Mouginot M., Smith R.C., Malek H., Leleu M., Rodriguez D., Khadka J., **Rosa P.,** Cousin P., Iseli C., Restrepo S., Guex N., McCabe B.D., Jankowski A., Levine M.S., Gambetta M.C. “Chromosome-level organization of the regulatory genome in the Drosophila nervous system” *Cell* **186**(18) (2023)